Response to Reviewers' comments on the manuscript:

CMEMS-LSCE: A global 0.25-degree, monthly reconstruction of the surface ocean carbonate system

T. T. T. Chau, M. Gehlen, N. Metzl, F. Chevallier

We would like to thank the two reviewers for reading the manuscript thoroughly and providing constructive feedback. Based on their comments, we have improved the manuscript. Detailed replies are given hereafter. Each section comprises replies for general comments and minor (or specific) comments. Relies to Reviewer 2 start at page 22. The text quoted from the initial manuscript is in blue and revisions are presented in green. The revised manuscript with track changes is attached in this document (after all the replies to the two reviewers).

On behalf of the authors,
Thi-Tuyet-Trang Chau

Replies to comments by Reviewer 1

General comments by Reviewer 1 (GC1)

GC1.1. *Chau et al. present a exclusive approach using discrete ocean surface data of pCO2 and total alkalinity (TA) to obtain a new monthly reconstruction for the period 1985 to 2021 with 0.25º resolution of the marine carbonate system variables. The reconstruction is based on the use of a feed-forward neural network (FFNN) for pCO2. For TA they use locally interpolated alkalinity regression (LIAR). The reconstruction is based on the CMEMS (Copernicus Marine Environment Monitoring Service) product, which provides global reconstructions of sea surface temperature (SST) and surface salinity (SSS) for the same period, including chlorophyll and other physical variables such as sea surface height. The authors start from a previous work where they published a similar database made with a resolution of 1° where only pCO2 has been reconstructed. Here they expand the resolution by increasing it to 0.25º with the inclusion of TA, and then using the thermodynamic equations of the marine carbonate system they obtain the variables: Dissolved Inorganic Carbon (DIC), pH and degree of saturation of aragonite and calcite. In this way a product is generated that can be used to evaluate the impact of ocean acidification by other users and stake-holders. The quality of the reconstruction is contrasted with values observed at a series of oceanic and other coastal time stations. The authors provide two databases, one with 1ºC resolution and the other with 0.25º resolution.*

The motivation and idea behind the paper is not original in the sense that this has been done before on a seasonal climate scale, but instead, here, the authors exploit the potential of CMEMS to obtain a reconstruction of all carbonate system variables on a spatial scale that has not been achieved so far and that can certainly be very useful in the evaluation of biogeochemical models and for the study of ocean acidification and in coastal regions of higher variability.

Authors:

We thank **Reviewer 1** for highlighting potential use cases of our new CMEMS-LSCE datasets of surface ocean carbonate variables at high resolution. The two key points that set this contribution apart from previous studies include (1) a model upgrade for monthly $p\mathrm{CO_2}$ reconstructions in spatial resolution from 1º (Chau et al., 2022) to 0.25º (this study) and (2) an extension to provide high-resolution datasets of A_T, DIC, *p*H, and calcium carbonate saturation states covering the 37-year period. We hope the CMEMS-LSCE data product will be explored in further analyses of fine-scale spatiotemporal variations in marine carbonate variables complementary to previous contributions.

%%%%%%%%%%%%%%%%%%%%%%%%%%%%%%%%

GC1.2. *The article is well written and provides detailed information both in the formalization of the equations and in the graphical information that is extended in the figures and equations of the appendix. However, it does not develop a specific discussion section of this new database or a comparison with other climatologies of pCO2, DIC, AT and pH that would allow us to see the benefits, improvements and qualities of the new product. The authors, instead, compare in the 'Conclusions and Discussion' section the acidification rates with other observational results of other authors.*

Authors:
We thank **Reviewer 1** for appreciating the manuscript presentation. Our evaluation strategy is based on gridded SOCAT, GLODAP, and various time series station data. As suggested by **Reviewer 2** (comment **GC2.2.**) to gain reliability for our data evaluation, in this revision, we have shown new results at additional 38 time series stations with $p\mathrm{CO}_2$ and pH measurements and 4 sites with A_T and DIC measurements. Our product assessment is now stretched across the tropics, the subpolar sector, and the Southern Ocean to complement our previous data evaluation over the subtropical regions (See Figure A1b and statistics added in Tables A3 and A4 in the revised manuscript). An intercomparison with 1°-climatological data reconstructions (e.g., Broullon et al., 2019, 2020; Keppler et al., 2020) seems to us too outside the scope of our study given the importance of underlying methodological choices in such intercomparisons: (1) the discrepancy in mapping methods, input data resource, and the ratio of training and validation datasets used in model fitting, (2) uncertainty from post-processing applied for some products (e.g., filtering, smoothing, calibration), (3) the normalization of different data covering periods, and (4) quality of evaluation (or reference) data; e.g., observation data paucity should be one major concern to evaluate seasonal cycle reconstructions. The effect of such methodological choices calls into question the interpretation of differences between products if the different data providers do not actively contribute with sensitivity studies.

%%%%%%%%%%%%%%%%%%%%%%%%%%%%%%%

GC1.3. *The source of information for the pCO2 reconstruction is the Surface Ocean CO2 Atlas version 2022 (SOCATv2022, 1985-2021) observations of CO2 fugacity (fCO2). This database provides not only fCO2 but the data are REQUIRED to be accompanied by SST and SSS. The fCO2 data cannot be used independently of the SST and SSS with which it has been reported, since the temperature in the observation of fCO2 has a high impact on the fCO2 value itself (a bias of 1°C generates a bias in pCO2 of 4.2%, ~18 µatm). The development of the pCO2 reconstruction expressed in equation (1) does not meet that requirement. The authors mix the SOCAT observations with the SST and SSS reconstructions of the CMEMS product. This generates important errors as they themselves show in the reconstruction at oceanic (Figure 7) and coastal (Figure 5) fixed stations. Similarly, with TA, the observations used in LIAR also use temperature and salinity in Global Ocean Data Analysis Project bottle data version 2.2022 (GLODAPv2.2022, Lauvset et al., 2022). GLODAPv2 does not report TA without temperature and salinity observations so neither should different data sources be mixed when applying the LIAR methodology as is done in equation 2. Therefore, methodologically, the manuscript is seriously flawed in its numerical approach. The process should be done in two stages, first obtaining a set of FFNNs trained with fCO2, SST and SSS with the SOCAT data (and additionally the variables already included in equation 1), and then projecting that FFNN onto CMENS' own reconstructions of SST and SSS. The same is true for TA and the use of LIAR. At least the SSS used in equation 2 should include the GLODLAP SSS and not the CMEMS SSS. Better is to include the GLODAP SST, also. Then the coefficients developed with LIAR are used on the CMENS reconstruction. This would greatly improve the reliability of the algorithms by better reproducing both the oceanic and coastal time series, not to mention that the GLODAP reconstructions shown in Figure 8 will do so as well. All this allows us to have a better estimate of the quality of the obtained algorithms since we can apply them to both oceanic and coastal time series with their own predictors and validate these algorithms. As currently performed in the manuscript, this validation is strongly biased because the SST and SSS reconstructions of CMENS on these series clearly disagree when comparing point data with monthly means as indicated in the manuscript itself in Figure A8. In addition, a simple linear regression of TA versus salinity would report a better fit than the LIAR model applied in the manuscript.*

As shown above, the monthly reconstruction proposed by the authors would be strongly improved if the two-step process is applied. The current product shown has a very poor quality in terms of validity since its comparison with the fixed time-series station used shows very high RMSD values (Figure 5, Table 7 and A3).

Authors:

- **For pCO$_2$**: Our FFNNs formally link a specific pCO$_2$ estimate (from the gridded SOCAT products) and specific estimates of environmental conditions (from the datasets listed in Table 1[(1)]), as expressed in Equation 1. There is no flaw in this approach that simply exploits the power of FFNNs (which are themselves non-linear regressors). The two-step approach proposed by the

[1] Table 2 in the initial manuscript (Table 1 has been removed as suggested by **Review 2**, comment **SC2.2**.).

reviewer unnecessarily complicates the reconstruction process. In addition, how the second step ("*projecting that FFNN onto CMENS' own reconstructions of SST and SSS*") can be made is not obvious: it seems to us that it would lose all the benefit gained by the first step.

Note that the bias between CMEMS SST and SOCAT data (or in situ observations) is relatively small (see Figures **GC1.3.** and **MC1.13.** in this document and also Figure A10 in the manuscript). Besides, the quality control has not been done for SOCAT salinity. There are some cruises in SOCAT with no salinity data and they have been replaced by SSS from the World Ocean Atlas (WOA) to recalculate CO2 fugacity (see Pfeil et al, 2013). SOCAT SSS would not be used in data reconstruction unless a critical quality control is performed. We have not changed the method.

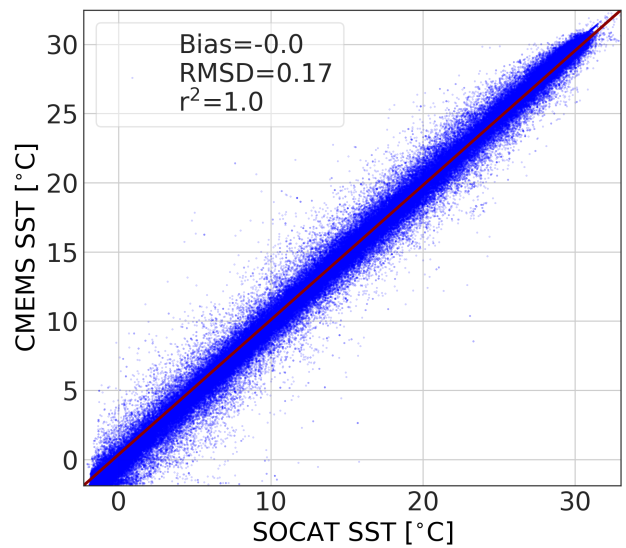

***Figure* GC1.3.** *Scatter plot of SOCAT SST and CMEMS SST gridded data over the global ocean in the period 1985-2021. The two datasets well fit to the bisector (red line) with no systematic bias, a RMSD of 0.17 and a r^2 of 1.*

- **For A_T**: **Reviewer 1**'s comment (**GC1.3.**) quoted below does not reflect precisely our method application.
  "*Similarly, with TA, the observations used in LIAR also use temperature and salinity in Global Ocean Data Analysis Project bottle data version 2.2022 (GLODAPv2.2022, Lauvset et al., 2022). GLODAPv2 does not report TA without temperature and salinity observations so neither should different data sources be mixed when applying the LIAR methodology as is done in*

equation 2. Therefore, methodologically, the manuscript is seriously flawed in its numerical approach."

LIAR coefficients were estimated with GLODAPv2 data (Olsen el al., 2016) of SSS, SST, A_T,... (Carter et al., 2018). In this study, we do not retrain LIAR models but use these existing coefficients to predict A_T with CMEMS SSS and SST (see Lines 257-260[2] in the revision attached at the end of this document):

"*Locally interpolated alkalinity regression (LIAR; Carter et al., 2016, 2018) is an ensemble-based regression method developed for the global reconstruction of total alkalinity (AT). Regression coefficients were learned on GLODAPv2 data (Olsen et al., 2016) binned within regular windows of 5◦ × 5◦. For prediction, the LIAR software interpolates between the regression coefficients to arbitrary resolutions specified by the users.*"

%%%%%%%%%%%%%%%%%%%%%%%%%%%%%%%%%%

Minor comments by Reviewer 1 (MC1)

Reviewer's comments	Replies from Authors	Notes
MC1.1. Line 18 "*reconstructions with root-of-mean–square–deviation from observations less than 8%, 4%, and 1% relative to the global mean*" The relative percentage of RMSD over the mean is not a good parameter to evaluated the goodness of the results. For example, the accuracy of AT is better than 0.1%, and pCO2 is similar. The percentages of	Lines 17-19 (abstract): we quote the full sentence below. "*Product qualification with observation-based data confirms reliable reconstructions with root-of-mean–square–deviation from observations less than 8%, 4%, and 1% relative to the global mean of pCO_2, A_T (DIC), and pH.*" We are surprised by this comment because normalizing the RMSD, for instance over the mean, may simplify the interpretation of this statistical quantity. In the quoted sentence of the abstract, it allows using the same metric (the relative amplitude of the error) for the four variables. We have not changed the sentence.	

[2] Lines 231-234 in the initial manuscript

RMSD reported are about two orders of magnitude higher.	**Reviewer 1** mentions that "*the accuracy of A_T is better than 0.1%, and pCO_2 is similar*". These values likely correspond to analytical errors based on measurement quality controls at each station/location, e.g., 4 µmol kg−1 for GLODAPv2.2022 A_T (Lauvset et al, 2022) and 2-5 µatm for SOCATv2.2022 pCO_2 (Bakker et al, 2022). Unsurprisingly, our reconstruction RMSD is substantially larger than analytical errors, which is only a minor source of uncertainty in the reconstruction process. Our reconstruction RMSD (e.g. 14.3 µatm, 22.1 µmol kg−1, 22.7 µmol kg−1, 0.022 for pCO_2, A_T, DIC, and pH) is in line with those reported in the previous studies (see our discussion in Lines 661-667* quoted below): *"For instance, Iida et al. (2021) calculated 1σ-uncertainty based on the median absolute deviation of regression model fits from open-ocean observations. Their approach yielded global σ-averages of 17.8 µatm, 11.5 µmol kg−1, 0.018, and 0.110 for* pCO_2*, normalized DIC, pH, and Ωar, respectively. In Gregor and Gruber (2021), the authors propagated the sum squared errors (global RMSD and measurement uncertainties) of* pCO_2 *(15 µatm) and* A_T *(22 µmol kg−1) obtaining global uncertainty estimates of 19 µmol kg−1 in DIC and 0.022 in pH."*	*Lines 615-619 in the initial manuscript
MC1.2. Line 20 *"and 0.4% for pH"* It is a bit odd to report percentages of a logarithmic magnitude such as pH.	In the statistical sense, we consider *p*H as a variable similar to pCO_2 and other carbonate system variables. All statistics are therefore reported with respect to the reconstructed variable. As explained in the previous comment (**MC1.1.**), with the intention of having a concise abstract, we choose to show the percentage of errors against the global mean value of each variable. It is noteworthy that percentages are also used in the scientific report SDG 14.3.1 (Table 1).	

MC1.3. Line 92 The associated uncertainty reported in the article (σ) refers only to the uncertainty of the 100 replicate FFNNs, but they do not incorporate the uncertainty that each of the FFNNs has with respect to the SOCAT pCO2 values they are trying to replicate. The paper is only assessing a part of the uncertainty, by the way the smallest part and therefore not evaluating the ability of the FFNN set to reconstruct the input values.	The CMEMS-LSCE-FFNN 100-ensemble approach subsamples the gridded data of $p\mathrm{CO_2}$ and predictors to compose different training and test datasets, i.e., 100 training datasets for 100 FFNN models. In practice, it would allow to account for multiple sources of input data uncertainty from measurement errors, data sampling bias, data post-processing, etc, which have been poorly quantified in the input data products so far. In addition, the first layer of FFNNs is also initialized randomly at each of the 100 iterations. Therefore, our ensemble-based uncertainty includes the randomness in both subsampling datasets of $p\mathrm{CO_2}$ and predictors and in FFNN initialization. In Chau et al. (2022) (Section Methods), the authors described the ensemble approach comprehensively. This study extends the model by Chau et al. (2022) and thus recaps its principle. We modify the text in Lines 239-241* and add another one (in green) as follow for clarification: "*After excluding the data in the reconstruction month, the data within the 3-month window are* ***randomly*** *separated into FFNN training and validation subsets with a ratio of 2 : 1.* ***The subsampling process is repeated for each 100 FFNN runs that results in 100 different datasets for model fitting.***"	*Lines 214-215 in the initial manuscript

MC1.4. Table 1, Table 2 and also Table 3 should include a value or an estimate of the uncertainty of each of the variables, either in their analytical determination or that which each product or reconstruction generates for each of the variables. This helps the reader to evaluate the quality of the reconstruction as a function of own error in the determination of each of the reconstructed variables.	Thank you. We have added the measurement errors with respect to each variable in Tables 1 and 2* if they are available from input data resources.	*Tables 2 and 3 in the initial manuscript (Table 1 has been removed as suggested by **Review 2**, comment SC2.2)
MC1.5. Line 126 Table 3 is cited before Table 2	We have revised the manuscript and cited Tables/Figures in order.	
MC1.6. Line 214 It is not sufficiently clear how to proceed with the reconstruction. It talks about excluding data in the month of reconstruction. Therefore, it would appear that for each month 100 FFNN reconstructions are performed. If this is correct, the RMSD for each month should be included in the figure or table of the SOCAT pCO2 reconstruction since that data is not used in the month-specific reconstruction.	We quote Lines 238-241* from the revised manuscript for a straightforward response to **Reviewer 1** (modification in green corresponding to our reply to comment **MC.1.3.**): "*The datasets of SOCAT fCO_2 and predictors are first reprocessed to match model fitting requirements (Sect. 2.1). After excluding the data in the reconstruction month, the data within the 3-month window are **randomly** separated into FFNN training and validation subsets with a ratio of 2 : 1. **The subsampling process is repeated for each 100 FFNN runs that results in 100 different datasets for model fitting.** The excluded SOCATv2022 datasets are used in model evaluation.*" Here we specify the three independent datasets for FFNN training, validation, and evaluation. In the fitting phase of FFNN, we do not use SOCAT fCO_2 in the month specified for reconstruction to train and validate	*Lines 213-215 in the initial manuscript

	FFNN models. In the reconstruction step, predictors data are available over the global ocean and FFNNs reconstruct *f*CO_2 for the target months. This exclusion strategy, called cross-validation, is widely used within machine learning approaches to avoid overfitting.	
MC1.7. Line 249 Fig A7 is not cited in order.	Thank you. We have revised the manuscript and cited Tables/Figures in order.	
MC1.8. Lines 285 and 210 How do you solve the discontinuities of the variable 'longitude' around the prime meridian 0°. This is usually solved using the sine and cosine functions of longitude. Any reason for not doing so? Does this variable really bring any improvement in the FFNN?	To preserve the continuity of longitude at 0°, we have applied both the sine and cosine functions to that coordinate. Hence, our global maps of carbonate variables (e.g. Figures 1, 6, 9) do not show discontinuity at the prime meridian. The sine is also used to transform latitude. Data transformation of predictor variables is explicitly presented in a sequence of preceding studies for the CMEMS-LSCE-FFNN model development (Denvil-Sommer et al 2021, Chau et al 2022). In the first manuscript version, we avoided repeating part of the data processing and model description from the previous studies. As the readers would concern, we have called back this information in the revision (Lines 162-164): "***The sine function is applied to convert latitude while both the sine and cosine are used to transform longitude to conserve their periodical behaviors***."	
MC1.9. Table 4 First of all, it should be pointed out that there is an excess of significant figures, not only in this table but throughout the text. Regarding the pCO2 results, the	The manuscript describes and evaluates long-term datasets of multiple variables. A significant number of figures and tables corresponds to the presentation of many results of these variables. *p*CO_2 errors (e.g. Bias, RMSD) have been reported with 1-2 decimals in previous studies (Landschuter et al 2020; Denvil et al 2019, Gregor et al.	

authors should remove all decimal places since analytically its precision is 2 µatm as described in the article. But more importantly, once the superfluous decimal places have been removed, what is observed is that there is practically no significant improvement between the product 'r025' and 'r100'.	2019, 2021). In this revision, we reduce the decimals from 2 to 1 for pCO_2, $A_{T,}$ and DIC. The modification has been applied for Tables, Figures, and texts involving these variables. Note that 2-5 µatm reported in the manuscript represents the precision of measurement replications or analytical errors based on measurement quality control at each station/location (Sutton et al., 2019; Bakker et al., 2022). Table 3* shows a marginal improvement from r100 to r025 in terms of global evaluation metrics. For the open ocean, we expect to obtain similar skill scores for both FFNN models as the spatial autocorrelation of open-ocean pCO_2 is estimated within 400±250 km (Jones et al., 2012) and the SOCAT 1°-open-ocean dataset was used in model fitting. As also noted by Chau et al., (2022), pCO_2 over the coastal ocean is characterized by high variability at small scales. For instance, pCO_2 levels can vary with a horizontal gradient as large as 470 µatm over a distance of less than 0.5 km (Chavez et al., 2018; Feely et al., 2008). Probably, statistical models would need a spatial resolution much finer than 0.25° (25 km) and a temporal resolution higher than monthly in order to capture such high variability in surface ocean pCO_2 present in observations (see also Bakker et al., 2016; Laruelle et al., 2017). In addition, measurement uncertainty of SOCAT gridded data due to undersampling is possibly one of the major sources of the irreducible model-data errors. Please refer to our reply to comment **MC1.11.** for a discussion on the benefits of the higher resolution.	*Tables 4 in the revied manuscript (Table 1 has been removed as suggested by **Review 2**, comment SC2.2)
MC1.10. Line 350 How is the regriding process performed? What type of interpolation is performed?	All the 3-dimensional datasets provided in this study have been saved as netCDF numerical files. To regrid these datasets, we use the Climate Data Operators (CDO) remapping operator, namely "remap". CDO remap supports converting netCDF datasets from one horizontal grid to another. This operator	

	has been widely used in standard processing for numerical and statistical model outputs. We have revised the last sentence in Lines 374-377* to make it clear to the readers. "*Table ~~4~~**3*** ** *also presents statistics for the monthly FFNN products of surface ocean* pCO_2 *at spatial resolutions of 0.25◦ (r025) and 1◦ (r100) together with their variants (r100 → 025 and r025 → 100). The latter are respectively extrapolation and interpolation versions of the original r100 and r025 datasets~~, i. e.,~~* ***. We used the Climate Data Operators (CDO) remap operator to regrid*** *FFNN model outputs (r100 and r025)~~ regridded~~ to a finer or coarser spatial resolution.*"	*Lines 348-350 in the initial manuscript **Table 4 in the initial manuscript (Table 1 has been removed as suggested by **Review 2**, comment **SC2.2.**)
MC1.11. Line 354 "*The FFNN(r025) central to this study yields a lower RMSD and a higher correlation to the SOCAT data than the FFNN(r100→ 025)*". Unfortunately, there is no significant difference between the two products. This statement is not correct. Line 393. It seems a very marginal the 2% improvement in pCO2 reconstruction capability	Our statement is upheld even though the increment in global skill scores relative to a low to high spatial resolution is not large. Here we do not mention getting a significant improvement but still obtained higher scores in RMSD and r^2 when increasing the model spatial resolution. Please refer to Table 3* for verifying the statistics with respect to FFNN(r025) and FFNN(r100→r025) and our reply to comment **MC.1.9.** for analysis. Apart from Table 3*, benefits by increasing model spatial resolution from 1° to 0.25° are also demonstrated in Figures 2-4 with analyses shown in Lines 414-420**: "*The two FFNN reconstructions (r025 and r100) share similarities in overall structures of* pCO_2 *over the coastal-open-ocean continuum (Figs. 2-4). However, the higher spatial resolution outperforms its lower resolution counterpart in reproducing fine-scale features of* pCO_2 *in the transition from nearshore regions to the adjacent open ocean. The increase in model spatial resolution translates into a greater spatial coverage of the continental shelves such as Labrador Sea, Northern Europe, and Sea of Japan (Fig. 3), and thus*	*Table 4 in the initial manuscript (Table 1 has been removed as suggested by **Review 2**, comment **SC2.2.**) **Lines 387-394 in the initial manuscript

	an increase in the number of data over the coastal domain. The increase in spatial resolution allows a gain in prediction probability of pCO_2 *variations on the order of roughly 2% over the Eastern Boundary Currents to 8% over the Western South Atlantic (Figs. 2-3b).*" This study also points out temporal data sampling bias as a source of uncertainty that would highly constrain model reconstruction skills. Based on the assessment at station time series (Figure 5 and Table A3), we found that in situ observations have been sampled with low frequency and the bias of sampling date is about a week from a month center. With the low number of observations and high variability of $p$$CO_2$ (20.12 to 69.98 µatm) over these stations, it would not be statistically sufficient to refer to their temporal mean as a representative of monthly averages. A large model-data deviation would be retained even if we increase spatial resolution (see text in Lines 434-447*** for further analysis).	***Lines 403-414 in the initial manuscript
MC1.12. Line 375 and 393 Line 375. The differences in RMSD between the regridded r100 and r025 products are very small, or even in some as in Canary Current System it is larger (strange?). There is no significant improvement in the coastal regions between the two products.	Thank you for pointing this out. We have revised Figures 2-4. In the previous version, we made a technical error in co-locating the two model outputs to coastal SOCAT grid cells so statistics were not precise enough. The revision slightly modifies RMSD and r^2 values over all regions but does change our conclusion.	
MC1.13. Lines 404-423 "*Analyzing the eight station time series, we have found that data have been sampled within a few days with an average offset of about a week from the month center. At*	We have demonstrated the better performance of FFNNr025 in terms of intra-seasonal to interannual variability of coastal sites (Sutton et al., 2019). By increasing the model resolution by 16-fold, this study partly resolves the spatial sampling bias from $p$$CO_2$ observations (lower RMSD and higher r^2 for	

these coastal sites, the temporal standard deviation from monthly averages of pCO2 (σ_t^{pCO2}) exceeds measurement errors (2 µatm, Sutton et al., 2019). σ_t^{pCO2} ranges from 20.12 µatm at GREYREFF to values as large as 65.6 µatm at CAPEARAGO or 69.98 µatm at FIRSTLANDING. The monthly average of pCO2 might not be adequately represented by discreet samples at sites with a large temporal standard deviation of pCO2. The misfit between the monthly reconstruction and discreet observations is exacerbated in dynamical coastal environments and might explain in part the large RMSD of reconstructions of monthly coastal pCO2 (e.g., GREYREEF: 38.34 µatm, CAPEARAGO: 79.86 µatm, FIRSTLANDING: 77.32 µatm) for the r025 reconstruction. The RMSD is mostly lower for the FFNN reconstruction at 0.25° resolution compared to the FFNN at 1° resolution by 2.11 µatm (CCE2) to 23.32 µatm (COASTALMS). Similarly, r2 increases between 7%-23% at higher resolution. Overall, seasonal to interannual variations of coastal-ocean pCO2 are better reproduced in the	the higher resolution) although large model-observation mismatches still persist. As replied to comments **MC1.9.** and **MC1.11.**, the sparsity of data samples (biases from observation locations to the grid cell center about 0.34° ± 0.14° as reported in Sabine et al., 2013) and high variability of coastal $p\mathrm{CO_2}$ (e.g., 470 µatm in a distance of 0.5km; see in Chavez et al., 2018 and Feely et al., 2008) would draw the conclusion that much higher resolution or extensions of observing system are necessary to fully capture coastal $p\mathrm{CO_2}$. Temporal data sampling bias should be considered as a great source of uncertainty contributing to large model-observation mismatch even though model spatial resolution is getting finer. We illustrate this through Figure 5 with the corresponding analysis being in the paragraph (Lines 437-439*) quoted by **Review 1**. The key discussion we found is as follows "*Analyzing the ~~eight~~ station time series, we have found that data have been sampled within a few days with an average offset of about a week from the month center. At these coastal sites, the temporal standard deviation from monthly averages of* $p\mathrm{CO_2}$ *(σ_t^{pCO2}) exceeds ~~measurement~~**analytical** errors (2 µatm, Sutton et al., 2019)*". With the low number of observations and high variability of $p\mathrm{CO_2}$ over these stations, it would not be statistically sufficient to refer to the temporal mean of instantaneous observations as a representation of monthly averages. We then provide evidence that the large values σ_t^{pCO2} at time series stations (e.g., GREYREEF: 20.12 µatm, CAPEARAGO: 65.6 µatm, FIRSTLANDING: 69.98 µatm) correspond to high RMSDs (e.g., GREYREEF: 38.34 µatm, CAPEARAGO: 79.86 µatm, FIRSTLANDING: 77.32 µatm). About the effect of model-observation bias of SST on the reconstruction skills of $p\mathrm{CO_2}$, we refer to our reply to the general comment **GC1.3** above.	*Lines 403-405 in the initial manuscript

reconstruction at 0.25° resolution (Fig. 5)."

Here, it becomes evident that comparing monthly reconstructions with point values in coastal areas of high variability results in very low predictive ability on the part of the product produced. As indicated in the general comment, this should be evaluated considering the variability of SST and SSS in the study area because in this way the biases that the CMENS product has to reproduce point values from monthly mean values are being transferred to pCO2. The aforementioned increases in r2 are relatively small if we consider the important biases involved, which in some products even increase as the resolution improves, as in FIRSTLANDING or CHEECAROCKS.

Also illustrated in Figure **MC.1.13.**, the bias between SST^{CMEMS} and in situ SST from Sutton et al's time series is always lower than 0.5°C for many stations. A bias in SST would not be the dominant source of high reconstruction errors at these stations.

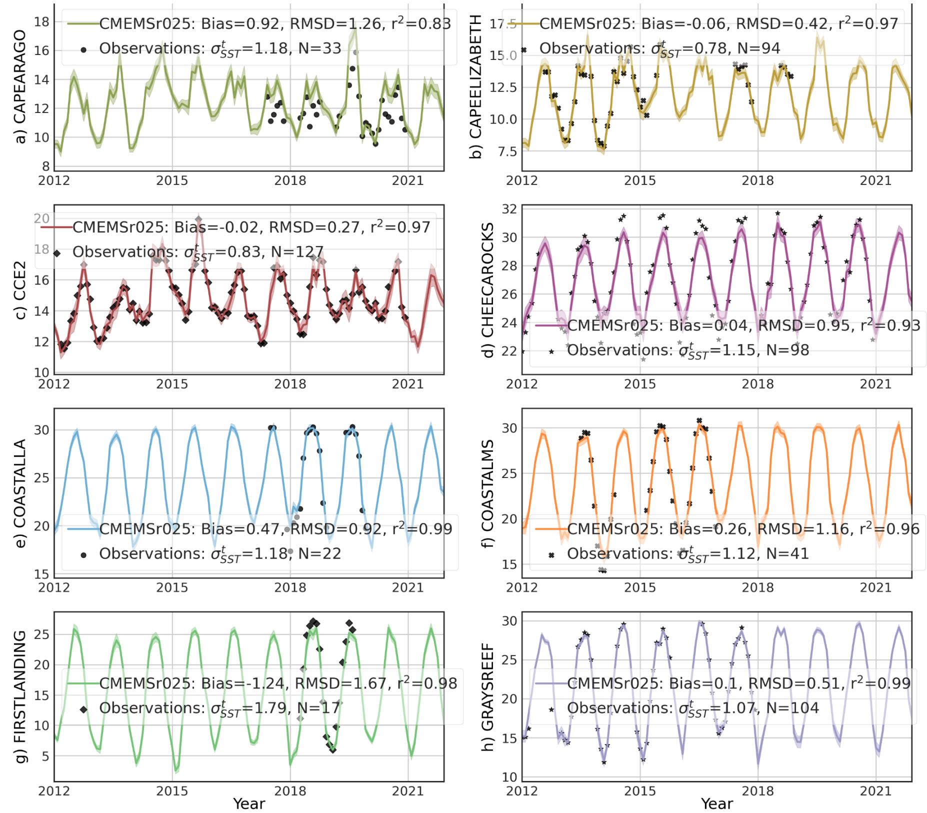

***Figure* MC1.13.** *Time series of surface ocean SST (°C) at coastal observing stations**: CMEMS SST estimate (curve), associated 1σ-uncertainty (envelope), and monthly average of in situ observations (point). CMEMS reanalysis data at 0.25° (r025) resolutions are co-located to in situ observations provided by Sutton et al. (2019). Statistics include number of months with observations (N), Bias, RMSD, and r^2. σ_t^{SST} stands for temporal standard deviation from monthly averages of SST observations.*

*** See Table A2 and Fig. A1b in the manuscript.*

MC1.14. Lines 437-438 "*The largest model uncertainty (σ > 30 μmol kg-1) is computed nearshore and surrounding oceanic islands, a feature inherited from input uncertainty associated with the CMEMS salinity product (Fig. A8a).*" This described here is very relevant. In fact, it would be necessary to show graphically the correlation between the uncertainty in TA and SSS in the CMEMS product in both the coastal and oceanic domains. Possibly it shows a very relevant correlation. A similar should be done with the uncertainties of pCO2 and SST in the CMEMS product.	Total alkalinity (A_T) is predominantly controlled by the processes that govern sea surface salinity (SSS) (Broecker and Peng, 1982; Millero et al, 1998). The typical relationship between these two variables is linear and can be estimated at a high precision (Lee et al, 2006; Carter et al, 2018; Broullon et al, 2019). From the statistical point of view, the distribution of A_T uncertainty is generally driven by SSS uncertainty: A_T uncertainty increases as SSS uncertainty increases (see Figure **MC1.17.**). To the contrary, pCO_2 is characterized by multiple physical, biological, and chemical processes. Uncertainties from many input data products thus contribute to pCO_2 uncertainty estimates. Drivers of pCO_2 uncertainty are not analyzed as input uncertainty has not been fully quantified or published so far for many environmental variables.	
MC1.15. Lines 451-465 "*The reconstruction of AT distributions relies on LIAR coefficients fit with GLODAPv2 data (Olsen et al., 2016) covering the years before 2015. These data are also part of the latest version GLODAPv2.2022 (Lauvset et al., 2022). They do therefore not correspond to an independent dataset for the evaluation data of the CMEMS-LSCE reconstruction. To overcome this limitation, reconstructions of AT and DIC are*	First of all, Lines 488-496* quoted by **Reviewer 1** describes the evaluation of our data product of A_T and DIC and time series of in situ observations. This complements the assessment with GLODAP data. As opposed to the interpretation by **Reviewer 1**, these lines do not contain any analysis about "*how a large part of the discrepancies between the TA and DIC reconstruction is due to the discrepancies in SSS and SST of the CMEMS product and observations*". But we have revised the following sentence to have a better sense (other modifications follow the revisions according comment **GC2.2.**) "*To ~~overcome this limitation~~* ***accomplish a cross-validation****, reconstructions of A_T and DIC are compared to observations for ~~Eulerian~~* ***eight*** *time series*	*Lines 451-465 in the initial manuscript

compared to observations for Eulerian time series stations: BATS, DYFAMED, ESTOC, and HOT (see Table 3 and Fig. A1b for data sources and station locations). Figure 7 illustrates the comparison between monthly time series of AT and DIC extracted from the CMEMS-LSCE datasets and measurements at these long-term monitoring sites". These lines and Figure 7 show again how a large part of the discrepancies between the TA and DIC reconstruction is due to the discrepancies in SSS and SST of the CMEMS product, indicating that the reconstruction is not well done. In the case of the DYFAMED station it is very noticeable and contrasts that other products such as climatologies like those cited in the article (Lauvset et al. 2016; Broullón et al. 2019) do not show bias as high as the reconstruction performed here.	*stations:* ***AWIPEV****, BATS, DYFAMED, ESTOC, ~~and~~ HOT,* ***ICELAND, IRMINGER, and KERFIX*** *(see Table 3 and Fig. A1b for data sources and station locations).*" In Figure 7 we illustrate both the relatively good and poor reconstructions at long-term time series of observations. Note that, Lauvet et al, (2016) and Broullon et al, (2019) provided climatologies of A_T and DIC and associated mapping errors. As the climatology is smoother than the monthly fields (with intra- to interannual variability) proposed in this study, the errors reported in the previous studies are evidently smaller than those presented here. Their magnitudes are not comparable. In addition, Lauvet et al, (2016) and Broullon et al, (2019) did not evaluate the reconstruction at DYFAMED as mentioned by **Reviewer 1**. Please kindly refer to our reply to **SC2.14.** for a profound analysis of high model-data mismatch of A_T at DYFAMED.	
MC1.16. Line 473 "*The lowest prediction skill of temporal variability is obtained for ESTOC. Particularly, seasonality to multiyear variations in DIC are predicted at r2=0.47*	We thank the reviewer for highlighting our good estimates of A_T and DIC at ESTOC in terms of RMSD. We skipped this element in the initial manuscript. We have added it in Lines 515-520*:	*Line 473-476 in the initial manuscript

for ESTOC compared to r2 > 0.7 for BATS and HOT." This is not correct. The regression coefficient is not the only criterion for assessing predictive ability. In this case the variability observed at ESTOC is lower than at BATS and HOT, so a lower r2 does not mean lower skill. In fact, the RMSD at is the lowest of all the stations evaluated in TA. In terms of DIC the three stations show similar RMSD.	"***Despite showing good estimates of A_T and DIC in RMSD at ESTOC, temporal variability of observations are reconstructed at the lowest r^2.*** ~~*The lowest prediction skill of temporal variability is obtained for ESTOC.*~~ *Particularly, seasonality to multi-year variations in DIC are predicted at r2 = 0.47 for ESTOC compared to r^2 > 0.7 for* ***AWIPEV, ICELAND, IRMINGER,*** *BATS and HOT. Over all the stations, the model underestimates temporal changes of A_T (Fig. 7a; BATS: r^2 = 0.33, DYFAMED: r^2 = 0.12, ESTOC: r^2 = 0.03, HOT: r^2 = 0.32) which can be attributed to the large discrepancy in variability between in situ measurements and the CMEMS time series of salinity (Fig. A10a; BATS: r2 = 0.33, DYFAMED: r^2 = 0.19, ESTOC: r^2 = 0.03, HOT: r^2 = 0.35).*" We indeed analyze both RMSD and r^2 throughout the manuscript. To be precise, r^2 is not '*regression coefficient*' but the determination coefficient. This metric allows evaluating the model predictive ability in temporal variations of the variables of interest. As shown in Eq (11) in the manuscript, r^2 is the model-data covariance normalized with the temporal variability of A_T and DIC reproduced by FFNN and observed at each station. Therefore, r^2 values at BATS and HOTs are comparable to the one at ESTOC even though the two former stations show higher temporal variability of A_T and DIC. Our analysis in Lines 515-520* holds true.	
MC1.17. Line 478 "*Model uncertainty (1σ-envelop) of monthly AT and DIC estimates (Fig. 7a) is also inflated somewhat proportional to the CMEMS salinity product uncertainty (Fig. A10a).*" Evidently. A figure showing that would be useful. That is why including this product in the LIAR training phase for	We include here Figure MC2.17 showing the relationship of AT and SSS uncertainty. It is indeed well-known that SSS is the dominant driver of A_T and same for their uncertainty. Please refer to our replies to comments **MC1.14.** and **GC.1.3.** for a further analysis.	

TA does not help to obtain the best possible reconstruction.	**Figure MC2.17.** Scatter plot of monthly uncertainty values of a) CMEMS-LSCE A_T (Figure 7) against CMEMS SSS (Figure A10) at four stations. 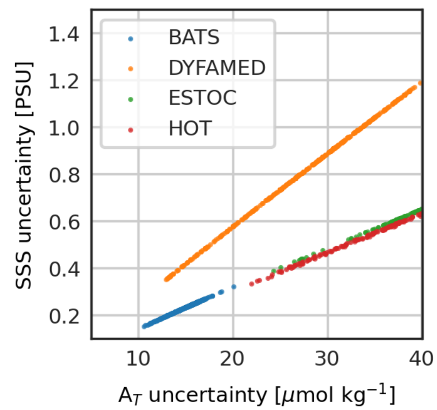 	
MC1.18. Line 527 "*The reconstructed pH time series reproduce measurement variability with relatively high correlation, r2 in [0.21,0.69], that reinforces the reliability of CMEMS-LSCE pH*". It does not seem that the level of correlation obtained with this reconstruction is significant with such low levels of r2. Additionally, the fact that there is no discussion in the article where these levels are compared with other products even if they are only climatic such as those of Takahashi et al. 2014, or others cited in the article for AT and DIC.	Similar to pCO$_2$, measurements of pH are subject to undersampling (see also our reply to comment **MC1.11.**). The data density is even lower for pH (see Figures 8 and A3 and Table A3). Remember that the comparison is between monthly mean estimates of pH and the mean of observations which are normally available within some days to a week. Temporal data sampling bias should be considered as a great source of uncertainty attributed to large model-observation mismatch (and thus moderate values of r^2) even with a finer model spatial resolution. We show that through Table A3 and an analysis is given in the paragraph (Lines 558-576*). Please note that the published data cited by Reviewer 1 are climatology. Strictly speaking, statistical evaluations between the climatological product and in situ observation data (sampled with very low frequency) is not robust (see also our reply to the general comment **GC1.2.**)	*Lines 514-530 in the initial manuscript

MC1.19. Line 576 "Conclusions and Discussion" It should be "Discussion and Conclusions" But on the other hand the discussion is made not in terms of the assessment of the quality of the reconstruction of the product but in terms of the results in terms of ocean acidification.	Thank you for your suggestion. We have changed Section "Conclusions and Discussion" to "Summary" as proposed by **Reviewer 2** (comment **SC2.16.**).	
MC1.20. Line 594 "*In comparison to CMEMS-LSCE at monthly and 1° resolutions (Chau et al., 2022b), the reconstructions over coastal areas are improved at higher resolution (Figs. 2-4).*" This is not demonstrated in the article. The reduction in RMSD between the two products is very small or marginal.	We modify the sentences below (Lines 640-643*) to better summarize our results: "*In comparison to CMEMS-LSCE at monthly and 1◦ resolutions (Chau et al., 2022b), the reconstructions over coastal areas are improved at higher resolution~~ (Figs. 2-4). Furthermore,~~*. *~~t~~The monthly, 0.25◦ reconstruction outperforms its 1◦ counterpart in reproducing horizontal and temporal gradients of $p\mathrm{CO_2}$ over a variety of oceanic regions as well as at nearshore time series stations (Figs. 2-5).*" The improvement in terms of global metrics is marginal but we still gain advantages when increasing model spatial resolution from 1° to 0.25° (e.g. better capturing horizontal and temporal gradients). In this manuscript, we also try to address the question why increasing the spatial resolution by 16-fold does not impressively reduce model-observation discrepancy. Please kindly refer to our reply to comments **MC1.9.** and **MC1.11.** for a comprehensive explanation.	*Lines 594-597 in the initial manuscript
MC1.21. Line 609 Line 609 "The spatial distribution of long-term mean 1σ-uncertainty estimates	The reviewer is correct, but, as discussed in Chau et al (2022b), the ensemble spread is a good proxy for the reconstruction uncertainty.	

(Figs. 1b, 6cd, and 9cd) indicates higher confidence levels for open-ocean estimates than over the coastal sector". This is very unrepresentative of product quality since it represents there producibility of the 100 FFNN but does not evaluate the RMSD between input and reconstructed data.		
MC1.22. Table 7 Both pCO2, AT and DIC quantities should not have decimal places (mean, RMSD).	pCO$_2$, A$_{T,}$ DIC, and their reconstruction errors/uncertainty have been reported with 1-2 decimals in the previous studies (Landschuter et al 2013, 2020; Denvil et al 2019, Gregor et al. 2019, 2021, Chau et al. 2022b). In this revision, we reduce the decimals from 2 to 1 for pCO$_2$, A$_{T,}$ and DIC. The modification has been applied for Tables, Figures, and texts involving these variables.	
MC1.23. Line 655 No comparisons with other reconstructions like MODO-DIC of Keppler et al. 2020, or AT from Broullon et al. 2019 or Lee et al. 2006.	Please see our answer to comments **GC1.2**. and **MC1.15.**	

Replies to comments by Reviewer 2

General comments by Reviewer 2 (GC2)

GC2.1. *The authors reconstructed 0.25-degree monthly full carbonate system variables during the period 1985-2021 based on surface ocean observation data. Distributions of pCO2 were reconstructed based on the machine learning method established by the authors (Trang-Chau et al. 2022) and those of TA were based on the LIAR method (Carter et al. 2016; 2018). While few reconstructions of full carbonate system variables are available at this moment, a comprehensive understanding of global surface ocean pH distributions is essential for monitoring ocean acidification, which is related to the SDG indicator 14.3.1. This study can enhance researches on the global carbon cycle as well as provide critical information to policymakers and stakeholders. I think this study has sufficient value to be published in this journal, but major concerns listed below should be addressed appropriately. I would like to encourage the authors to improve the study and revise the manuscript for better understanding.*

Authors:
We are grateful for **Reviewer 2**'s positive evaluation and constructive comments which help us to improve our manuscript. Please kindly find our replies to address his/her concerns below.

%%%%%%%%%%%%%%%%%%%%%%%%%%%%%%%%%%%

GC2.2. *The concept of this study itself is not novel, and the assessment of uncertainty in the reconstructed fields and the validation of the method become important. The authors derived uncertainty distributions in reconstructed parameters from the spread of 100 model ensemble. They also demonstrated the validity of the method by comparing the result of this study with observation data that were not used for learning and those of time-series points. The time-series used in this study are biasedly located in the subtropical region, so comparing their data with the results of this study does not seem a good indicator of uncertainty. For validation of this method, the authors must take a comparison with other reconstruction(s) into account, if needed.*

Authors:

Further to the reviewer's suggestion, we have added comparisons to 38 time series stations located outside the subtropics (the tropics, the subpolar sector, and the Southern Ocean). The results appear in Figure A1b, Tables A3 and A4. They confirm the reliability of CMEMS-LSCE datasets (see our analysis in Lines 421-447, 488-522, 558-576 in the revised manuscript attached at the end of this document).

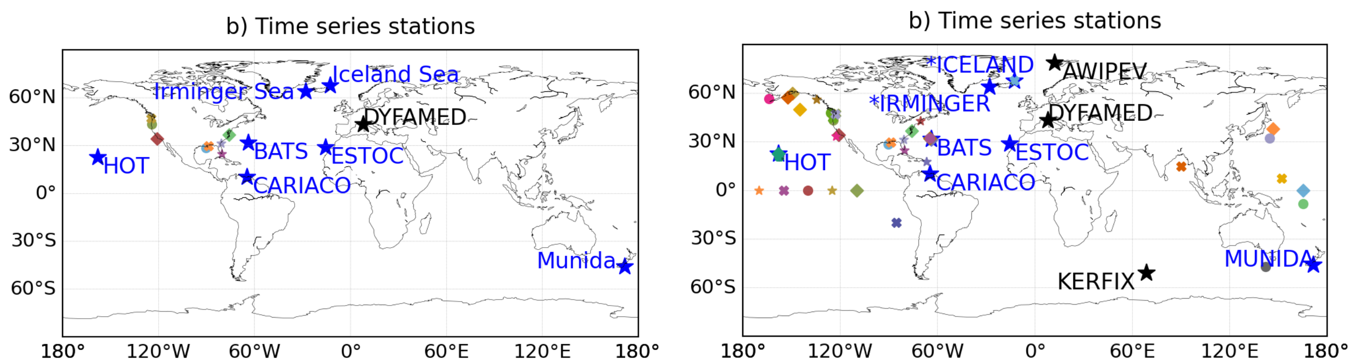

Figure GC2.2. Revised Figure A1b (right): *b) Location of time series stations recording in situ observations used in data evaluation (Table **2**): blue stars* ***for ocean acidification*** *(Bates et al., 2014), black stars* ***for A_T and DIC (Metzl et Lo Monaco, 1998;*** *Coppola et al., 2021;* ***Gattuso et al., 2023****), and other coloured scattered objects* ***for pCO_2 and pH*** *(Sutton et al., 2019)****. Asterisk (*) marks the two stations with A_T and DIC observations (Olafsson et al., 2010) available for assessments.***

Suggestions from the two reviewers about an intercomparison with other products are interesting but would bring us well outside the scope of our study if we take them carefully enough. Such intercomparison between data products deserve proper investigations on (1) the discrepancy in mapping methods, input data resource, and the ratio of training and validation datasets used in model fit, (2) uncertainty from post-processing applied for some products (e.g., filtering, smoothing, calibration), (3) the normalization of different data covering periods, and (4) quality of evaluation (or reference) data; e.g., data paucity should be one major concern to evaluate seasonal cycle reconstructions. For $p\mathrm{CO_2}$, the evaluation of multiple products including CMEMS-LSCE at 1°, monthly resolutions (Chau et al., 2022) was done in the previous studies (Hauck et al., 2020; Gregor et al., 2021; Friedlingstein et al., 2022), and it is well confirmed that the quality of CMEMS-LSCE is in line with the others. This manuscript investigates an upgrade of multi-year reconstructions of $p\mathrm{CO_2}$ and other carbonate system variables by increasing spatial resolution from 1° to 0.25°, that has not been done in the previous studies.

%%%%%%%%%%%%%%%%%%%%%%%%%%%%%%%%

GC2.3. *The authors use external SST and SSS instead of those incorporated in the datasets in the learning process. This seems unusual because the oceanographic condition represented by temperature and salinity considerably affects the ocean biogeochemistry in the observed area. If the authors think the use of external SST/SSS to be essential, they must demonstrate that the impact of differences between external SST/SSS and those in the datasets is negligible.*

Authors:
Our reconstructions require gridded SST and SSS datasets without any gaps, which is not available from SOCAT. We therefore use other data sources**.** Based on statistical assessments, the difference between CMEMS SST and SOCAT SST (or in situ observations) is relatively small (see Figures **GC1.3.** and **MC1.13.** in this document and also Figure A10 in the manuscript). Besides, no quality control has been done for SOCAT salinity. There are some cruises in SOCAT with no salinity data and SOCAT has alternatively used SSS from the World Ocean Atlas (WOA) to recalculate CO_2 fugacity (see Pfeil et al, 2013). We have not changed the method.

%%%%%%%%%%%%%%%%%%%%%%%%%%%%%%%%

GC2.4. *In addition, the manuscript seems to contain unnecessary sentences and be lengthened. Shortening the manuscript will increase readability.*

Authors:
Thank you. We have shortened the manuscript, in particular based on the reviewer's specific comments.

%%%%%%%%%%%%%%%%%%%%%%%%%%%%%%%%

Specific comments by Reviewer 2 (SC2)

Reviewer's comments	Replies from Authors	Notes
SC2.1. Introduction This section seems too long and needs to be shortened.	We have revised the manuscript and removed part of the unnecessary sentences.	
SC2.2. L71 not only "extrapolate" but also "interpolate".	Thank you. "interpolate" was added.	
SC2.3. L91 Table 1 and Appendix A Table 1 only shows six carbonate system variables and is not necessary. Reference to them in the text is enough. In the same context, Appendix A is also unnecessary because it only contains general explanations of carbonate system variables as written in, e.g., Dickson et al. 2007.	We removed both Table 1 and Appendix A.	

SC2.4. L95-131 All or a part of these explanations had better be transferred to the beginning of the "3 Reconstruction method" section.	These lines were modified accordingly.	
SC2.5. L135 Which were used, sea surface height anomaly (SLA) or sea surface dynamic height (SLA+MDT)? Please clarify.	As defined by data providers of CMEMS SSH, we revised the text as follows: "*sea surface height **above geoid***".	
SC2.6. L155 SOCAT's full name was already mentioned in L66.	We replaced the full name with its abbreviation.	
SC2.7. L160-165 Using global 0.25 deg binned data derived from SOCAT cruise data is a usual way, even though using 1 deg binned data does not significantly affect the result.	Using a global 0.25° dataset gridded from SOCAT underway measurements for FFNN model training is indeed our ultimate goal. We have contacted SOCAT experts to investigate further how to grid measurements into 0.25° open-ocean datasets knowing that quality control of measurements is critical.	
SC2.8. L213 It should be clarified how you dealt with longitude and latitude parameters.	To preserve the continuity of longitude at 0°, we have applied the sine and cosine functions to that coordinate. Hence, our global maps of carbonate variables (e.g. Figures 1, 6, 9) do not show discontinuity at the prime meridian. The sine is also used to transform latitude. Data transformation of predictor variables is explicitly presented in a sequence of preceding studies	

	for the CMEMS-LSCE-FFNN model development (Denvil-Sommer et al,. 2021, Chau et al,. 2022). In the first manuscript version, we avoided repeating part of the data processing and model description from the previous studies. As the readers would concern, we have called back this information in the revision (Lines 162-164): "***The sine function is applied to convert latitude while both the sine and cosine are used to transform longitude to conserve their periodical behaviors***."	
SC2.9. Table 4 This table contains RMSDs and coefficients of determination, and the name "skill score" is not appropriate. RMSDs of r025 are not significantly different from those of r100 according to Table 4, and therefore the authors should not emphasize an improvement of the prediction skill. The results only show that a fine-scale reconstruction was achieved with no adverse effect.	We have changed "Skill scores" to "**Evaluation statistics**" in the Table caption. Table 3* shows a marginal improvement from r100 to r025 in terms of global evaluation metrics. For the open ocean, we expect to obtain similar skill scores for both FFNN models as the spatial autocorrelation of open-ocean pCO_2 is estimated within 400±250 km (Jones et al., 2012) and the same SOCAT 1°-open-ocean dataset was used in model fitting. As also reviewed in Chau et al., (2022), pCO_2 over the coastal ocean is characterized with high variability at small scales. For instance, pCO_2 levels can vary with a horizontal gradient as large as 470 µatm over a distance of less than 0.5 km (Chavez et al., 2018; Feely et al., 2008). Statistical models would need a spatial resolution much finer than 0.25° (25 km) and a temporal resolution higher than monthly in order to capture such high variability in surface ocean pCO_2 present in observations (see also Bakker et al., 2016; Laruelle et al., 2017) (see our discussion in Section Summary**). Apart from Table 3*, benefits of increasing the model spatial resolution from 1° to 0.25° are also demonstrated in Figures 2-4 with analyses shown in Lines 414-420***	*Table 4 in the initial manuscript (Table 1 has been removed as suggested by **Review 2**, comment **SC2.2.**) ** Section Conclusion and Discussions in the initial manuscript

	"*The two FFNN reconstructions (r025 and r100) share similarities in overall structures of pCO_2 over the coastal-open-ocean continuum (Figs. 2-4). However, the higher spatial resolution outperforms its lower resolution counterpart in reproducing fine-scale features of pCO_2 in the transition from nearshore regions to the adjacent open ocean. The increase in model spatial resolution translates into a greater spatial coverage of the continental shelves such as Labrador Sea, Northern Europe, and Sea of Japan (Fig. 3), and thus an increase in the number of data over the coastal domain. The increase in spatial resolution allows a gain in prediction probability of pCO_2 variations on the order of roughly 2% over the Eastern Boundary Currents to 8% over the Western South Atlantic (Figs. 2-3b).*" This study also points out temporal data sampling bias as a source of uncertainty that would highly constrain model reconstruction skills. Based on the assessment at station time series (Figure 5 and Table A3), we found that in situ observations have been sampled with low frequency and the bias of sampling date is about a week from a month center. With the low number of observations and high variability of $p$$CO_2$ (20.12 to 69.98 µatm) over these stations, it would not be statistically sufficient to refer to their temporal mean as a representative of monthly averages. A large model-data deviation would be retained even if we increase spatial resolution (see text in Lines 421-447 for further analysis).	***Lines 387-394 in the initial manuscript
SC2.10. Fig 2-4 The results from the two methods, r100 and r025, have almost the same structure. Please explain the reason why the authors focused on the comparison of them.	As expressed in Line 384-393*, the motivation for a comparison between r100 and r025 in Figures 2-4 to show improvements of horizontal gradients in the higher resolution over different oceanic conditions. The three figures respectively present results in:	*Line 358-367 in the previous version

	☐ permanent Eastern Boundary current upwelling systems with relatively high *p*CO_2, ☐ regions characterized by low *p*CO_2 values driven by cold water temperatures and strong biological production, ☐ other regions either under the influence of strong river runoff or monsoon-driven upwelling. It is expected that the two models with different resolutions share the same large-scale structure described above. In Line 413-420** (below), we further analyse the benefits obtained with the higher resolution. "*The two FFNN reconstructions (r025 and r100) share similarities in overall structures of* pCO_2 *over the coastal-open-ocean continuum (Figs. 2-4). However, the higher spatial resolution outperforms its lower resolution counterpart is reproducing fine-scale features of* pCO_2 *in the transition from nearshore regions to the adjacent open ocean. The increase in model spatial resolution translates into a greater spatial coverage of the continental shelves such as Labrador Sea, Northern Europe, and Sea of Japan (Fig. 3), and thus an increase in the number of data over the coastal domain.*"	**Line 387-391 in the previous version
SC2.11. L374 Fig. 3 RMSD for the Sea of Japan is suppressed by using data in the subtropical regions (Tsushima warm current area and Kuroshio area) which generally can be estimated more easily. The RMSD must be calculated from data restricted north of the subtropical front.	Thank you for the comment. However, we should use all the available SOCAT data over the Sea of Japan to evaluate RMSD setting the assessment consistent with the other coastal regions. The evaluation over specific sub-basins can be considered in a regional study of *p*CO_2 variability.	

SC2.12. L403-414 The discrepancy between the estimated and observed pCO2 not only originated from the timescale but also from the method itself. The method cannot express short-term phenomena inherently because it used external SST and SSS instead of those incorporated in the datasets in the learning process.	We agree with the reviewer. As explained above (replies to comments **GC1.3.** and **GC2.3.**), the use of gridded SST and SSS is a necessity for the reconstruction and there is no significant descrepancy between SOCAT (or in situ) data and CMEMS gridded data.	
SC2.13. 5.2 Total alkalinity and dissolved inorganic carbon In the method of this study, discrepancies in estimated and observed DIC were initially derived from pCO2 and TA estimation and propagated via carbonate system calculations. The discussion on uncertainty should be written along with such a concept.	Thank you for this point. We have added the discussion in the revised manuscript (see Lines 471-474*): "*~~The largest model uncertainty~~* ***DIC uncertainty is computed through CO2SYS error propagation with reconstruction uncertainties of pCO_2 and A_T set as inputs. The largest values*** *~~model uncertainty~~ (σ > 30 $\mu mol\ kg^{-1}$)* ***appear*** *~~is computed~~ nearshore and surrounding oceanic islands* ***(Fig. 6d). A similar feature is found on the field of A_T (Fig. 6c)***, *~~a feature~~ inherited from input uncertainty associated with the CMEMS salinity product (Fig. A8a).*"	*Lines 437-438 in the initial manuscript
SC2.14. L467-469 The authors attributed a large σ of DYFAMED estimates to a limited number of observations in the Mediterranean, but GLODAPv2 includes alkalinity measurement data in the Mediterranean. Schneider et al. 2007 successfully derived	There exists indeed a few observations over the surface Mediterranean Sea in GLODAPv2.2022 (Lauvset et al., 2022) used for model evaluation (see f.i. Figure 8 in the manuscript), and even lower data density in GLODAPv2 (Olsen et al., 2016) used for LIAR coefficients fits (Carter et al. 2018). As illustrated in Figure **SC2.14.**, the bias between CMEMS SSS and observations is tiny compared to that of LIAR A_T and observations. The paucity of	

the salinity-alkalinity relationship. The discrepancy in DYFAMED seems to be attributable to salinity discrepancy only.	GLODAPv2 data over the Mediterranean Sea and the distinction in AT-SSS relationship over this region from other basins would lead to a biased LIAR estimate of A_T (-145.1 µmol kg^{-1}). Schneider et al., (2007) derived the estimates of A_T-SSS relationship by using local observations, but the estimated A_T is also subject to a large error range (±114.94 µmol kg^{-1}), see Eq 1 quoted below: $$A_T = 73.7(\pm 3.0) \cdot S - 285.7(\pm 114.94)\mu mol\ kg^{-1}$$ **Figure SC2.14**. Monthly time series of A_T (Figure 7) and SSS (Figure A10) at DYFAMED. 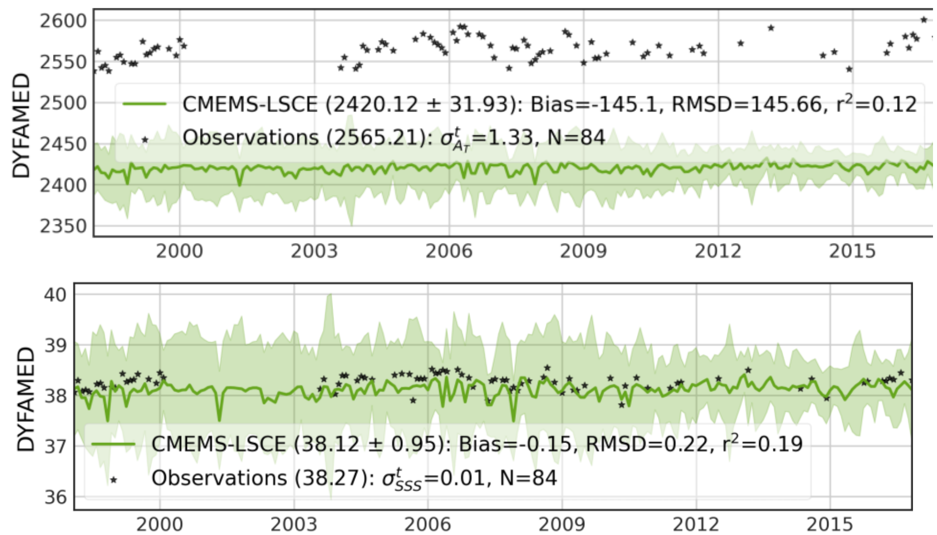 We have added one sentence in Lines 508-510* for clarification. "***Although the bias between reanalysed SSS and observations (Fig. A10) is relatively small (-0.15 µmol kg⁻¹)***, *LIAR (Carter et al., 2018) was trained on GLODAPv2 (Olsen et al., 2016) including* ~~*a*~~ ***only*** *few observations in this area. The distinct relationship between alkalinity and salinity prevailing in*	*Lines 467-469 in the initial manuscript

	the Mediterranean Sea is likely not reproduced by LIAR leading to an underestimation of A_T and a systematic bias to DIC at DYFAMED (Fig. 7)."	
SC2.15. L539-540 I think that SDG indicator 14.3.1, "Average marine acidity (pH) measured at agreed suite of representative sampling stations", is worth mentioning here. Global mean pH based on observation can be a proxy for the indicator. In addition, it is also valuable information that the global mean pH becomes 8.0 with one decimal place, not 8.1 often said.	Thank you. In lines 686-689, we have mentioned the SDG 14.3.1 indicator for ocean acidification. ***"The global maps of CMEMS-LSCE pH, Ω, and their trend estimates would be potential indicators for ocean acidification along with the SDG 14.3.1 - "Average marine acidity (pH) measured at agreed suite of representative sampling stations" (https://sdgs.un.org/goals/goal14: last access 31/07/2023)."*** However, the global mean CMEMS pH over 1985-2022 is about 8.082 (Table 6*). With one decimal, it becomes 8.1, the same value as reported previously.	*Table 7 in the initial manuscript (Table 1 has been removed as suggested by **Review 2**, comment **SC2.2.**)
SC2.16. 6. Conclusion and discussion This section had better be titled "Summary". It does not seem to include discussion.	Thank you. We have modified the section title as suggested.	

Other changes:

- Data repository: the following sentence is added at the end of the Introduction (Lines 136-138) to make data repository visible to the users (details of data access can be found in Section Data availability):
  "***The high-resolution data product described in this manuscript (netCDF format) can be accessed via repository under data DOI: 10.14768/a2f0891b-763a-49e9-af1b-78ed78b16982.***"
- Contribution of GLODAP for this study: we add one sentence in Acknowledgement.
  "***The Global Ocean Data Analysis Project (GLODAP, www.glodap.info, last access: 21 August 2023) provides access to ocean surface-to-bottom quality controlled data of carbonate system variables collected through international cruises.***"
- Typo errors / references: they are corrected / updated in the revised manuscript.

References

1. Bakker, D., Alin, S., Becker, M., Bittig, H., Castaño-Primo, R., Feely, R. A., Gritzalis, T., Kadono, K., Kozyr, A., Lauvset, S. K., Metzl,N., Munro, D., Nakaoka, S.-i., Nojiri, Y., O'Brien, K., Olsen, A., Pfeil, B., Pierrot, D., Steinhoff, T., Sullivan, K., Sutton, A., Sweeney, C., Tilbrook, B., Wada13, C., Wanninkhof, R., Wranne, A. W., et al.: SOCAT version 2022 for quantification of ocean CO2 uptake, https://www.socat.info/wp-content/uploads/2022/06/2022_Poster_SOCATv2022_release.pdf, 2022.
2. Bakker, D. C. E., Pfeil, B., Landa, C. S., Metzl, N., O'Brien, K. M., Olsen, A., Smith, K., Cosca, C., Harasawa, S., Jones, S. D., Nakaoka, S., Nojiri, Y., Schuster, U., Steinhoff, T., Sweeney, C., Takahashi, T., Tilbrook, B., Wada, C., Wanninkhof, R., Alin, S. R., Balestrini, C. F., Barbero, L., Bates, N. R., Bianchi, A. A., Bonou, F., Boutin, J., Bozec, Y., Burger, E. F., Cai, W.-J., Castle, R. D., Chen, L., Chierici, M., Currie, K., Evans, W., Featherstone, C., Feely, R. A., Fransson, A., Goyet, C., Greenwood, N., Gregor, L., Hankin, S., Hardman-Mountford, N. J., Harlay, J., Hauck, J., Hoppema, M., Humphreys, M. P., Hunt, C. W., Huss, B., Ibánhez, J. S. P., Johannessen, T., Keeling, R., Kitidis, V., Körtzinger, A., Kozyr, A., Krasakopoulou, E., Kuwata, A., Landschützer, P., Lauvset, S. K., Lefèvre, N., Lo Monaco, C., Manke, A., Mathis, J. T., Merlivat, L., Millero, F. J., Monteiro, P. M. S., Munro, D. R., Murata, A., Newberger, T., Omar, A. M., Ono, T., Paterson, K., Pearce, D., Pierrot, D., Robbins, L. L., Saito, S., Salisbury, J., Schlitzer, R., Schneider, B., Schweitzer, R., Sieger, R., Skjelvan, I., Sullivan, K. F., Sutherland, S. C., Sutton, A. J., Tadokoro, K., Telszewski, M., Tuma, M., van Heuven, S. M. A. C., Vandemark, D., Ward, B., Watson, A. J., and Xu, S.: A multi-decade record of high-quality f CO2 data in version 3 of the Surface Ocean CO2 Atlas (SOCAT), Earth System Science Data, 8, 383–413, https://doi.org/10.5194/essd-8-383-2016, 2016.
3. Broecker, W. S., & Peng, T. H.:. *Tracers in the Sea* (Vol. 690). Palisades, New York: Lamont-Doherty Geological Observatory, Columbia University, 1982.
4. Broullón, D., Pérez, F. F., Velo, A., Hoppema, M., Olsen, A., Takahashi, T., Key, R. M., Tanhua, T., González-Dávila, M., Jeansson, E., et al.: A global monthly climatology of total alkalinity: a neural network approach, Earth System Science Data, 11, 1109–1127, 2019.
5. Broullón, D., Pérez, F. F., Velo, A., Hoppema, M., Olsen, A., Takahashi, T., Key, R. M., Tanhua, T., Santana-Casiano, J. M., and Kozyr, A.: A global monthly climatology of oceanic total dissolved inorganic carbon: a neural network approach, Earth Syst. Sci. Data, 12, 1725–1743, https://doi.org/10.5194/essd-12-1725-2020, 2020.
6. Carter et al. 2016, Locally interpolated alkalinity regression for global alkalinity estimation, Limnol. Oceanogr. Methods, 14, 268–277, https://doi.org/https://doi.org/10.1002/lom3.10087.
7. Carter et al. 2018, Updated methods for global locally interpolated estimation of alkalinity, pH, and nitrate, Limnology and Oceanography: Methods, 16, 119–131, https://doi.org/https://doi.org/10.1002/lom3.10232, 2018.
8. Chau, T. T. T., Gehlen, M., and Chevallier, F.: A seamless ensemble-based reconstruction of surface ocean pCO2 and air–sea CO2 fluxes over the global coastal and open oceans, Biogeosciences, 19, https://doi.org/10.5194/bg-19-1087-2022.
9. Chavez, F. P., Sevadjian, J., Wahl, C., Friederich, J., and Friederich, G. E.: Measurements of pCO2 and pH from an autonomous surface vehicle in a coastal upwelling system, Deep-Sea Res. Pt. 2, 151, 137–146, https://doi.org/10.1016/j.dsr2.2017.01.001, 2018.
10. Coppola, L., Boutin, J., Gattuso, J.-P., Lefevre, D., and Metzl, N.: The Carbonate System in the Ligurian Sea, chap. 4, pp. 79–103, John Wiley & Sons, Ltd, https://doi.org/https://doi.org/10.1002/9781119706960.ch4, 2020.
11. Coppola, L., Diamond, R. E., and Carval, T.: Dyfamed observatory data. SEANOE [dataset], https://doi.org/0.17882/43749, 2021.
12. Denvil-Sommer, A., Gehlen, M., Vrac, M., and Mejia, C.: LSCE-FFNN-v1: a two-step neural network model for the reconstruction of surface ocean pCO2 over the global ocean, Geoscientific Model Development, 12, 2091–2105, https://doi.org/10.5194/gmd-12-2091-2019, 2019.

13. Dickson et al (Eds.) 2007, Guide to Best Practices for Ocean CO2 Measurements. PICES Special Publication 3, 191 pp.
14. Feely, R. A., Sabine, C. L., Hernandez-Ayon, J. M., Ianson, D., and Hales, B.: Evidence for upwelling of corrosive "acidified" water onto the continental shelf, Science, 320, 1490–1492, https://doi.org/10.1126/science.1155676, 2008.
15. Friedlingstein, P., O'Sullivan, M., Jones, M. W., Andrew, R. M., Gregor, L., Hauck, J., Le Quéré, C., Luijkx, I. T., Olsen, A., Peters, G. P., Peters, W., Pongratz, J., Schwingshackl, C., Sitch, S., Canadell, J. G., Ciais, P., Jackson, R. B., Alin, S. R., Alkama, R., Arneth, A., Arora, V. K., Bates, N. R., Becker, M., Bellouin, N., Bittig, H. C., Bopp, L., Chevallier, F., Chini, L. P., Cronin, M., Evans, W., Falk, S., Feely, R. A., Gasser, T., Gehlen, M., Gkritzalis, T., Gloege, L., Grassi, G., Gruber, N., Gürses, O., Harris, I., Hefner, M., Houghton, R. A., Hurtt, G. C., Iida, Y., Ilyina, T., Jain, A. K., Jersild, A., Kadono, K., Kato, E., Kennedy, D., Klein Goldewijk, K., Knauer, J., Korsbakken, J. I., Landschützer, P., Lefèvre, N., Lindsay, K., Liu, J., Liu, Z., Marland, G., Mayot, N., McGrath, M. J., Metzl, N., Monacci, N. M., Munro, D. R., Nakaoka, S.-I., Niwa, Y., O'Brien, K., Ono, T., Palmer, P. I., Pan, N., Pierrot, D., Pocock, K., Poulter, B., Resplandy, L., Robertson, E., Rödenbeck, C., Rodriguez, C., Rosan, T. M., Schwinger, J., Séférian, R., Shutler, J. D., Skjelvan, I., Steinhoff, T., Sun, Q., Sutton, A. J., Sweeney, C., Takao, S., Tanhua, T., Tans, P. P., Tian, X., Tian, H., Tilbrook, B., Tsujino, H., Tubiello, F., van der Werf, G. R., Walker, A. P., Wanninkhof, R., Whitehead, C., Willstrand Wranne, A., Wright, R., Yuan, W., Yue, C., Yue, X., Zaehle, S., Zeng, J., and Zheng, B.: Global Carbon Budget 2022, Earth System Science Data, 14, 4811–4900, https://doi.org/10.5194/essd-14-4811-2022, 2022.
16. Gattuso, J.-P., Alliouane, S., and Fischer, P.: High-frequency, year-round time series of the carbonate chemistry in a high-Arctic fjord (Svalbard), Earth Syst. Sci. Data, 15, 2809–2825, https://doi.org/10.5194/essd-15-2809-2023, 2023.
17. Gregor, L., Lebehot, A. D., Kok, S., and Scheel Monteiro, P. M.: A comparative assessment of the uncertainties of global surface ocean CO2 estimates using a machine-learning ensemble (CSIR-ML6 version 2019a) – have we hit the wall?, Geoscientific Model Development, 12, 5113–5136, https://doi.org/10.5194/gmd-12-5113-2019, 2019.
18. Gregor, L. and Gruber, N.: OceanSODA-ETHZ: a global gridded data set of the surface ocean carbonate system for seasonal to decadal studies of ocean acidification, Earth System Science Data, 13, 777–808, https://doi.org/10.5194/essd-13-777-2021, 2021.
19. Hauck, J., Zeising, M., Le Quéré, C., Gruber, N., Bakker, D. C. E., Bopp, L., Chau, T. T. T., Gürses, z., Ilyina, T., Landschützer, P., Lenton, A., Resplandy, L., Rödenbeck, C., Schwinger, J., and Séférian, R.: Consistency and Challenges in the Ocean Carbon Sink Estimate for the Global Carbon Budget, Front. Mar. Sci., 7, 852, https://doi.org/10.3389/fmars.2020.571720, 2020.
20. Intergovernmental Oceanographic Commission (2019), Indicator methodology for SDG 14.3.1: Indicator description; Metadata template; Data template; Metadata instructions. Paris, France, Intergovernmental Oceanographic Commission of UNESCO. DOI: http://dx.doi.org/10.25607/OBP-655
21. Iida, Y., Takatani, Y., Kojima, A., and Ishii, M.: Global trends of ocean CO2 sink and ocean acidification: an observation-based reconstruction of surface ocean inorganic carbon variables, Journal of Oceanography, 77, 323–358, 2021.
22. Jones, S., Le Quéré, C., and Rödenbeck, C.: Autocorrelation characteristics of surface ocean pCO2 and air-sea CO2 fluxes, Global biogeo-chemical cycles, 26, 2012.
23. Keppler, L., Landschützer, P., Gruber, N., Lauvset, S. K., & Stemmler, I. (2020). Seasonal carbon dynamics in the near-global ocean. Global Biogeochemical Cycles, 34, e2020GB006571. https://doi.org/10.1029/2020GB006571
24. Landschützer, P., Laruelle, G. G., Roobaert, A., and Regnier, P.: A uniform pCO2 climatology combining open and coastal oceans, Earth System Science Data, 12, 2537–2553, https://doi.org/10.5194/essd-12-2537-2020, 2020.
25. Lauvset, S. K., Lange, N., Tanhua, T., Bittig, H. C., Olsen, A., Kozyr, A., Alin, S., Álvarez, M., Azetsu-Scott, K., Barbero, L., Becker, S., Brown, P. J., Carter, B. R., da Cunha, L. C., Feely, R. A., Hoppema, M., Humphreys, M. P., Ishii, M., Jeansson, E., Jiang, L.-Q., Jones, S. D., Lo Monaco, C., Murata, A., Müller, J.

D., Pérez, F. F.References, Pfeil, B., Schirnick, C., Steinfeldt, R., Suzuki, T., Tilbrook, B., Ulfsbo, A., Velo, A., Woosley, R. J., and Key, R. M.: GLODAPv2.2022: the latest version of the global interior ocean biogeochemical data product, Earth System Science Data, 14, 5543–5572, https://doi.org/10.5194/essd-14-5543-2022, 2022.

26. Lauvset, S. K., Key, R. M., Olsen, A., van Heuven, S., Velo, A., Lin, X., Schirnick, C., Kozyr, A., Tanhua, T., Hoppema, M., Jutterström, S., Steinfeldt, R., Jeansson, E., Ishii, M., Perez, F. F., Suzuki, T., and Watelet, S.: A new global interior ocean mapped climatology: the 1° × 1° GLODAP version 2, Earth Syst. Sci. Data, 8, 325–340, https://doi.org/10.5194/essd-8-325-2016, 2016.
27. Laruelle, G. G., Landschützer, P., Gruber, N., Tison, J.-L., Delille, B., and Regnier, P.: Global high-resolution monthly pCO2 climatology for the coastal ocean derived from neural network interpolation, Biogeosciences, 14, 4545–4561, 2017.
28. Lee, K., Tong, L. T., Millero, F. J., Sabine, C. L., Dickson, A. G., Goyet, C., Park, G.-H., Wanninkhof, R., Feely, R. A., and Key, R. M.: Global relationships of total alkalinity with salinity and temperature in surface waters of the world's oceans, Geophysical research letters, 33, 2006.
29. Metzl, N. and Lo Monaco, C.: OISO - Ocean Indien Service d'Observation [dataset], https://doi.org/10.18142/228, 1998.
30. Millero, F. J., Lee, K., & Roche, M.:. Distribution of alkalinity in the surface waters of the major oceans. *Marine Chemistry*, *60*(1-2), 111-130, 1998.
31. Olsen, A., Key, R. M., Van Heuven, S., Lauvset, S. K., Velo, A., Lin, X., Schirnick, C., Kozyr, A., Tanhua, T., Hoppema, M., et al.: The Global Ocean Data Analysis Project version 2 (GLODAPv2)–an internally consistent data product for the world ocean, Earth System Science Data, 8, 297–323, 2016.
32. Olafsson, J., Olafsdottir, S., Benoit-Cattin, A., and Takahashi, T.: The Irminger Sea and the Iceland Sea time series measurements of sea water carbon and nutrient chemistry 1983–2008, Earth System Science Data, 2, 99–104, 2010.
33. Pfeil, B., Olsen, A., Bakker, D. C., Hankin, S., Koyuk, H., Kozyr, A., Malczyk, J., Manke, A., Metzl, N., Sabine, C. L., et al.: A uniform, quality–controlled Surface Ocean CO2 Atlas (SOCAT), Earth System Science Data, 5, 125–143, 2013.
34. Rödenbeck, C., Keeling, R. F., Bakker, D. C., Metzl, N., Olsen, A., Sabine, C., and Heimann, M.: Global surface-ocean pCO2 and sea–air CO2 flux variability from an observation-driven ocean mixed-layer scheme, Ocean Science, 9, 193–216, 2013.
35. Sabine, C. L., Hankin, S., Koyuk, H., Bakker, D. C. E., Pfeil, B., Olsen, A., Metzl, N., Kozyr, A., Fassbender, A., Manke, A., Malczyk, J., Akl, J., Alin, S. R., Bellerby, R. G. J., Borges, A., Boutin, J., Brown, P. J., Cai, W.-J., Chavez, F. P., Chen, A., Cosca, C., Feely, R. A., González-Dávila, M., Goyet, C., Hardman-Mountford, N., Heinze, C., Hoppema, M., Hunt, C. W., Hydes, D., Ishii, M., Johannessen, T., Key, R. M., Körtzinger, A., Landschützer, P., Lauvset, S. K., Lefèvre, N., Lenton, A., Lourantou, A., Merlivat, L., Midorikawa, T., Mintrop, L., Miyazaki, C., Murata, A., Nakadate, A., Nakano, Y., Nakaoka, S., Nojiri, Y., Omar, A. M., Padin, X. A., Park, G.-H., Paterson, K., Perez, F. F., Pierrot, D., Poisson, A., Ríos, A. F., Salisbury, J., Santana-Casiano, J. M., Sarma, V. V. S. S., Schlitzer, R., Schneider, B., Schuster, U., Sieger, R., Skjelvan, I., Steinhoff, T., Suzuki, T., Takahashi, T., Tedesco, K., Telszewski, M., Thomas, H., Tilbrook, B., Vandemark, D., Veness, T., Watson, A. J., Weiss, R., Wong, C. S., and Yoshikawa-Inoue, H.: Surface Ocean CO2 Atlas (SOCAT) gridded data products, Earth Syst. Sci. Data, 5, 145–153, https://doi.org/10.5194/essd-5-145-2013, 2013.
36. Schneider et al. 2007, Alkalinity of the Mediterranean Sea, Geophys. Res. Lett., 34, L15608, doi:10.1029/2006GL028842.
37. Sutton, A. J., Feely, R. A., Maenner-Jones, S., Musielwicz, S., Osborne, J., Dietrich, C., Monacci, N., Cross, J., Bott, R., Kozyr, A., et al.: Autonomous seawater pCO2 and pH time series from 40 surface buoys and the emergence of anthropogenic trends, Earth System Science Data, 11, 421–439, 2019.

CMEMS-LSCE: A global 0.25-degree, monthly reconstruction of the surface ocean carbonate system

Thi-Tuyet-Trang Chau[1], Marion Gehlen[1], Nicolas Metzl[2], and Frédéric Chevallier[1]

[1]Laboratoire des Sciences du Climat et de l'Environnement, LSCE/IPSL, CEA-CNRS-UVSQ, Université Paris-Saclay, F-91191 Gif-sur-Yvette, France

[2]Laboratoire LOCEAN (IPSL), Sorbonne Université, CNRS–IRD–MNHN, Paris, F-75005, France

Correspondence: Thi-Tuyet-Trang CHAU (trang.chau@lsce.ipsl.fr, thi.tuyet.trang.chau@gmail.com)

Abstract. Observation-based data reconstructions of global surface ocean carbonate system variables play an essential role in monitoring the recent status of ocean carbon uptake and ocean acidification as well as their impacts on marine organisms and ecosystems. So far ongoing efforts are directed towards exploring new approaches to describe the complete marine carbonate system and to better recover its fine-scale features. In this respect, our research activities within the Copernicus Marine Environment Monitoring Service (CMEMS) aim at developing a sustainable production chain of observation-derived global ocean carbonate system datasets at high space-time resolution. As the start of the long-term objective, this study introduces a new global $0.25°$ monthly reconstruction, namely CMEMS-LSCE, for the period 1985-2021. The CMEMS-LSCE reconstruction derives datasets of six carbonate system variables including surface ocean partial pressure of CO_2 ($p$$CO_2$), total alkalinity ($A_T$), total dissolved inorganic carbon (DIC), surface ocean pH, and saturation states with respect to aragonite (Ω_{ar}) and calcite (Ω_{ca}). Reconstructing $p$$CO_2$ relies on an ensemble of neural network models mapping gridded observation-based data provided by the Surface Ocean CO_2 ATlas (SOCAT). Surface ocean A_T is estimated with a multiple linear regression approach, and the remaining carbonate variables are resolved by CO_2 system speciation given the reconstructed $p$$CO_2$ and A_T. 1σ-uncertainty associated with these estimates is also provided. Here, σ stands for either ensemble standard deviation of $p$$CO_2$ estimates or total uncertainty for each of the five other variables propagated through the processing chain with input data uncertainty. We demonstrate that the $0.25°$-resolution $p$$CO_2$ product outperforms a coarser spatial resolution ($1°$) thanks to a higher data coverage nearshore and a better description of horizontal and temporal variations in $p$$CO_2$ across diverse ocean basins, particularly in the coastal-open-ocean continuum. Product qualification with observation-based data confirms reliable reconstructions with root-of-mean–square–deviation from observations less than 8%, 4%, and 1% relative to the global mean of $p$$CO_2$, A_T (DIC), and pH. The global average 1σ-uncertainty is below 5% and 8% for $p$$CO_2$ and Ω_{ar} (Ω_{ca}), 2% for A_T and DIC, and 0.4% for pH relative to their global mean values. Both model-observation misfit and model uncertainty indicate that coastal data reproduction still needs further improvement, wherein high temporal and horizontal gradients of carbonate variables and representative uncertainty from data sampling would be taken into account in priority. This study also presents a potential use case of the CMEMS-LSCE carbonate data product in tracking the recent state of ocean acidification.

1 Introduction

Between 1750 and 2019, the ocean took up an estimated 25% (or 170 ± 20 PgC) of total cumulated anthropogenic CO_2 (685 ± 75 PgC) emitted to the atmosphere (IPCC AR6 - the Sixth Assessment Report of the United Nations Intergovernmental Panel on Climate Change, Canadell et al., 2021). While the uptake of anthropogenic CO_2 mitigates global warming it also profoundly modifies seawater chemistry in a suite of well-understood reactions (Orr et al., 2005) leading to an increase in hydrogen ion concentration ($[H^+]$), as well as a decrease in carbonate ion concentration ($[CO_3^{2-}]$) and in the saturation state of seawater (Ω) with respect to calcium carbonate minerals ($CaCO_3$). The increase in hydrogen ion concentration ($[H^+]$) is commonly reported as a decrease in pH (pH = - $\log[H^+]$) and referred to as ocean acidification.

Changes in carbonate chemistry impact calcifying plankton and benthos as a direct result of decreasing seawater saturation state with respect to $CaCO_3$ (Fabry et al., 2008; Thomsen et al., 2015). Ocean acidification also modifies the production of marine trace gases exchanged at the air-sea interface (Hopkins et al., 2020), the availability of nutrients fueling primary production (Doney et al., 2009), as well as the speciation of pollutants (Millero et al., 2009; Hoffmann et al., 2012). These chemical changes interact with warming and ocean deoxygenation to drive major changes in marine ecosystems (Doney et al., 2020) and to alter global biogeochemical cycles with the potential for feeding back on radiative forcing (Gehlen et al., 2011; Hopkins et al., 2020). The likelihood for major disruptive impacts of ocean acidification on marine ecosystems, if future CO_2 emissions were to go unabated, is reflected by the Sustainable Development Goal 14.3 (SDG 14.3) - "Reduce Ocean Acidification: minimize and address impacts of ocean acidification" (https://www.globalgoals.org/14-life-below-water, last access: 20/03/2023). Albeit not specifically mentioned, moving towards SDG 14.3 implies the understanding of historical and contemporary carbonate chemistry, its mean state, trends and variability.

~~Earth system models have been widely used to track changes in ocean pH over the historical period and to project its future evolution under different CO_2 emission pathways (Bopp et al., 2013; Gattuso et al., 2015; Kwiatkowski et al., 2020; Cooley et al., 2022; Ji . The present-day global surface ocean pH is roughly 0.1 pH units less than at the beginning of the industrial era (Gattuso et al., 2015; Jiang e corresponding to an increase in hydrogen ion concentration of 26% (Doney, 2010). By the end of the 21^{st} century, the pH is projected to decrease by 0.16 ± 0.002 pH units in response to the IPCC AR6 low emission scenario (SSP1-2.6), respectively by 0.44 ± 0.005 pH units in response to the IPCC AR6 high emission pathway (SSP5-8.5) relative to 1870–1899 (Kwiatkowski et al., 2020). Understanding impacts on marine biota requires to move towards finer spatial and temporal scales than resolved by the current generation of Earth system models (Torres et al., 2021), as well as to expand the analysis from pH to other carbonate system variables such as the saturation state with respect to calcium carbonate minerals and the buffer capacity. The development and implementation of environmental management strategies equally rely on understanding and attributing the variability of the carbonate system from diurnal to decadal time scales to underlying physical-chemical-biological processes.~~

In situ time series have played an important role in monitoring ocean acidification over the last decades (Bates et al., 2014; Lauvset et al., 2015; Sutton et al., 2019; Pérez et al., 2021; Leseurre et al., 2022; Skjelvan et al., 2022). At these sites, seawater pH (Ω) has been either directly measured or calculated from measurements of other carbonate system variables. These variables include surface ocean partial pressure of CO_2 ($p$$CO_2$), total alkalinity ($A_T$), and dissolved inorganic carbon (DIC). While changes in time series of carbonate system variables well reflect impacts of enhanced anthropogenic CO_2 uptake on ocean chemistry at a local scale (Steinberg et al., 2001; González-Dávila and Santana-Casiano, 2009; Dore et al., 2009; Bates et al., 2014; Pérez et al., 2021), the reliable upscaling to large ocean regions or entire basins requires a significant extension of the existing observing network (Lauvset et al., 2015; Bakker et al., 2016; Sutton et al., 2019; Lauvset et al., 2022a).

Time series data are completed by bottle data from international cruises. These data are synthesized by the Global Ocean Data Analysis Project v2.2022 (GLODAPv2.2022) and include about 1.4 million measurements of surface-to-interior ocean pH, A_T, DIC, and other parameters ~~(Lauvset et al., 2022a, https://www.glodap.info/, last access: 30/9/2022)~~(Lauvset et al., 2022b, https://www.gl . Likewise, underway measurements of near-surface CO_2 fugacity, i.e., $p$$CO_2$ corrected for non-ideal gas behavior, are compiled in the Surface Ocean CO_2 Atlas (SOCAT) since its first release in 2011 (Pfeil et al., 2013). That latest version SOCATv2022 yields approximately 33.7 million high-quality controlled data (Bakker et al., 2022, http://www.socat.info/, last access: 17/6/2022). Despite millions of observations available, data coverage is still modest, e.g., CO_2 fugacity samples over the global ocean cover less than 2% of its surface for each month in the last three decades (Bakker et al., 2016; Hauck et al., 2020). Mapping methods have thus become an essential tool in ocean carbon cycle research allowing to interpolate or extrapolate these sparse measurements into space-time varying fields of carbonate system variables~~(e.g., Rödenbeck et al., 2015) and used for global carbon budget estimates (Friedlingstein et al., 2022).~~ .

Recent years have seen the rapid development of machine learning approaches to map global surface ocean $p$$CO_2$ (see Rödenbeck et al., 2013; Landschützer et al., 2016; Denvil-Sommer et al., 2019; Gregor et al., 2019; Chau et al., 2022b, for instance). Thanks to these efforts, the carbon cycle community can now draw on an ensemble of reconstructions for the observation-based assessment of the ocean carbon sink (Friedlingstein et al., 2022). However, only a few global observation-based reconstructions are available for pH, A_T, DIC, and Ω with respect to calcite and aragonite (see Gregor and Gruber, 2021, for a review). The reconstruction of global distributions of these variables is hampered by an insufficient amount of direct measurements (Bakker et al., 2016; Lauvset et al., 2022a). Alternatively, the complete carbonate system can be obtained by speciation given the information of any couple of $p$$CO_2$, pH, A_T or DIC together with chemical (e.g., phosphate, silicate, nitrate) and physical variables (e.g., temperature, salinity), as well as corresponding dissociation constants (Park, 1969; Lewis and Wallace, 1998; Dickson et al., 2007).

Regardless of the developments in different observation-based estimation methods, Takahashi et al. (2014), Iida et al. (2021), and Gregor and Gruber (2021) propose global climatologies or monthly varying fields of all variables of the carbonate system, i.e., $p$$CO_2$, pH, A_T, DIC, and Ω. These data products have a spatial resolution of $1°$ ($\sim 100\mathrm{km} \times 100\mathrm{km}$) or even coarser. Nevertheless, the variations of carbonate system variables over the coastal regions where their instantaneous gradients are driven by smaller-scale features like ocean upwelling, wind turbulence, eddies, water runoff, and sharp biological productivity (Jones et al., 2012; Bakker et al., 2016; Laruelle et al., 2017) are poorly described at such spatial resolutions. Here we improve on existing studies by providing a global $0.25°$, monthly observation-based ~~surface ocean carbonate system~~ product consisting of datasets of six core surface ocean carbonate system variables of the marine carbonate system ~~(see Table 1 and Appendix A for definitions)~~ and their associated 1σ-uncertainty. This high-resolution data product covers the years from 1985 to 2021.

Laboratoire des Sciences du Climat et de l'Environnement (LSCE) is in charge of the product within the European Copernicus Marine Environment Monitoring Service (CMEMS). Our product is referred to as CMEMS-LSCE hereafter.

The reconstruction of surface ocean carbonate system variables starts with the reconstruction of surface ocean $p\mathrm{CO_2}$ and $\mathrm{A_T}$ in each regular grid of $1\mathrm{month} \times 0.25° \times 0.25°$ in the period 1985-2021 (444 months in total). Next, variables pH, DIC, and Ω are derived by speciation. Advantages of the combination of $p\mathrm{CO_2}$ and $\mathrm{A_T}$ over others for the speciation of the carbonate system are: (1) $p\mathrm{CO_2}$ is the most extensively measured parameter, (2) $\mathrm{A_T}$ can be accurately predicted from salinity, temperature, and nutrient concentrations, and (3) the combination of these two prior variables results in the slightest uncertainty of pH estimates (Zeebe and Wolf-Gladrow, 2001; Lauvset and Gruber, 2014; Takahashi et al., 2014; Orr et al., 2018). The three main successive modules used in the CMEMS-LSCE production chain are summarized as follows.

Table 1. ~~CMEMS-LSCE carbonate system variables.~~

~~Standard names~~	~~Notations~~	~~Units~~
~~1. Partial pressure of CO_2 in surface seawater~~	~~$p\mathrm{CO_2}$~~	~~µatm~~
~~2. Total alkalinity in surface seawater~~	~~$\mathrm{A_T}$~~	~~µmol kg^{-1}~~
~~3. Surface ocean dissolved inorganic carbon~~	~~DIC~~	~~µmol kg^{-1}~~
~~4. Surface seawater pH reported on total scale~~	~~pH~~	-
~~5. Saturation state for surface seawater with respect to aragonite~~	~~Ω_{ar}~~	-
~~6. Saturation state for surface seawater with respect to calcite~~	~~Ω_{ca}~~	-

i) *Reconstruction of pCO_2* (Sect. 3.1): ~~a modified version of~~ the CMEMS-LSCE-FFNN ensemble-based approach (Chau et al., 2022b) is ~~applied~~ modified to map gridded datasets of SOCATv2022 CO_2 fugacity and predictors in order to reconstruct $p\mathrm{CO_2}$ at a ~~spatial~~ finer spatial scale resolution of $0.25°$ for every month in the period 1985-2021 (444 months in total). The ~~CMEMS-LSCE-FFNN works on an ensemble of 100~~ spatial resolution of new feed-forward neural networks (FFNNs) is 16-fold higher than the original. By design, ~~100-member ensemble model outputs allow~~ the ensemble of model outputs allows to yield the best model estimate (i.e., ensemble mean) and model uncertainty (i.e., ensemble standard deviation) ~~for surface ocean $p\mathrm{CO_2}$ in each grid~~ at each $0.25°$-grid cell and each month. ~~The primary modification of this study's version and the original CMEMS-LSCE-FFNN (Chau et al., 2022b) is an increase of 16-fold in model spatial resolution.~~ Global monthly reconstructions of $p\mathrm{CO_2}$ proposed by this study complement the previous climatological product by Landschützer et al. (2020), i.e., a combination of the two existing datasets covering respectively the open ocean at $1°$ (Landschützer et al., 2016) and the coastal sector at $0.25°$ (Laruelle et al., 2017).

ii) *Reconstruction of A_T* (Sect. 3.2): locally interpolated alkalinity regression (LIAR; Carter et al., 2016, 2018) is chosen to estimate ~~total alkalinity on regular grids of $1\mathrm{month} \times 0.25° \times 0.25°$~~ monthly total alkalinity over the global surface ocean~~for the years 1985-2021. LIAR works with multiple linear regression models, each representing a combination of predictor variables. The best linear model, which has the lowest prediction error among the others, is retained for the final estimation of $\mathrm{A_T}$~~. Various reconstruction methods for $\mathrm{A_T}$ exist (see Carter et al., 2016; Broullón et al., 2019; Gregor and Gruber, 2021, for a review), but we choose LIAR due to its global applicability, simplicity in setting, and accuracy compared to other published approaches (Carter et al., 2018; Gregor and Gruber, 2021). Importantly, LIAR allows determining reconstruction uncertainty propagated from multiple sources of input uncertainties at desired model resolutions.

iii) *Reconstruction of pH, DIC, and saturation states with respect to aragonite* (Ω_{ar}) and calcite (Ω_{ca}) (Sect. 3.3): CO2SYS (Lewis and Wallace, 1998; Van Heuven et al., 2011) is a standard software used for the speciation of carbonate parameters in the marine CO_2 system (see Olsen et al., 2016; Bresnahan et al., 2021; Gregor and Gruber, 2021; Woosley, 2021, for a few). ~~The CO2SYS speciation is built on a set of equilibrium equations (Dickson et al., 2007; Dickson, 2010). Given the reconstructed pCO$_2$ and A$_T$, non-CO$_2$ acid-base constituents, physical variables, and equilibrium constants, this method allows solving pH, DIC, Ω_{ar}, and Ω_{ca} at the same input resolutions.~~ A complementary of the CO2SYS software developed by Orr et al. (2018) is used to quantify the uncertainty associated with these carbonate system variables. All the input data uncertainties are propagated through the CO2SYS processing chain.

The global monthly, 0.25°-resolution datasets of ~~pCO$_2$, A$_T$, pH, DIC, Ω_{ar}, and Ω_{ca}~~ surface carbonate variables are intensively evaluated against different observation-based products independent from our model fitting at a global scale to in situ locations~~(Table 2)~~. In Section 4, multiple metrics are proposed for product ~~analyzes~~ analyses and assessments. Results are presented in section 5 with emphasis on the evaluation of the best reconstruction and associated model uncertainty for each variable (Sect. 5). This section also highlights the advantages obtained with an increase in spatial resolution and presents an application of the CMEMS-LSCE product in tracking ocean acidification over the last three decades. Section 6 summarizes key results, discusses the potential for future model upgrades, and introduces possible product use cases. The high-resolution data product described in this manuscript (netCDF format) can be accessed via repository under data DOI: 10.14768/a2f0891b-763a-49e9-af1b-78ed78b16982.

2 Data used and reprocessing

2.1 Input data products for surface ocean carbonate system reconstructions

Many observation-based products are used as predictors of our target carbonate system variables (Table 1). Global ocean maps of sea surface temperature (SST), sea surface salinity (SSS), ~~height~~ sea surface height above geoid (SSH), chlorophyll-*a* (Chl-*a*) come from the Copernicus Marine Environment Monitoring Service (CMEMS: Good et al., 2020; Nardelli et al., 2016; Droghei et al., 2018; Maritorena et al., 2010). Mixed layer depth (MLD) fields belong to Estimating the Circulation and Climate of the Ocean project Phase II (ECCO2, Menemenlis et al., 2008). CO_2 mole fractions (xCO$_2$) are derived from the CO_2 atmospheric inversion of the Copernicus Atmosphere Monitoring Service (CAMS, Chevallier et al., 2005, 2010; Chevallier, 2013). Surface ocean concentrations of nitrate (NO_3), silicate (SiO_2), and phosphate (PO_4) are extracted from the World Ocean Atlas 2018 (WOA18, Garcia et al., 2019). The climatological pCO$_2$ ($p\mathrm{CO}_2^{clim}$) product is provided by Lamont Doherty Earth Observatory (LDEO, Takahashi et al., 2009). Details of these products including resource access, data coverage, and resolutions are presented in Table 1.

Table 1. Input data used in the reconstructions of CMEMS-LSCE carbonate system variables over the global ocean in 1985-2021.

Variables	Notations	Units	Products	Resolutions	References
1. CO_2 fugacity	$f\mathrm{CO_2}$	$\mu\mathrm{atm}$	Surface Ocean CO_2 Atlas version 2022 (SOCATv2022, 1985-2021)	monthly, $1°$ (open ocean) and $0.25°$ (coastal ocean)	Bakker et al. (2022)
2. Sea surface temperature	SST	$°\mathrm{C}$	CMEMS SST_GLO_SST_L4_REP_OBSERVATIONS_010_011 and SST_GLO_SST_L4_NRT_OBSERVATIONS_010_001 (1985-2021)	daily, $0.05°$	Good et al. (2020)
3. Sea surface salinity	SSS	PSU	CMEMS MULTIOBS_GLO_PHY_S_SURFACE_MYNRT_015_013 (1993-2021)	monthly, $0.25°$	Nardelli et al. (2016); Droghei et al. (2018)
4. Sea surface height	SSH	m	CMEMS SEALEVEL_GLO_PHY_L4_MY_008_047 and SEALEVEL_GLO_PHY_L4_NRT_OBSERVATIONS_008_046 (1993-2021)	daily, $0.25°$	CLS-TOULOUSE
5. Mixed layer depth	MLD	m	Estimating the Circulation and Climate of the Ocean project Phase II (ECCO2, 1992-2021)	daily, $0.25°$	Menemenlis et al. (2008)
6. Chlorophyll-*a*	CHL-*a*	$\mathrm{mg\,m^{-3}}$	CMEMS OCEANCOLOUR_GLO_CHL_L4_REP_OBSERVATIONS_009_082 and OCEANCOLOUR_GLO_CHL_L4_NRT_OBSERVATIONS_009_033 (1998-2021)	daily, $0.25°$	GLOCOLOUR, Maritorena et al. (2010)
7. CO_2 mole fraction	$x\mathrm{CO_2}$	ppm	CO_2 atmospheric inversion from the Copernicus Atmosphere Monitoring Service (CAMS, 1985-2021)	3-hourly, $1.9° \times 3.75°$	Chevallier et al. (2005, 2010); Chevallier (2013)
8. $p\mathrm{CO_2}$ climatology	$p\mathrm{CO_2^{clim}}$	$\mu\mathrm{atm}$	Lamont Doherty Earth Observatory (LDEO, climatology)	monthly, $4° \times 5°$	Takahashi et al. (2009)
9. Nitrate 10. Silicate 11. Phosphate	NO_3 SiO_2 PO_4	$\mu\mathrm{mol\,kg^{-1}}$	World Ocean Atlas 2018 (WOA18, climatologies)	monthly, $1°$	Garcia et al. (2019)

* Last access was on 15/4/2022 for all input databases except for SOCATv2022 data (17/6/2022) and WOA18 data (30/7/2022).

** Data products 1-8 are used in the $p\mathrm{CO_2}$ reconstruction. Products 2-3 and 9-11 are used to compute A_T, DIC, pH, Ω_{ar}, and Ω_{ca}.

*** Global values of product uncertainty (data† or analysis errors expressed as σ) have been reported for $f\mathrm{CO_2^\dagger}$ ($< 5\ \mu\mathrm{atm}$), SST ($0.15\ °\mathrm{C}$), SSS (0.2 PSU), SSH (0.02 m), MLD (-), CHL-*a* ($0.03\mathrm{mg\,m^{-3}}$), $x\mathrm{CO_2}$ (-), $p\mathrm{CO_2^{clim}}$ ($10\ \mu\mathrm{atm}$), NO_3 ($1.8\ \mu\mathrm{mol\,kg^{-1}}$), SiO_2 ($3.6\ \mu\mathrm{mol\,kg^{-1}}$), PO_4 ($0.12\ \mu\mathrm{mol\,kg^{-1}}$).

With the exception of $x\mathrm{CO_2}$, nutrient concentrations, and $p\mathrm{CO_2^{clim}}$, these input data products have original resolutions equivalent to or even finer than a spatial resolution of $0.25°$ and a temporal resolution of monthly. When mismatches in data resolutions appear, input data products are interpolated to fit the pre-defined model resolutions. The datasets of SST and $x\mathrm{CO_2}$ - the two key variables driving global $p\mathrm{CO_2}$ changes (Bates et al., 2014; Gruber et al., 2019; Landschützer et al., 2019; Chau et al., 2022b; Friedlingstein et al., 2022) - cover the full learning period and the whole globe as expected. The other predictor data are not available before the 1990s, when new types of satellite measurements started, and one of them (i.e., Chl-*a*) does not cover the high latitudes of the winter hemisphere. We therefore gap-fill the time series in an ad hoc manner, as in previous studies (Landschützer et al., 2016; Gregor et al., 2019; Chau et al., 2022b). Monthly climatologies of SSS, Chl-*a*, and MLD computed on the available data are used for each missing year. Likewise, climatologies plus linear trends of SSH following global warming effects serve for the pre-1993 period. Missing Chl-*a* data in the high latitudes of the winter hemisphere are replaced by the minimum concentration of Chl-*a* over the available data for the same grid cell ($\sim$0.01 $\mathrm{mg\,m^{-3}}$). WOA18 nutrients and LDEO $p\mathrm{CO_2^{clim}}$ are already climatolgies per se and we apply them for all the analysis years 1985-2021. The sine function is applied to convert latitude while both the sine and cosine are used to transform longitude to conserve their periodical behaviors.

CO_2 fugacity from ~~Surface Ocean CO_2 ATlas version 2022 (SOCATv2022, Bakker et al., 2022)~~ SOCATv2022 (Bakker et al., 2022) is used as the target data in our monthly $p\mathrm{CO_2}$ reconstructions. The SOCAT project collects and qualifies underway observations via international vessels, moorings, or autonomous platforms. It grids the observations at spatial resolutions of 1° or 0.25° resulting in the two major SOCAT gridded data products. The temporal resolution of these two products is monthly. While the 1°-data product (SOCATv2022r100) covers the global ocean, the 0.25° covers solely the coastal regions. The SOCAT coastal areas is within 400 km from the shoreline (Sabine et al., 2013; Bakker et al., 2016); see Fig. A1a for an illustration. To merge the two resolutions, we first duplicate the 1°-open-ocean SOCATv2022 data ($\sim 2 \times 10^5$ data points) over its sixteen 0.25° sub-cells. This 0.25°-open-ocean data are then combined with the 0.25°-coastal-ocean SOCATv2022 data ($\sim 4 \times 10^5$ data points) to generate a global monthly 0.25° ocean data product fed to our reconstruction model of $p\mathrm{CO_2}$ (Sect. 3.1). The merged SOCATv2022 product at monthly, 0.25° resolutions is referred to as SOCATv2022r025 hereafter. The assumption of open-ocean data homogeneity of $p\mathrm{CO_2}$ within 1°-grid boxes ($\sim 100\ \mathrm{km} \times 100\ \mathrm{km}$) does not degrade the reconstruction skill over the global open ocean (see Sect. 5 for results) where $p\mathrm{CO_2}$ observations are spatially auto-correlated within a global median distance of $400 \pm 250\ \mathrm{km}$ (Jones et al., 2012). The data distribution of SOCATv2022 CO_2 fugacity before and after combining is shown in Fig. A2 and Table 3.

2.2 Product qualification and comparison

The monthly, 0.25°-resolution reconstructions of carbonate system variables are qualified with gridded observation-based datasets and in-situ time series which are not used in our model fitting (Table 2).

- The SOCAT data in each reconstruction month are excluded from the model fitting, which avoids overfitting and ensures fairness in the model evaluation (Chau et al., 2022b). The global monthly, 0.25°-resolution CMEMS-LSCE-FFNN $p\mathrm{CO_2}$ fields ~~at a spatial resolution of 0.25°~~ can therefore be evaluated against the $p\mathrm{CO_2}$ data converted from SOCATv2022 CO_2 fugacity ~~(Eq. A2)~~ (Körtzinger, 1999) at the same resolution. Doing this, CMEMS-LSCE-FFNN $p\mathrm{CO_2}$ is assessed with more than 32×10^5 open-ocean data and 4×10^5 coastal-ocean data (Table 3). The SOCATv2022 ~~measurements~~ data have low random uncertainty (2-5 $\mathrm{\mu atm}$) but the spatio-temporal sampling bias from the month and grid centers is significant (Bakker et al., 2016). The 0.25°-data reconstruction is also compared to its previous version with a spatial resolution of 1° (Chau et al., 2022a, b).

- The monthly, 0.25° reconstructions of $\mathrm{A_T}$, DIC, and $p\mathrm{H}$ are qualified based on ~~Global Ocean Data Analysis Project bottle data version 2.2022 (GLODAPv2.2022, Lauvset et al., 2022a)~~GLODAPv2.2022 data (Lauvset et al., 2022b). GLODAP provides non-gridded datasets of ocean carbon variables which have been compiled and bias-corrected from water samples taken at various depths. The measurement uncertainty is $4\ \mathrm{\mu mol\,kg^{-1}}$ in $\mathrm{A_T}$ and DIC and between $0.01 - 0.02$ in $p\mathrm{H}$ (Lauvset et al., 2022a). Only direct measurements at depths shallower than 10 m and with a flag of 2 (best quality control) are selected for this evaluation. Measurements in each box of $1\mathrm{month} \times 10\mathrm{m} \times 0.25^\circ \times 0.25^\circ$ are averaged to obtain representative data of surface A_T, DIC, and pH at $0.25°$-grid cells for months in the period 1985-2021. This results in roughly 16×10^3 data points for A_T and DIC over the global ocean (Table 4). Only half of that amount stems from direct pH measurements. Another half, referred to as indirect measurements (i.e., pH calculated with A_T and DIC), is excluded from this data evaluation. Over 30% of ~~these~~ GLODAP data are distributed along the coasts. ~~The number of the GLODAPv2.2022 gridded data (Table 4) is much less than the SOCATv2022 gridded data (Table 3).~~

- In situ time series of direct measurements of carbonate system variables ($p\mathrm{CO_2}$, A_T, DIC, and pH) are used to qualify our product at local scale (Table 2).

  a) Sutton et al. (2019) present data over multiple sites equipped with autonomous moorings measuring surface ocean $p\mathrm{CO_2}$ and pH ~~from the open ocean to the continental shelves~~ since 2004. These ~~time series were used to qualify the CMEMS-LSCE-FFNN reconstruction in Chau et al. (2022b). This study only revisits eight coastal sites (Table A2)where both~~ stations cover a wide range of oceanic conditions from the tropics to high latitudes (Fig. A1b). More than half of 42 stations distribute over the continental shelves, and many of them observe $p\mathrm{CO_2}$ and pH ~~have been measured and the 1°-reconstruction poorly constrains most of these measurements (see later in Sect. 3.1). The eight stations are located along the US coast, the Gulf of Mexico, and in a Caribbean coral reef (Fig. A1b and Table A2~~ in the regime of coral reefs (Tables A2 and A3). Measurement uncertainty is up to 2 µatm reported for $p\mathrm{CO_2}$ and 0.02 for pH.

  b) For A_T and DIC, we consider ~~four time series : (1)~~ eight time series accessible to provide insights into changes in the surface ocean carbonate system over the recent decades (Bates et al., 2014; Coppola et al., 2020; Gregor and Gruber, 2021; Pére . Two of them belong to the biogeochemical observing systems located in the subtropical Atlantic: Bermuda Atlantic Time Series (BATS, Michaels and Knap, 1996; Steinberg et al., 2001) ~~, (2) Atmospheric Flux Dynamics Time Series in the Mediterranean (DYFAMED, Coppola et al., 2021), (3)~~ and European Station for Time-Series in the Ocean Canary islands (ESTOC, González-Dávila and Santana-Casiano, 2009)~~, and (4) Hawaii Ocean~~ . The other two provide direct measurements in the same ocean basin but in the subpolar region: Irminger Sea and Iceland Sea (IRMINGER and ICELAND, Olafsson et al., 2010). Further mentions time series distributed in specific conditions including a high-Arctic fjord in Svalbard (AWIPEV, Fischer et al., 2017; Gattuso et al., 2023) and the Mediterranean basin (DYFAMED, Coppola et al., 2021). Hawaii Ocean Time-series ~~(HOT, Dore et al., 2009) . The first three stations are in the North Atlantic while the latter is located in~~ in the subtropical North Pacific (HOT, Dore et al., 2009) and OISO time series in the ~~North Pacific (Fig. A1b). These long-term time series provide insights into changes in the surface ocean carbonate system over the recent decades (Bates et al., 2014; Coppola et al., 2020; Gre . The~~ subpolar Southern Ocean (KERFIX, Metzl and Lo Monaco, 1998) allow to complete the reconstruction qualification in different ocean basins. Measurement uncertainty (f.i., from replication experiments) reported at these sites is below 3 $\mathrm{\mu mol kg^{-1}}$. Except for HOT and ESTOC ~~stations provide surface ocean observations of A_T and DIC, and BATS and DYFAMED data~~ (surface ocean measurements), data over all the stations are extracted at seawater depth shallower than $10\ \mathrm{m}$. A monthly average is applied for all the mentioned time series in order to be compatible with output from the CMEMS-LSCE chain of models.

Table 2. Data sources used in product evaluation and comparison. Values in brackets of each variable present measurement-based data uncertainty or analysis[‡] uncertainty.

Product		Data type	Evaluation variables	Reference
Global ocean	1. Surface Ocean CO_2 Atlas version 2022 (SOCATv2022, 1985-2021), last access: 17/6/2022	observation-based gridding, resolution: 1° (global ocean) and 0.25° (coastal ocean), monthly	$p\mathrm{CO_2}$ ($< 5\ \mu\mathrm{atm}$)	Bakker et al. (2022)
	2. CMEMS global ocean surface carbon product (MULTI-OBS_GLO_BIO_CARBON_SURFACE_REP_015_008, 1985-2021), last access: 05/12/2022	SOCAT-based reconstruction, resolution: 1°, monthly	$p\mathrm{CO_2^{\ddagger}}$ ($8\ \mu\mathrm{atm}$)	Chau et al. (2022a, b)
	3. Global Ocean Data Analysis Project bottle data version 2.2022 (GLODAPv2.2022, 1985-2021), last access: 30/9/2022	observation	A_T ($4\ \mu\mathrm{mol\,kg^{-1}}$) DIC ($4\ \mu\mathrm{mol\,kg^{-1}}$) pH ($0.01-0.02$)	Lauvset et al. (2022a, b)
Time series stations	4. Autonomous time series from surface buoys since 2004 (see details in Table A2), last access: 15/10/2022	observation	$p\mathrm{CO_2}$ ($2\ \mu\mathrm{atm}$) pH (0.02)	Sutton et al. (2019)
	5. Bermuda Atlantic Time Series (BATS: 31.7°N-64.2°W, 1988-2021), last access: 30/10/2022	observation	A_T ($3\ \mu\mathrm{mol\,kg^{-1}}$) DIC ($1\ \mu\mathrm{mol\,kg^{-1}}$)	Michaels and Knap (1996); Steinberg et al. (2001)
	6. Atmospheric Flux Dynamics Time Series in the Mediterranean (DY-FAMED: 43.5°N-7.9°E, 1998-2017), last access: 23/03/2023	observation	A_T, DIC	Coppola et al. (2020, 2021)
	7. European Station for Time-Series in the Ocean Canary islands (ES-TOC: 29.2°N-15.5°W, 1995-2009), last access: 30/10/2022	observation	A_T, DIC	González-Dávila and Santana-Casiano (2009)
	8. Hawaii Ocean Time-series (HOT: 22.5°N-158.1°W, 1988-2020), last access: 30/10/2022	observation	A_T, DIC	Dore et al. (2009)
	9. Underwater observatory in Spitsbergen (Svalbard) (AWIPEV: 78.93°N-11.92°E, 2015-2020), last access: 20/07/2023	observation	A_T ($2.6\ \mu\mathrm{mol\,kg^{-1}}$) DIC ($3\ \mu\mathrm{mol\,kg^{-1}}$)	Fischer et al. (2017); Gattuso et al. (2023)
	10. Irminger Sea and the Iceland Sea time series (IRMINGER: 64.33°N-28.00°W, 2014-2021; ICELAND: 68.00°N-12.67°W, 2014-2021), last access: 20/07/2023	observation	A_T (-) DIC ($2\ \mu\mathrm{mol\,kg^{-1}}$)	Olafsson et al. (2010)
	11. Southern Ocean time series under the OISO project (KERFIX: 50.67°S-68.42°E, 1992-2018), last access: 20/07/2023	observation	A_T ($3\ \mu\mathrm{mol\,kg^{-1}}$) DIC ($3\ \mu\mathrm{mol\,kg^{-1}}$)	Metzl and Lo Monaco (1998)

3 Reconstruction methods

3.1 Ensemble $p\mathrm{CO_2}$ mapping feed-forward neural networks

The CMEMS-LSCE-FFNN (Chau et al., 2022b) is based on an ensemble of 100 feed-forward neural network (FFNN) models mapping SOCAT $\mathrm{CO_2}$ fugacity ($f\mathrm{CO_2}$) and predictor variables (Eq. 1).

$$f\mathrm{CO_2} = \mathrm{FFNN}\left(\mathrm{SST}, \mathrm{SSS}, \mathrm{SSH}, \mathrm{Chl}-a, \mathrm{MLD}, x\mathrm{CO_2}, f\mathrm{CO_2^{\mathit{clim}}}, \text{ latitude, longitude}\right) \quad (1)$$

The predictors of $f\mathrm{CO_2}$ include sea surface temperature (SST), salinity (SSS), surface height (SSH), chlorophyll-a (Chl-a), mixed layer depth (MLD), $\mathrm{CO_2}$ mole fraction ($x\mathrm{CO_2}$), $f\mathrm{CO_2}$ climatologies ($f\mathrm{CO_2^{\mathit{clim}}}$), and the geographical coordinates (latitude and longitude). The datasets of SOCAT $f\mathrm{CO_2}$ and predictors are first reprocessed to match model fitting requirements (Sect. 2.1). After excluding the data in the reconstruction month, the data within the 3-month window are randomly separated into FFNN training and validation subsets with a ratio of $2:1$. The subsampling process is repeated for each 100 FFNN runs that results in 100 different datasets for model fitting.The excluded SOCATv2022 datasets are used in model evaluation. The CMEMS-LSCE-FFNN approach was originally developed for $p\mathrm{CO_2}$ reconstructions at monthly, $1°$ resolutions where $p\mathrm{CO_2}$ is converted from $f\mathrm{CO_2}$ following the formulation by Körtzinger (1999). The model best estimate and its uncertainty are defined as the ensemble mean (μ) and ensemble spread (σ) of 100 model outputs of $p\mathrm{CO_2}$.

This study slightly modifies the CMEMS-LSCE-FFNN ensemble approach by Chau et al. (2022b) to achieve $p\mathrm{CO_2}$ reconstructions at monthly, $0.25°$ resolutions. Some of the input datasets presented here (Table 1) are different from those presented in Chau et al. (2022b) (Table S1). The up-to-date input datasets have higher resolutions and a better coverage over the coastal ocean as well as in the high latitudes. Furthermore, the new CMEMS data resources offer space-time varying uncertainty fields which are important in quantifying carbonate system variable uncertainties.

For comparable evaluations in this study, we execute 100-member ensembles of FFNN models at spatial resolutions of both $1°$ (FFNNr100) and $0.25°$ (FFNNr025) using the same lot of input data resources (Table 1). Remind that the training data of $f\mathrm{CO_2}$ is extracted from the SOCATv2022r100 product for FFNNr100 while it comes from the SOCATv2022r025 product (i.e., the merged product of the $1°$-open-ocean dataset and the $0.25°$-coastal-ocean dataset) for FFNNr025. All input datasets are reprocessed with respect to each model resolution (Sect. 2.1). Sect. 3.1 compares these two CMEMS-LSCE-FFNN versions and highlights the skill of the finer resolution data product.

3.2 Locally interpolated alkalinity regression

Locally interpolated alkalinity regression (LIAR; Carter et al., 2016, 2018) is an ensemble-based regression method developed for the global reconstruction of total alkalinity ($\mathrm{A_T}$). Regression coefficients were learned on GLODAPv2 data (Olsen et al., 2016) binned within regular windows of $5° \times 5°$. For prediction, the LIAR software interpolates between the regression coefficients to arbitrary resolutions specified by the users. This study employs eight LIAR models (Carter et al., 2018, Table 2) for calculating $\mathrm{A_T}$ at monthly, $0.25°$ resolutions. Each model represents a combination of predictor variables (see the full presentation in Eq. 2),

$$A_T = \mathrm{LIAR}\,(\mathrm{SSS}, \mathrm{SST}, \mathrm{NO_3}, \mathrm{SiO_2}). \tag{2}$$

The eight regression models include salinity (SSS) - the predominant predictor of A_T - and some combinations of temperature (SST), nitrate (NO_3), and silicate (SiO_2). The model which has the smallest propagation uncertainty is chosen to provide the best estimate of A_T.

Global monthly total alkalinity and 1σ-uncertainty are estimated with given input data from the monthly CMEMS SSS and SST fields and from the WOA18 datasets of nutrient concentrations (Table 1). Uncertainty of the A_T field is estimated systematically through input uncertainty propagation along the processing chain (Carter et al., 2018). Here we define the input uncertainty of predictors in terms of standard deviations (1σ). Input uncertainty fields associated to the monthly CMEMS SSS and SST are products' analysis errors (see e.g., Fig. A7) while uncertainties of the WOA18 NO_3 and SiO_2 climatologies are set to 15% of data values per cell. The 15% quantity refers to the median percentage of standard analysis errors against climatological means of nutrient concentrations (see product standard errors in Table 6, Garcia et al., 2019). The WOA18 standard analysis errors are defined as misfits between their interpolated data and GLODAPv2 bottle data (Olsen et al., 2016). Spatial distribution of the error percentage of the WOA18 nutrient concentrations at the ocean surface is illustrated in Fig. A8.

3.3 Carbonate system speciation

The CO2SYS speciation software was first developed by Lewis and Wallace (1998) to determine carbonate system parameters in the marine CO_2 system based on a set of equilibrium equations (Dickson et al., 2007). Here we use the speciation program written by Van Heuven et al. (2011) and its extension with uncertainty propagation proposed by Orr et al. (2018). To obtain a complete description of the ocean carbonate system, the CO2SYS initialization requires the following input conditions:

i) values of any couple of the parameters $p\mathrm{CO_2}$, A_T, DIC, and pH,

ii) temperature and pressure,

iii) total concentrations of all the non-CO_2 acid-base systems,

iv) equilibrium constants used to describe seawater acid-base chemistry.

The (iii)-condition involves total concentrations of both conservative and non-conservative constituents in the non-CO_2 acid-base systems. The amount of conservative constituents such as borate, fluoride, and sulfate in surface seawater is estimated with salinity. The total concentration of non-conservative constituents (nutrients) is computed approximately with silicate (SiO_2), and phosphate (PO_4). Further information of the carbonate system speciation can be found in Dickson et al. (2007) and Dickson (2010).

With the reconstructions of $p\mathrm{CO_2}$ and A_T (Sects 3.1 and 3.2), the CO2SYS speciation software is used to derive pH, DIC, Ω_{ar}, and Ω_{ca}, and determine their uncertainty over the ocean surface at a resolution of $0.25°$. Equation 3 expresses all input-output variables of CO2SYS for this study. Note that the estimates for other carbonate system variables such as hydrogen ion

(H^+) concentration and Revelle Factor (RF) - a measure of the carbonate buffer capacity- are also available (Figs. A4 and A6) but beyond the scope of our data evaluation.

$$p\mathrm{H},\ \mathrm{DIC},\ \Omega_{ar},\ \Omega_{ca} = \mathrm{CO2SYS}\left(p\mathrm{CO_2}, \mathrm{A_T}, \mathrm{SST}, \mathrm{SSS}, \mathrm{P}, \mathrm{SiO_2}, \mathrm{PO_4}, \mathrm{constants}\right) \tag{3}$$

The FFNN best estimate (ensemble mean) of $p\mathrm{CO_2}$ reconstructions (Sect. 3.1) and the LIAR outputs of $\mathrm{A_T}$ (Sect. 3.2) are used as the prior inputs of the CO2SYS at each grid cell for every month in the period 1985-2021. We take the same data products of SST, SSS, and nutrient concentrations as for the previous reconstructions (Table 1). Pressure (P) is assumed to be $0\ \mathrm{dbar}$ at the ocean surface. For equilibrium constants, we choose the best empirical values recommended by Dickson et al. (2007) and Dickson (2010). These settings include (1) the dissociation constants K_1 and K_2 from Lueker et al. (2000) and $K_{\mathrm{HSO_4}}$ from Dickson (1990) in combination with the total boron-ratio-salinity formulation by Uppstrom (1974).

The uncertainty of the CO2SYS variables is estimated by error propagation (Orr et al., 2018). Inputs for the CO2SYS error propagation include the reconstruction uncertainty of $p\mathrm{CO_2}$ (FFNN ensemble standard deviation) and of $\mathrm{A_T}$ (LIAR error propagation). The uncertainty of SST, SSS, and nutrient concentrations are set to the same values as in the previous section (Sect. 3.2). Equilibrium constants' standard errors are default values (see Table 1, Orr et al., 2018). As for FFNN and LIAR, uncertainty values of each carbonate system variable are computed for each month in 1985-2021 and at each $0.25°$-grid box over the global surface ocean.

4 Evaluation metrics

4.1 Model best estimate and uncertainty quantification

The 100 FFNN models result in an ensemble of 100 estimates of global monthly, $0.25°$ surface ocean $p\mathrm{CO_2}$ fields (Sect. 3.1). Specify any $t = 1:444\ (\mathrm{month})$, $i = 1:180\ (\mathrm{latitude})$, and $j = 1:360\ (\mathrm{longitude})$, the best estimate ($\mu_{tij}$) and uncertainty ($\sigma_{tij}$) at time t and grid cell ij are deduced from 100 FFNN $p\mathrm{CO_2}$ estimates $\left(X(t,i,j,m)\right)_{m=1}^{m=100}$ as follows.

$$\mu_{tij} = \frac{\sum_{m=1}^{m=100} X(t,i,j,m)}{100}, \tag{4a}$$

$$\sigma_{tij} = \sqrt{\frac{\sum_{m=1}^{m=100} \left[X(t,i,j,m) - \mu_{tij}\right]^2}{100}}. \tag{4b}$$

For $p\mathrm{H}$, $\mathrm{A_T}$, DIC, Ω_{ar}, and Ω_{ca}, the best estimates and associated uncertainties (μ_{tij} and σ_{tij}) are obtained directly from the LIAR and CO2SYS speciation tools and their error propagation (Sects. 3.2 and 3.3).

To assign representatives of μ and σ estimates for carbonate system variables at a specific space-time window, we define statistics with respect to each of the three following cases:

i) a representative over a period of time (T months)

$$\mu_{ij} = \frac{\sum_t \mu_{tij}}{T}, \tag{5a}$$

$$\sigma_{ij} = \sqrt{\frac{\sum_t \sigma_{tij}^2}{T}}. \tag{5b}$$

ii) a representative over a region (e.g., ocean basins and sub-basins, the global ocean)

$$\mu_t = \frac{\sum_{ij} \mu_{tij} \times A_{ij}}{\sum_{ij} A_{ij}}, \tag{6a}$$

$$\sigma_t = \sqrt{\frac{\sum_{ij} \sigma_{tij}^2 \times A_{ij}}{\sum_{ij} A_{ij}}}. \tag{6b}$$

iii) a representative over a period of time and a region

$$\mu = \frac{\sum_{t,ij} \mu_{tij} \times A_{ij}}{T \times \sum_{ij} A_{ij}}, \tag{7a}$$

$$\sigma = \sqrt{\frac{\sum_{t,ij} \sigma_{tij}^2 \times A_{ij}}{T \times \sum_{ij} A_{ij}}}. \tag{7b}$$

where t is in a time period with length T and A_{ij} is the area of each grid cell in a desired region. It is noteworthy that the statistics in Eqs. (5b)-(7b) are not the standard deviation associated to the mean quantities in Eqs. (5a)-(7a), but they stand for the best representative of uncertainty estimates over an ocean basin and/or time period. These statistics also support for the comparison with model-observation deviation (e.g., Eq. 10) which is typically used in the calculation of standard uncertainty proposed in the previous studies (Jiang et al., 2019; Iida et al., 2021; Gregor and Gruber, 2021). Subscripts in the notations of the best model estimates (μ) and model uncertainties (σ) in Eqs. (4)-(7) are dropped out for general situations.

The best model estimate (μ) is assessed against model uncertainty (σ) through σ-to-μ ratio ($\%$)

$$R(\mu,\sigma) = 100\% \, \frac{\sigma}{|\mu|}. \tag{8}$$

The σ-to-μ ratio allows evaluating the significance of the model estimate. Model estimates of carbonate variables are reliable with $R(\sigma,\mu)$ values less than 20% (Rose, 2013).

4.2 Model performance in comparison with evaluation data

Assume that μ_{tij} and O_{tij} are the best model estimate and an observation (or its gridded data) available at time t and grid cell ij, and μ and O are respectively their means over the total number of evaluation data (N). Model skills are assessed against observation data (Table 2) with the following metrics:

- mean model-observation differences (Bias)

$$\mathrm{Bias} = \frac{\sum_{t,ij} (\mu_{tij} - \mathrm{O}_{tij})}{N}, \tag{9}$$

- root-of-mean-square-deviation (RMSD)

$$\mathrm{RMSD} = \sqrt{\frac{\sum_{t,ij}\left(\mu_{tij} - \mathrm{O}_{tij}\right)^2}{N}}, \tag{10}$$

- coefficient of determination (r^2)

$$r^2 = \frac{\left[\sum_{t,ij}\left(\mu_{tij} - \mu\right) \times \left(\mathrm{O}_{tij} - \mathrm{O}\right)\right]^2}{\sum_{t,ij}\left(\mu_{tij} - \mu\right)^2 \times \sum_{t,ij}\left(\mathrm{O}_{tij} - \mathrm{O}\right)^2}. \tag{11}$$

5 Results

5.1 Surface ocean $p\mathrm{CO_2}$

This section presents the reconstruction of surface ocean $p\mathrm{CO_2}$ at monthly and $0.25°$ resolutions. The reconstruction skill is evaluated against SOCATv2022 data from global to ocean basin scale and at the level of grid cells (Sect. 2.2). We compare the novel reconstruction at a higher spatial resolution to the one at a coarser spatial resolution (Chau et al., 2022b). Emphasis is put on the skill to reproduce spatial and temporal variations of $p\mathrm{CO_2}$ across a variety of coastal regions and time series stations.

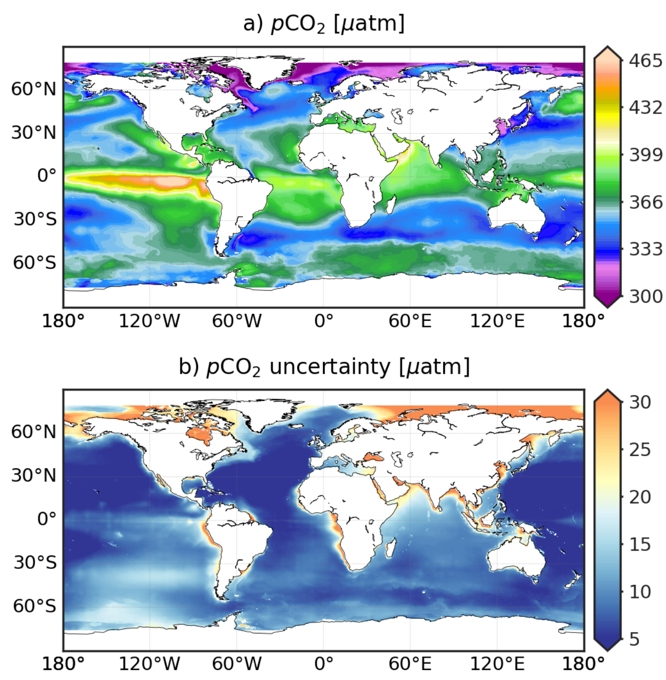

Figure 1. CMEMS-LSCE-FFNN $p\mathrm{CO_2}$ over the global ocean at a spatial resolution of $0.25°$. Temporal means of the model best estimate and 1σ-uncertainty per grid cell over 1985-2021 are calculated by using Eq. (5).

Table 3. ~~Skill scores~~ Evaluation statistics for monthly CMEMS-LSCE-FFNN reconstructions of $p\mathrm{CO_2}$ at 1° (r100) and 0.25° (r025) spatial resolutions computed over the period 1985-2021. r100 $\rightarrow$ 025 and r025 $\rightarrow$ 100 are referred to the versions ~~upscaled or~~ downscaled or upscaled from the original CMEMS-LSCE-FFNN $p\mathrm{CO_2}$ at 1° and 0.25° resolutions. SOCATv2022 gridded data independent from CMEMS-LSCE-FFNN training are used as benchmarks for model evaluation (see text for details). Statistics including total numbers of data, RMSD (Eq. 10), and r^2 (Eq. 11) are reported for both the open ocean (O) and coastal region (C). $*$ marks results with respect to the primary product proposed in this study.

Basins			Number of data		RMSD [µatm]				r^2			
			r100	r025*	r100	r025 → 100	r025*	r100 → 025	r100	r025 → 100	r025*	r100 → 025
0.	Globe	(O)	207174	3317273	~~14.32~~ 14.3	~~14.08~~ 14.1	~~14.29~~ 14.3	~~14.38~~ 14.4	0.83	0.83	0.83	0.83
		(C)	101007	431758	~~26.61~~ 26.6	~~26.48~~ 26.5	~~27.55~~ 27.6	~~28.50~~ 28.5	0.72	0.72	0.74	0.72
1.	Arctic	(O)	537	8589	~~27.93~~ 27.9	~~27.43~~ 27.4	~~28.04~~ 28.0	~~28.06~~ 28.1	0.69	0.69	0.67	0.67
		(C)	5897	25844	~~38.74~~ 38.7	~~38.56~~ 38.6	~~41.46~~ 41.5	~~43.17~~ 43.2	0.55	0.56	0.55	0.52
2.	Atlantic	(O)	54797	876116	~~13.76~~ 13.8	~~13.57~~ 13.6	~~13.69~~ 13.7	~~13.78~~ 13.8	0.81	0.81	0.81	0.81
		(C)	49770	227665	~~24.99~~ 25.0	~~24.78~~ 24.8	~~25.17~~ 25.2	~~26.05~~ 26.1	0.76	0.76	0.77	0.77
3.	Pacific	(O)	120604	1932981	~~14.59~~ 14.6	~~14.30~~ 14.3	~~14.54~~ 14.5	~~14.67~~ 14.7	0.85	0.85	0.85	0.85
		(C)	26847	104269	~~26.79~~ 26.8	~~26.90~~ 26.9	~~28.46~~ 28.5	~~28.95~~ 29.0	0.71	0.71	0.69	0.67
4.	Indian Ocean	(O)	4485	71719	~~10.34~~ 10.3	~~10.17~~ 10.2	~~10.26~~ 10.3	~~10.34~~ 10.3	0.88	0.88	0.88	0.88
		(C)	1522	6187	~~23.50~~ 23.5	~~22.82~~ 22.8	~~25.40~~ 25.4	~~26.51~~ 26.5	0.69	0.71	0.69	0.69
5.	Southern Ocean	(O)	26751	427868	~~14.42~~ 14.4	~~14.29~~ 14.3	~~14.52~~ 14.5	~~14.43~~ 14.4	0.69	0.69	0.69	0.69
		(C)	16971	67793	~~26.01~~ 26.0	~~25.80~~ 25.8	~~27.35~~ 27.4	~~28.80~~ 28.8	0.61	0.61	0.64	0.59

Figure 1 presents global maps at 0.25°-resolution of long-term averages of $p\mathrm{CO_2}$ and corresponding uncertainty estimates. Reconstructed $p\mathrm{CO_2}$ distributions reveal well documented large scale structures. Values are high over upwelling regions (e.g., Equatorial Pacific, California Boundary Current, Western Arabian Sea). Low $p\mathrm{CO_2}$ is associated with increased $\mathrm{CO_2}$ solubility in cold high latitudes seawater (e.g., Arctic), strong biological production (e.g., China Sea), or the combination of both (e.g., subpolar Northern Atlantic, Southern Ocean between $35-50^\circ$S). Spatial structures appear coherent from small to large spatial scales, both along the coast and moving towards the open ocean (see also in Figs. 2-4). The combination of a down-scaled version of open-ocean and higher-resolution coastal SOCATv2022 data (Sect. 2.1) yields $p\mathrm{CO_2}$ distributions without discontinuities. The uncertainty map (Fig 1b) represents the confidence level in surface ocean $p\mathrm{CO_2}$ estimates (Fig 1a). Predominantly low uncertainty estimates ($\sigma < 5$ µatm) indicate the global stability of the ensemble reconstruction. Exceptions are found in many coastal regions, open-ocean areas with sparse data coverage (e.g., Southern Pacific, Indian Ocean), or regions with substantially high or low surface ocean $p\mathrm{CO_2}$ (e.g., Arctic, eastern equatorial Pacific). However, $p\mathrm{CO_2}$ is reconstructed with a high degree of confidence over most of the global ocean with a σ-to-μ ratio (Eq. 8) below 10% (Fig. A9a).

Skill scores of the monthly, 0.25°-resolution reconstruction are presented in Table 3 (columns marked by an asterisk). The global RMSD (Eq. 10) between the best reconstruction and SOCATv2022r025 $p\mathrm{CO_2}$ over the entire period is ~~14.29~~14.3 µatm for the open ocean and ~~27.55~~27.6 µatm for the coastal ocean. These two model errors are lower than 4% and 8% of the global mean $p\mathrm{CO_2}$ (Table 6). Moreover, variability present in observation-based data is reproduced by the CMEMS-LSCE-FFNN with high values of r^2 (open ocean: 0.83, coast: 0.74). The reconstruction quality is similar among major ocean basins. Spatial distributions of SOCATv2022 data, bias, and RMSD are shown in Figs. A2-bd and A3-bdfh. Estimation skills are low in the ocean basins with sparse data coverage and significant space-time variability of $p\mathrm{CO_2}$ (e.g., Arctic, eastern Equatorial Pacific, land-ocean continuum).

Table 3 also presents statistics for the monthly FFNN products of surface ocean $p\mathrm{CO_2}$ at spatial resolutions of $0.25°$ (r025) and $1°$ (r100) together with their variants (r100 $\rightarrow$ 025 and r025 $\rightarrow$ 100). The latter are respectively extrapolation and interpolation versions of the original r100 and r025 datasets~~, i. e.,~~. We used the Climate Data Operators (CDO) remap operator to regrid FFNN model outputs ~~regridded~~ to a finer or coarser spatial resolution. For compatibility, we compare statistics between:

i) FFNN(r025) and FFNN(r100 $\rightarrow$ 025) by using SOCATv2022r025 as evaluation data,

ii) FFNN(r025 $\rightarrow$ 100) and FFNN(r100) by using SOCATv2022r100 as evaluation data.

The FFNN(r025) central to this study yields a lower RMSD and a higher correlation to the SOCAT data than the FFNN(r100 $\rightarrow$ 025). As expected, the improvement in reconstruction skill with higher model resolution is larger over coastal regions than in the open ocean. The FFNN(r025) product after interpolating to a coarser resolution, i.e., FFNN(r025 $\rightarrow$ 100), agrees with the original $1°$-resolution data product over all the ocean.

The motivation to increase the spatial resolution of the reconstruction is to improve the representation of horizontal gradients of $p\mathrm{CO_2}$ at fine scales. Figures 2-4 exemplify spatial distributions for the two reconstructions (r025 and r100) over the coastal-open-ocean continuum. Ten distinct oceanic regions are considered (see Fig. A1a and Table A1 for the ten locations), which can be classified into three groups:

- permanent Eastern Boundary current upwelling systems with relatively high $p\mathrm{CO_2}$ (California Current System - CCS, Humboldt Current System - HCS, Canary Current System - CnCS, and Benguela Current System - BCS),
- regions characterized by low $p\mathrm{CO_2}$ values driven by cold water temperatures and strong biological production (Labrador Sea, Western South Atlantic, Northern Europe, and Sea of Japan),
- other regions either under the influence of strong river runoff (Amazon ~~mount~~mouth) or monsoon-driven upwelling (Western Arabian Sea).

The legend of Figs 2-4 includes regional RMSD and r^2 computed between the best estimates of two models and coastal-ocean SOCATv2022r025 data. The coarser spatial resolution product is co-located at the same $0.25°$-grid cells for this analysis. These figures illustrate important discrepancies in $p\mathrm{CO_2}$ data density between coastal regions with poorly monitored regions (e.g., HCS, BCS, Amazon ~~mount~~mouth) contrasting with areas with higher data coverage (e.g., Northern Europe, Sea of Japan).

Over 7 out of the 10 analysed regions the reconstruction at monthly, $0.25°$ resolutions yields RMSDs below 10% of the global mean of coastal-ocean $p\mathrm{CO_2}$ estimates (Table 6) and r^2 values higher than 0.3; e.g., Northern Europe ($\cancel{\mathrm{RMSD} = 33.90}$ $\mathrm{RMSD} = 32.4$ µatm, $\cancel{r^2 = 0.80} r^2 = 0.81$), Sea of Japan ($\cancel{\mathrm{RMSD} = 20.84}$ $\mathrm{RMSD} = 20.8$ µatm, $\cancel{r^2 = 0.70} r^2 = 0.71$), and CnCS ($\cancel{\mathrm{RMSD} = 30.36}$ $\mathrm{RMSD} = 28.8$ µatm, $\cancel{r^2 = 0.35} r^2 = 0.4$). The CMEMS-LSCE-FFNN model projections of $p\mathrm{CO_2}$ lack skill over the HCS ($\cancel{\mathrm{RMSD} = 54.54}$ $\mathrm{RMSD} = 50.0$ µatm, $\cancel{r^2 = 0.29} r^2 = 0.33$), the region under influence of the Amazon river ($\cancel{\mathrm{RMSD} = 45.93}$ $\mathrm{RMSD} = 45.7$ µatm, $\cancel{r^2 = 0.37} r^2 = 0.38$), and the Western Arabian Sea ($\cancel{\mathrm{RMSD} = 45.31}$ $\mathrm{RMSD} = 44.8$

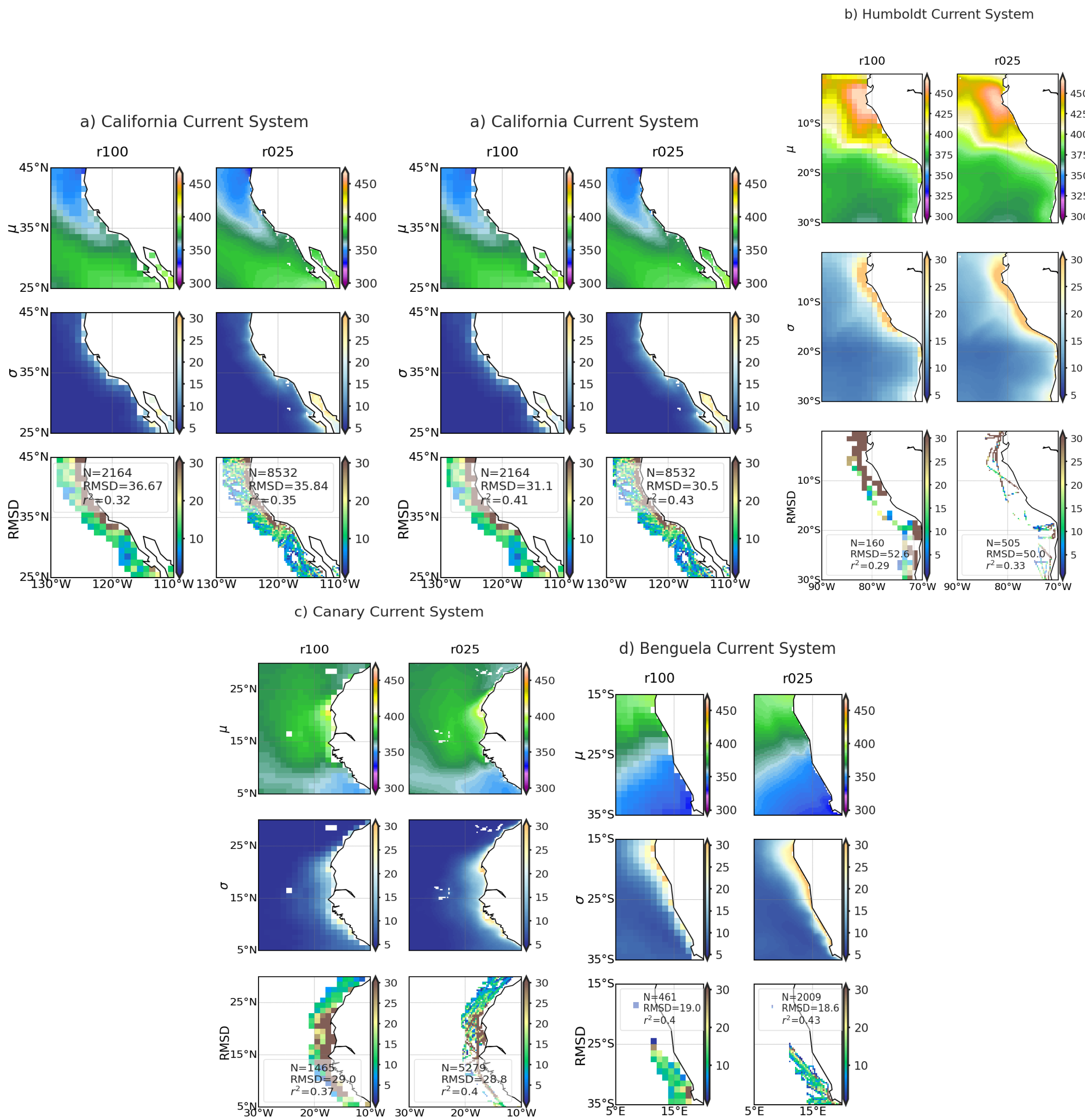

Figure 2. Comparison of CMEMS-LSCE-FFNN mapping $p\mathrm{CO_2}$ at 1° (r100) and 0.25° (r025) resolutions over 4 permanent upwelling regions associated with the Eastern Boundary Currents (California, ~~Peru~~Humboldt, Canary, and Benguela; see Figure A1-ABGH for geographical locations). For each region, spatial distributions of $p\mathrm{CO_2}$ (μ) and uncertainty (σ) estimates, and coastal-ocean RMSD of $p\mathrm{CO_2}$ averaged over 1985-2021 (Eqs. 5 and 10) are shown. Metrics presented in the legend for each of the 3rd row include the number of coastal-ocean SOCATv2022 data (N), regional RMSD (Eq. 10) and r^2 (Eq. 11).

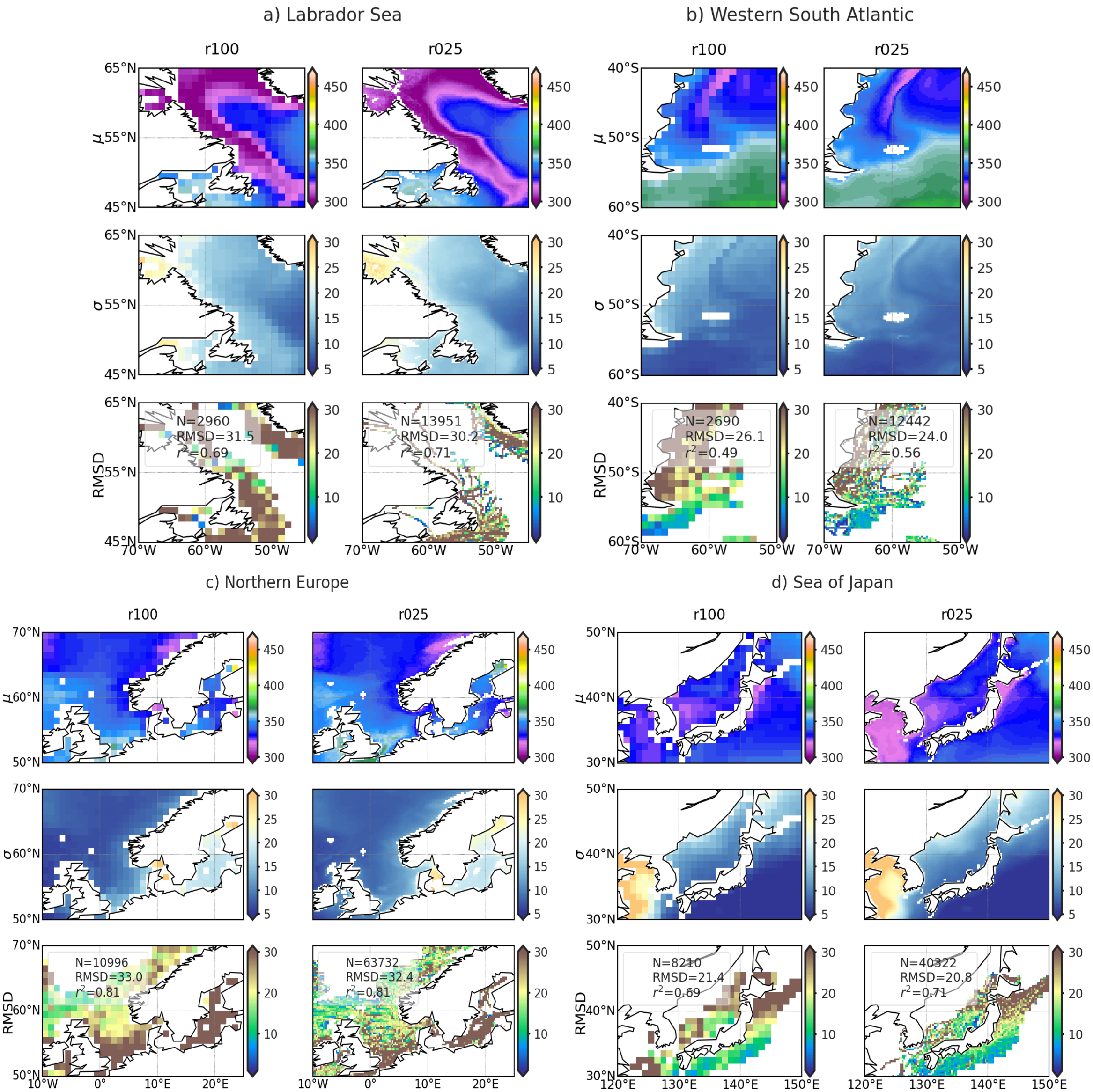

Figure 3. Comparison of CMEMS-LSCE-FFNN mapping $p\mathrm{CO_2}$ at 1° (r100) and 0.25° (r025) resolutions over 4 regions characterized with low $p\mathrm{CO_2}$ values (Labrador, Western South ~~America~~Atlantic, Northern Europe, and Japan; see Figure A1-CEFJ for geographical locations). For each region, spatial distributions of $p\mathrm{CO_2}$ (μ) and uncertainty (σ) estimates, and coastal-ocean RMSD of $p\mathrm{CO_2}$ averaged over 1985-2021 (Eqs. 5 and 10) are showed. Metrics present in the legend for each of the 3rd row include the number of coastal-ocean SOCATv2022 data (N), regional RMSD (Eq. 10) and r^2 (Eq. 11).

μatm, $\cancel{r^2 = 0.47}$ $r^2 = 0.49$). In nearshore sectors of these coastal areas, $p\mathrm{CO_2}$ estimates are also subject to a substantial amount of uncertainty ($\sigma > 20$ μatm). The lack of model skill reflects the combination of low data density and strong $p\mathrm{CO_2}$ gradients

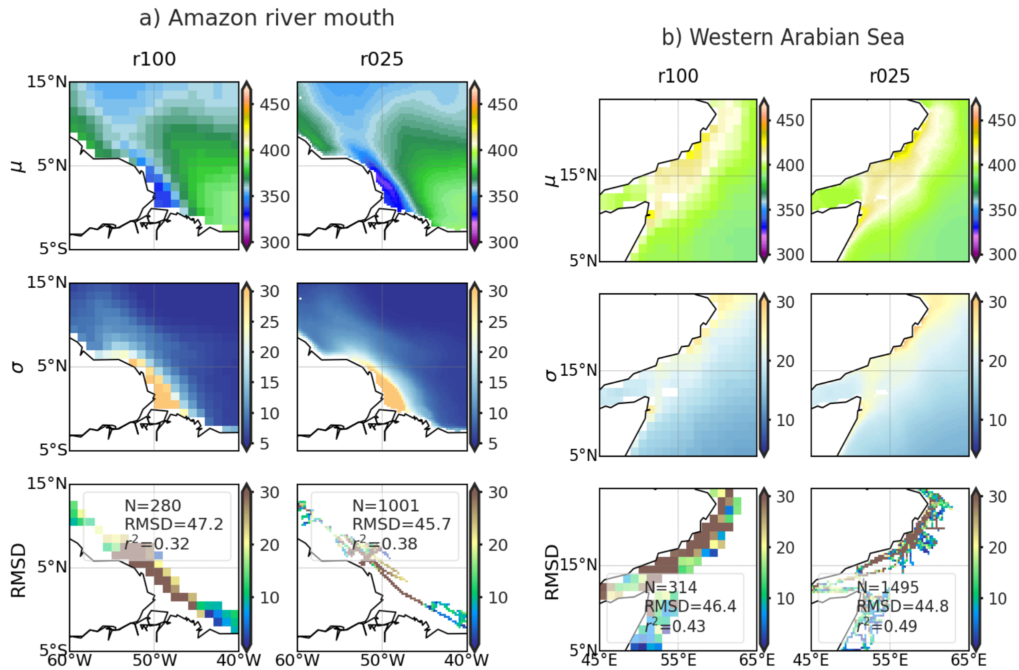

Figure 4. Comparison of CMEMS-LSCE-FFNN mapping $p\mathrm{CO_2}$ at 1° (r100) and 0.25° (r025) resolutions over the mouth of the river Amazon and the Western Arabian Sea (see Fig. A1-DI for geographical locations). For each region, spatial distributions of $p\mathrm{CO_2}$ (μ) and uncertainty (σ) estimates, and coastal-ocean RMSD of $p\mathrm{CO_2}$ averaged over 1985-2021 (Eqs. 5 and 10) are showed. Metrics present in the legend for each of the 3rd row include the number of coastal-ocean SOCATv2022 data (N), regional RMSD (Eq. 10) and r^2 (Eq. 11).

driven by multiple underlying physical and biogeochemical processes. The HCS, for instance, is characterized by the highest $p\mathrm{CO_2}$ levels (Fig. 2) among the four Eastern Boundary Current Systems, with interannual variability amplified with the El Niño–Southern Oscillation (ENSO) events (Feely et al., 1999; Landschützer et al., 2016). Similarly, high $p\mathrm{CO_2}$ levels with substantial seasonal variability are observed over the Western Arabian Sea (Fig. 4b), the key driver being monsoonal upwelling ~~(Sabine et al., 2002; Sarma et al., 2013)~~(Sabine et al., 2002; Sarma et al., 2013, 2023). In contrast to the two aforementioned coastal regions, high $\mathrm{CO_2}$ undersaturation as well as strong $p\mathrm{CO_2}$ gradients (Fig. 4a) are found in the area under the influence of Amazon river discharge (Olivier et al., 2022). Extreme values and large variability of $p\mathrm{CO_2}$ challenge any approach to estimate $p\mathrm{CO_2}$ data over these regions (Ibánhez et al., 2015; Bakker et al., 2016; Landschützer et al., 2020).

The two FFNN reconstructions (r025 and r100) share similarities in overall structures of $p\mathrm{CO_2}$ over the coastal-open-ocean continuum (Figs. 2-4). However, the higher spatial resolution outperforms its lower resolution counterpart is reproducing fine-scale features of $p\mathrm{CO_2}$ in the transition from nearshore regions to the adjacent open ocean. The increase in model spatial resolution translates into a greater spatial coverage of the continental shelves such as Labrador Sea, Northern Europe, and Sea of Japan (Fig. 3), and thus an increase in the number of data over the coastal domain. The increase in spatial resolution allows

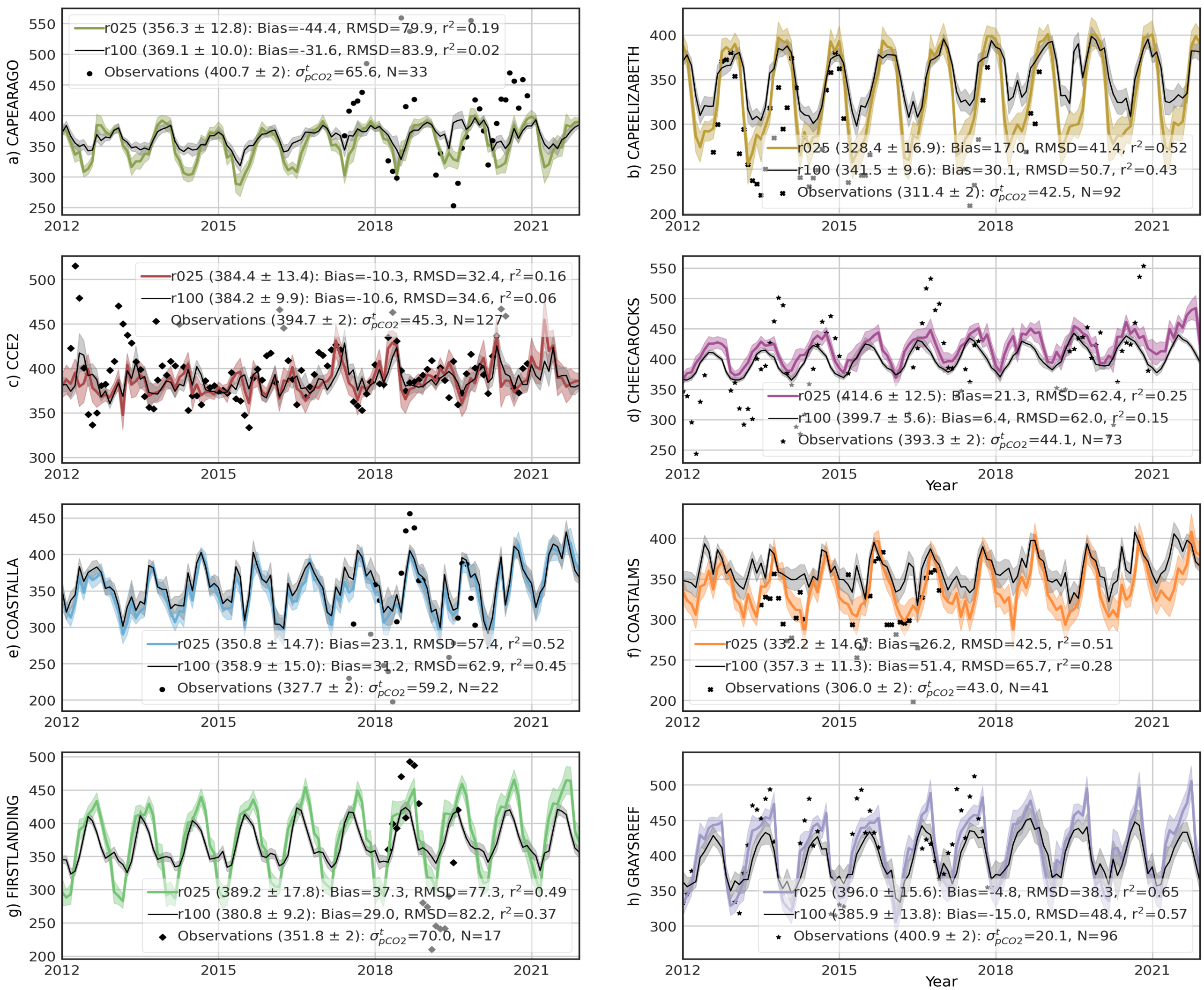

Figure 5. Time series of surface ocean $p\mathrm{CO}_2$ (µatm) at coastal observing stations (Table A2 and Fig. A1b): model best estimate (curve), 1σ-uncertainty (envelope), and monthly average of in situ observations (point). The reconstructed data at 1° (r100) and 0.25° (r025) resolutions are co-located to in situ observations provided by Sutton et al. (2019). Means of the best estimate and 1σ-uncertainty ($\mu \pm \sigma$) calculated over the observing time span are shown in brackets. Statistics include number of months with observations (N), Bias, RMSD, and r^2 computed for the two reconstructions. $\sigma^t_{p\mathrm{CO}_2}$ stands for temporal standard deviation from monthly averages of $p\mathrm{CO}_2$ observations.

a gain in prediction probability of $p\mathrm{CO}_2$ variations on the order of roughly 2% over the Eastern Boundary Currents to ~~8%~~ 7% over the Western South Atlantic (Figs. 2-3b).

~~Reconstruction skill of seasonal to inter-annual variability of~~ At local scale, the reconstruction of in situ $p\mathrm{CO}_2$ ~~is further assessed at eight coastal monitoring sites (Sutton et al., 2019) and illustrated in~~ (Sutton et al., 2019) over the open ocean is at the high order of confidence (Table A3). Low RMSD (between 7.8 and 23.5 µatm) and sustainably high r^2 (from 0.45 to 0.98) dominate evaluation statistics over the 18 open-ocean stations. Obviously, CMEMS-LSCE-FFNN has less skill in the coastal sector and model-observation deviation varies depending on a wide range of $p\mathrm{CO}_2$ conditions. However, coastal-ocean RMSD can be smaller than 10% of station climatology (e.g., KILONALU, KANEOHE, ALAWAI) and the reproduction availability of temporal variations of $p\mathrm{CO}_2$ possibly exceeds 70% (e.g., SEAK, KODIAK, DABOB). Through Fig. 5~~(see Sect. 2.2~~ , we further assess seasonal to inter-annual variability reproduced at the eight coastal sites (see Fig. A1b and Table A2 for ~~data description and Fig. A1b for station locations)~~ station location) where measurements are available for both $p\mathrm{CO}_2$ and pH (analyzed in Section 5.3) and they are poorly constrained by the 1°-reconstruction (Chau et al., 2022b). The temporal variability of $p\mathrm{CO}_2$ reported for these time series sites reflects a combination of processes (Sutton et al., 2019), e.g., California Current System (CAPEARAGO and CCE2), western coastal upwelling (CAPEELIZABETH), eutrophication enhancing respiration of CO_2 (FIRSTLANDING), and multiple stressors on coral reef environments (CHEECAROCKS, GREYREEF). ~~Results from reconstructions at two spatial resolutions are compared: 1° (100, black curve) and 0.25° (r025, color curve).~~ As shown in Fig. 5 (scattered points for observations) time series of coastal $p\mathrm{CO}_2$ are still short. The longest time series covers 127 months of $p\mathrm{CO}_2$ monitoring since 2010 (CCE2) while the shortest one contributes 17 months with observations (FIRSTLANDING).

Analyzing the ~~eight~~ station time series, we have found that data have been sampled within a few days with an average offset of about a week from the month center. At these coastal sites, the temporal standard deviation from monthly averages of $p\mathrm{CO}_2$ ($\sigma^t_{p\mathrm{CO}_2}$) exceeds ~~measurement~~ analytical errors (2 µatm, Sutton et al., 2019). $\sigma^t_{p\mathrm{CO}_2}$ ranges from ~~20.12~~20.1 $\mu\mathrm{atm}$ at GREYREFF to values as large as 65.6 $\mu\mathrm{atm}$ at CAPEARAGO or ~~69.98~~70 $\mu\mathrm{atm}$ at FIRSTLANDING. The monthly average of $p\mathrm{CO}_2$ might not be adequately represented by discreet samples at sites with a large temporal standard deviation of $p\mathrm{CO}_2$. The misfit between the monthly reconstruction and discreet observations is exacerbated in dynamical coastal environments and might explain in part the large RMSD of reconstructions of monthly coastal $p\mathrm{CO}_2$ (e.g., GREYREEF: ~~38.34~~38.3 $\mu\mathrm{atm}$, CAPEARAGO: ~~79.86~~79.9 $\mu\mathrm{atm}$, FIRSTLANDING: ~~77.32~~77.3 $\mu\mathrm{atm}$) for the r025 reconstruction. The RMSD is mostly lower for the FFNN reconstruction at 0.25° resolution compared to the FFNN at 1° resolution by ~~2.11~~2.2 $\mu\mathrm{atm}$ (CCE2) to ~~23.32~~23.2 $\mu\mathrm{atm}$ (COASTALMS). Similarly, r^2 increases between 7%-23% at higher resolution. Overall, seasonal to interannual variations of coastal-ocean $p\mathrm{CO}_2$ are better reproduced in the reconstruction at 0.25° resolution (Fig. 5).

5.2 Total alkalinity and dissolved inorganic carbon

This section presents and ~~analyzes~~ analyses global ocean surface reconstructions of total alkalinity ($\mathrm{A_T}$) and dissolved inorganic carbon (DIC) at monthly, 0.25° resolutions over 1985-2021. GLODAPv2.2022 bottle data (Sect. 2.2) serve as reference data for model evaluation. Model reconstruction skill is further assessed at the ~~four~~ eight Eulerian time series sites: AWIPEV, BATS, DYFAMED, ESTOC, ~~and HOTS~~ HOT, ICELAND, IRMINGER, and KERFIX (Table 2).

Figure 6 shows spatial distributions of the climatological mean and uncertainty (Eq. 5) for $\mathrm{A_T}$ and DIC. Despite being in part influenced by common biological and physical processes, both properties have contrasting distributions due to the strong correlation between surface ocean $\mathrm{A_T}$ and salinity (Lee et al., 2006; Broullón et al., 2019), as well as the contribution of air-sea gas exchange and biological productivity on surface ocean DIC levels (Feely et al., 2001; Takahashi et al., 2014). Over subtropical

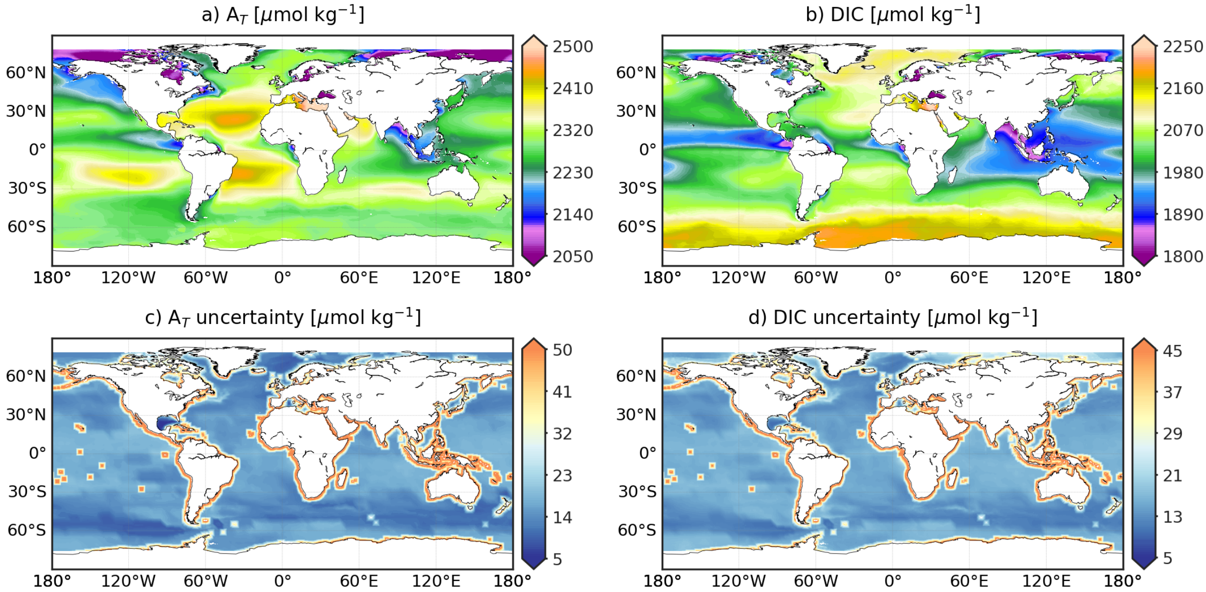

Figure 6. CMEMS-LSCE A_T and DIC over the global ocean at a spatial resolution of 0.25°. Temporal means of the model best estimate and 1σ-uncertainty per grid cell over 1985-2021 are calculated by using Eq. (5).

Atlantic gyres and the Mediterranean Sea, oceanic areas with net evaporation, A_T exceeds 2400 µmol kg^{-1}. Total alkalinity falls below 2150 µmol kg^{-1} in regions where precipitation, river freshwater runoff, or seasonal sea-ice melting dilute surface water salinity (e.g., subpolar North Pacific, Arctic, and equatorial river outflows). The distribution of DIC is relatively uniform between the Atlantic, Pacific, and Indian Ocean basins, but shows pronounced latitudinal gradients. High concentrations of DIC are found throughout the Southern Ocean (DIC > 2100 µmol kg^{-1}) where strong upwelling brings up subsurface water enriched in CO_2 and nutrients. The inefficient utilization of nutrients in this high nutrient low chlorophyll region limits the biological drawdown of DIC allowing the massive DIC input to be spread horizontally by westerlies (Key et al., 2004; Menviel et al., 2018). Levels of DIC below 1900 µmol kg^{-1} are reconstructed over the Equatorial Pacific, the Equatorial Eastern Atlantic, the Eastern Indian Ocean, and coastal areas on the Arctic Ocean. While low DIC levels associated with Equatorial upwelling reflect gas exchanges across the air-sea interface and enhanced biological production, the interaction between physical and biogeochemical processes at work in the Indian Ocean are less well understood (Takahashi et al., 2014). Low DIC levels found close to river mouths reflect outgassing of CO_2 across the salinity gradient, as well as enhanced biological uptake fueled by river nutrient inputs. Representation uncertainty (Fig. 6-cd) associated with monthly alkalinity and DIC reconstructions is lower than 20 µmol kg^{-1} throughout the open ocean. The open-ocean σ-to-μ ratio (Eq. 8) ranges between $0.5-1.5\%$ which is relatively small (Fig. A9-cd). ~~The largest model uncertainty~~ DIC uncertainty is computed through CO_2SYS error propagation with reconstruction uncertainties of pCO$_2$ and A_T set as inputs. The largest values ($\sigma > 30$ µmol kg^{-1}) ~~is computed~~ appear nearshore and surrounding oceanic islands ~~, a feature~~ (Fig. 6d). A similar feature is found on the field of A_T (Fig. 6c) inherited from input uncertainty associated with the CMEMS salinity product (Fig. A7a).

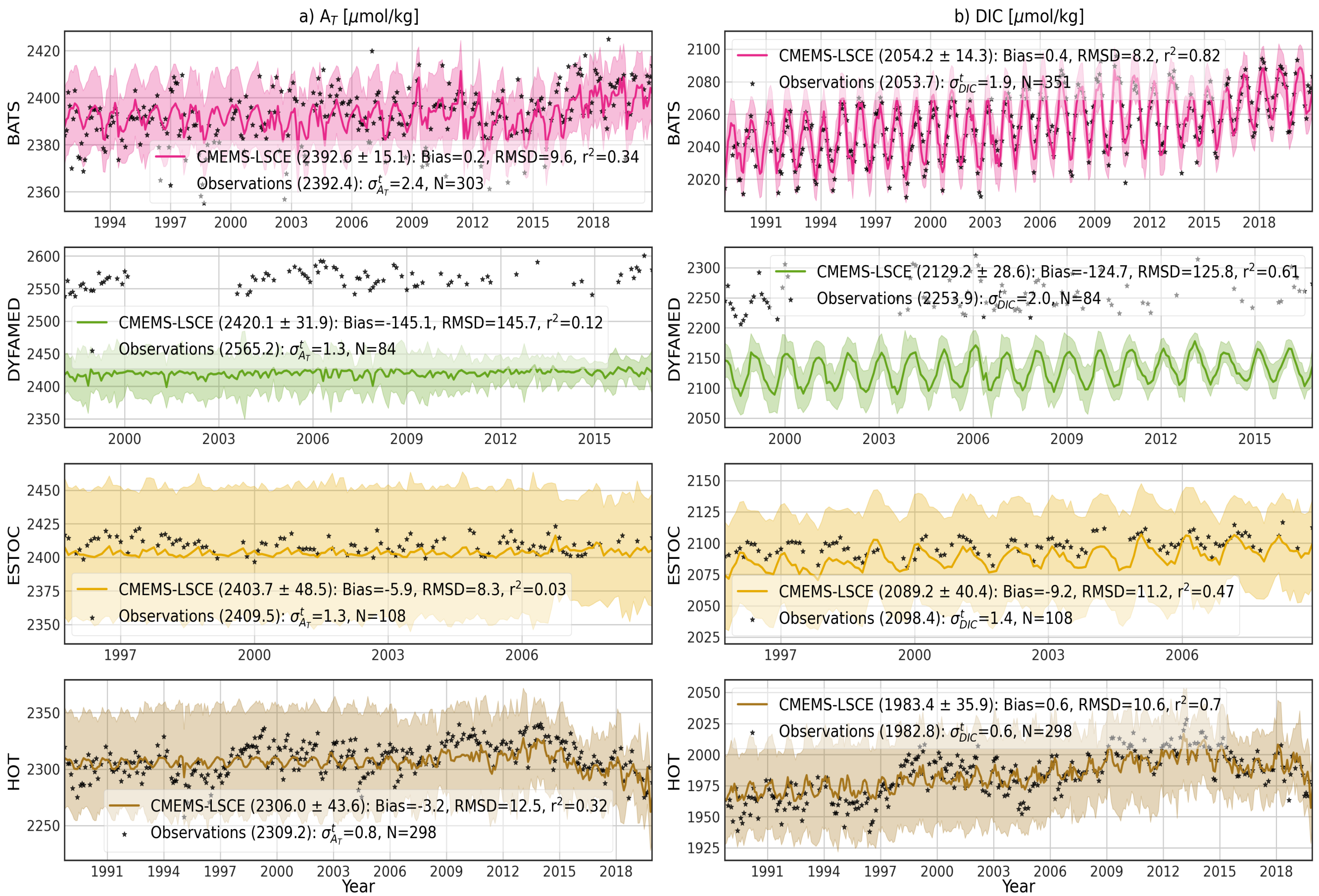

Figure 7. Monthly time series of A_T and DIC at BATS, DYFAMED, ESTOC and HOT stations (Table 2 and Fig. A1b): model best estimate (curve), 1σ-uncertainty (envelope), and monthly average of surface (0-10 m) observations (point). Means of the best estimate and 1σ-uncertainty ($\mu \pm \sigma$) calculated over the observing time span are shown in brackets if accessible. Statistics include number of months with observations (N), Bias, RMSD, and r^2. $\sigma^t_{A_T}$ [σ^t_{DIC}] stands for temporal standard deviation from monthly averages of A_T [DIC] observations.

We qualify monthly, $0.25°$ reconstructions of A_T and DIC with ~~measurements from~~ GLODAPv2.2022 data (Lauvset et al., 2022a) for the 37-year period (Table 4 and Fig. 8). The global open-ocean reconstruction scores a RMSD of ~~22.09~~22.1 $\mu mol\,kg^{-1}$ and a r^2 of 0.9 in A_T. Similar numbers are found for DIC (RMSD~~= 22.67~~= 22.7 $\mu mol\,kg^{-1}$ and $r^2 = 0.9$). The model scores the good fit in the open Indian Ocean with RMSD smaller than 15.5 $\mu mol\,kg^{-1}$ and r^2 above 0.92 for both variables. The reconstruction deviates from GLODAP data in the western North Atlantic, subpolar North Pacific, tropics, and nearby major rivers (Fig. 8-abcd).

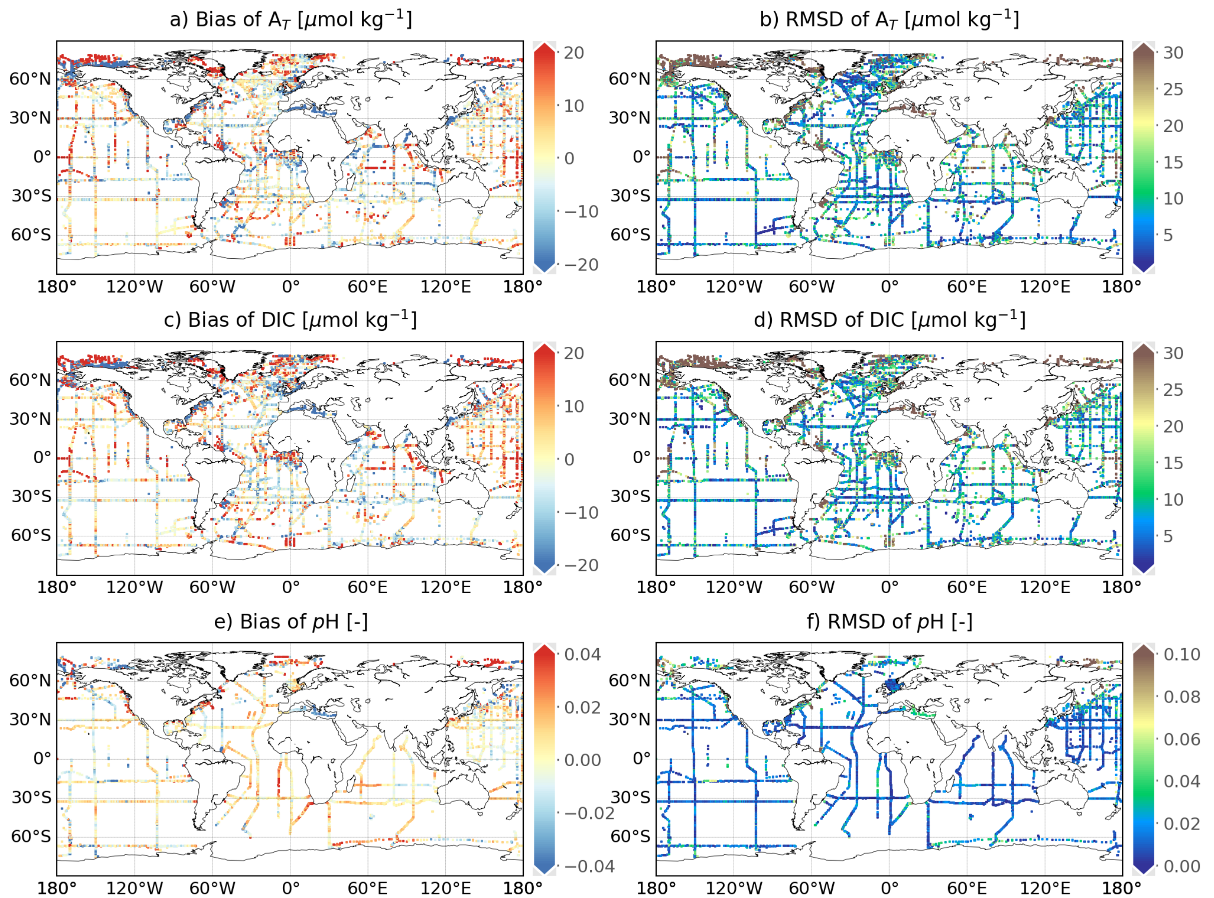

Figure 8. Spatial distribution of reconstruction skills for A_T, DIC, and pH over 1985-2021. Mean model-data difference (Bias) and root-of-mean square-deviation (RMSD) between the reconstruction and GLODAPv2.2022 surface data (0-10 m) at a spatial resolution of $0.25°$. The size of grid cells is scaled upon a better visualization.

A_T and DIC are underestimated in the continental shelves of north Alaska and the northeastern Atlantic, the Mediterranean Sea, South China Sea, and nearby river plumes (Fig. 8-ac). The Arctic yields the poorest estimations among all the ocean basins with a global RMSD over $100\ \mu\mathrm{mol\,kg}^{-1}$ (Table 4). The prediction probability of variability in A_T [DIC] is relatively large for the open ocean 79% [71%], but rather unsatisfying over the coastal ocean (46% [40%]). Extrapolating these carbonate variables towards the shore remains challenging with much higher errors and uncertainty estimates obtained over the continental shelf compared to the open-ocean reconstruction (Table 4, Figs. 6-cd and . 8-abcd). The coastal-ocean errors are on the order of 10% of the global mean values of A_T and DIC (Table 6).

The reconstruction of A_T distributions relies on LIAR coefficients fit with GLODAPv2 data (Olsen et al., 2016) covering the years before 2015. These data are also part of the latest version GLODAPv2.2022 (Lauvset et al., 2022a). They do therefore not correspond to an independent dataset for the evaluation data of the CMEMS-LSCE reconstruction. To ~~overcome this~~

Table 4. Skill scores computed between CMEMS-LSCE and GLODAPv2.v2022 in A_T, DIC, and pH over the period 1985-2021. Total numbers of data, RMSD (Eq. 10), and r^2 (Eq. 11) are reported for both the open ocean (O) and coastal region (C). Basin identification is shown in Fig. A1.

Basins			Number of data		A_T [μmol kg^{-1}]		DIC [μmol kg^{-1}]		pH [-]	
			A_T-DIC	(pH)	RMSD	r^2	RMSD	r^2	RMSD	r^2
0.	Globe	(O)	10269	(5411)	~~22.09~~ 22.1	0.90	~~22.67~~ 22.7	0.90	0.022	0.70
		(C)	6309	(2080)	~~82.01~~ 82.0	0.72	~~72.39~~ 72.4	0.62	0.060	0.45
1.	Arctic	(O)	103	(26)	~~107.09~~ 107.1	0.79	~~113.28~~ 113.3	0.71	0.106	0.32
		(C)	1635	(300)	~~148.71~~ 148.7	0.46	~~126.77~~ 126.8	0.4	0.107	0.48
2.	Atlantic	(O)	2785	(932)	~~30.10~~ 30.1	0.74	~~28.66~~ 28.7	0.72	0.028	0.58
		(C)	2422	(941)	~~44.50~~ 44.5	0.71	~~39.09~~ 39.1	0.69	0.046	0.45
3.	Pacific	(O)	4539	(3222)	~~13.61~~ 13.6	0.92	~~15.95~~ 16.0	0.92	0.019	0.74
		(C)	1380	(639)	~~28.43~~ 28.4	0.76	~~44.36~~ 44.4	0.45	0.057	0.34
4.	Indian Ocean	(O)	1177	(551)	~~15.05~~ 15.1	0.92	~~13.79~~ 13.8	0.96	0.012	0.90
		(C)	328	(62)	~~16.56~~ 16.6	0.92	~~21.97~~ 22.0	0.90	0.013	0.82
5.	Southern Ocean	(O)	1665	(680)	~~10.96~~ 11.0	0.64	~~13.21~~ 13.2	0.92	0.019	0.68
		(C)	544	(138)	~~22.53~~ 22.5	0.50	~~24.48~~ 24.5	0.77	0.023	0.65

~~limitation~~accomplish a cross-validation, reconstructions of A_T and DIC are compared to observations for ~~Eulerian~~ eight time series stations: AWIPEV, BATS, DYFAMED, ESTOC, ~~and HOT~~HOT, ICELAND, IRMINGER, and KERFIX (see Table 2 and Fig. A1b for data sources and station locations). Table A4 presents the evaluation statistics for all the stations and Figure 7 illustrates the comparison between monthly time series of A_T and DIC extracted from the CMEMS-LSCE datasets and measurements at ~~these long-term monitoring sites. The four stations stand out as~~ the four sustained long-term ~~observation time series for carbonate system variables~~monitoring sites. More than 270 [80] months in the years 1988-2021 [1995-2009 and 1998-2017] include measurements of A_T and DIC at BATS and HOT [ESTOC and DYFAMED]. As shown in Table A4, the Arctic site (AWIPEV) provides 52-month data in 2015-2020 while the three other stations sparsely observed A_T and DIC at the surface layer resulting in fewer than 30 monthly mean data in 2014-2021 (IRMINGER and ICELAND) and 1992-2018 (KERFIX). The reconstructed time series fit monthly averages of in situ measurements well. Mean estimates of A_T [DIC] over the observing period are about ~~2305~~ 2283 [1983] µmol kg^{-1} at ~~HOT~~ KERFIX [HOT] to 2420 [~~2129~~2219] µmol kg^{-1} at DYFAMED [AWIPEV]. At all the stations (DYFAMED and AWIPEV excepted) and for the two variables, model-observation misfit is small (Bias ~~< 10~~< 11 µmol kg^{-1}, RMSD ~~< 13~~< 14 µmol kg^{-1}) relative to the aforementioned mean estimates (Table A4). The highest offset between the CMEMS-LSCE estimation and observations for all the stations is found at DYFAMED (A_T: -145.1 µmol kg^{-1}, DIC: ~~-124.69~~-124.7 µmol kg^{-1}). DYFAMED provides long-term time series of A_T and DIC measurements in the Northwestern Mediterranean Sea (Fig. A1b). Salinity and alkalinity have substantial values due to the net evaporation (Coppola et al., 2020). The average of A_T in the Mediterranean Sea exceeds that for the global ocean by 10%

(Palmiéri et al., 2015). These characteristics set the Mediterranean Sea aside from the ocean basins. Although the bias between reanalysed SSS and observations (Fig. A10) is relatively small, LIAR (Carter et al., 2018) was trained on GLODAPv2 (Olsen et al., 2016) including ~~a~~ only few observations in this area. The distinct relationship between alkalinity and salinity prevailing in the Mediterranean Sea is likely not reproduced by LIAR leading to an underestimation of A_T and a systematic bias to DIC at DYFAMED (Fig. 7). ESTOC is located close to the North Atlantic east coast and under the influence of the Canary Current System (CCS, Fig. A1). Spatial gradients and temporal variability are higher in the CCS (Fig. 2c) compared to BATS and HOT which are both located in the center of subtropical gyres. ~~The lowest prediction skill of temporal variability is obtained for ESTOC~~Despite showing good estimates of A_T and DIC in RMSD at ESTOC, temporal variability of observations are reconstructed with the lowest r^2 (Table A4). Particularly, seasonality to multi-year variations in DIC are predicted at $r^2 = 0.47$ for ESTOC compared to $r^2 > 0.7$ for AWIPEV, ICELAND, IRMINGER, BATS and HOT. Over all the stations, the model underestimates temporal changes of A_T (Fig. 7a; BATS: $r^2 = 0.33$, DYFAMED: $r^2 = 0.12$, ESTOC: $r^2 = 0.03$, HOT: $r^2 = 0.32$) which can be attributed to the large discrepancy in variability between in situ measurements and the CMEMS time series of salinity (Fig. A10a; BATS: $r^2 = 0.33$, DYFAMED: $r^2 = 0.19$, ESTOC: $r^2 = 0.03$, HOT: $r^2 = 0.35$). Model uncertainty (1σ-envelop) of monthly A_T and DIC estimates (Fig. 7a) is also inflated somewhat proportional to the CMEMS salinity product uncertainty (Fig. A10a).

5.3 Surface ocean pH and saturation state with respect to carbonate minerals

Surface ocean pH and saturation states with respect to aragonite (Ω_{ar}) and calcite (Ω_{ca}) are critical indicators used to measure ocean acidification. This section first presents an overall evaluation of these variables. We then introduce estimates involved in the monitoring of ocean acidification in 1985-2021 as an essential application of the CMEMS-LSCE surface ocean carbon product.

5.3.1 General analysis and evaluation

The spatial distribution of surface ocean pH reported on total hydrogen ion (H^+) scale is shown in Fig. 9 (the corresponding figure for H^+, Fig. A4, is included in the supplementary). Both temporal means of the best model estimate and 1σ-uncertainty of pH share spatial patterns with $p\mathrm{CO_2}$ (Fig. 1). Variables pH and $p\mathrm{CO_2}$ correlate closely through equilibrium relationships of dissolved CO_2 in seawater: an increase in $p\mathrm{CO_2}$ generally corresponds to a decrease in pH. The distribution of the climatological mean of pH displays a gradient with latitude between 8.03 and 8.11 pH units across most of the basins (Fig. 9a). Values of pH below 8 are associated with the upwelling of CO_2-rich waters (e.g., Eastern Equatorial Pacific, Western Arabian Sea). pH exceeds 8.15 in sub- and polar cold surface water and in the regions with high biological productivity (e.g. Labrador Sea, Nordic Seas, Southern Ocean between 35°S-50°S).

The saturation state of surface ocean waters with respect to calcium carbonate minerals aragonite and calcite is defined as the ratio of the product of the concentrations of calcium ions (Ca^{2+}) and carbonate ions (CO_3^{2-}) to the solubility of the respective calcium carbonate mineral ($\mathrm{CaCO_3}$) in surface seawater~~(Eq. ??)~~. Aragonite being the more soluble polymorph, its degree of saturation (Ω_{ar}) is smaller than that of calcite (Ω_{ca}) (Mucci, 1983). With the exception of this offset, the spatial distributions

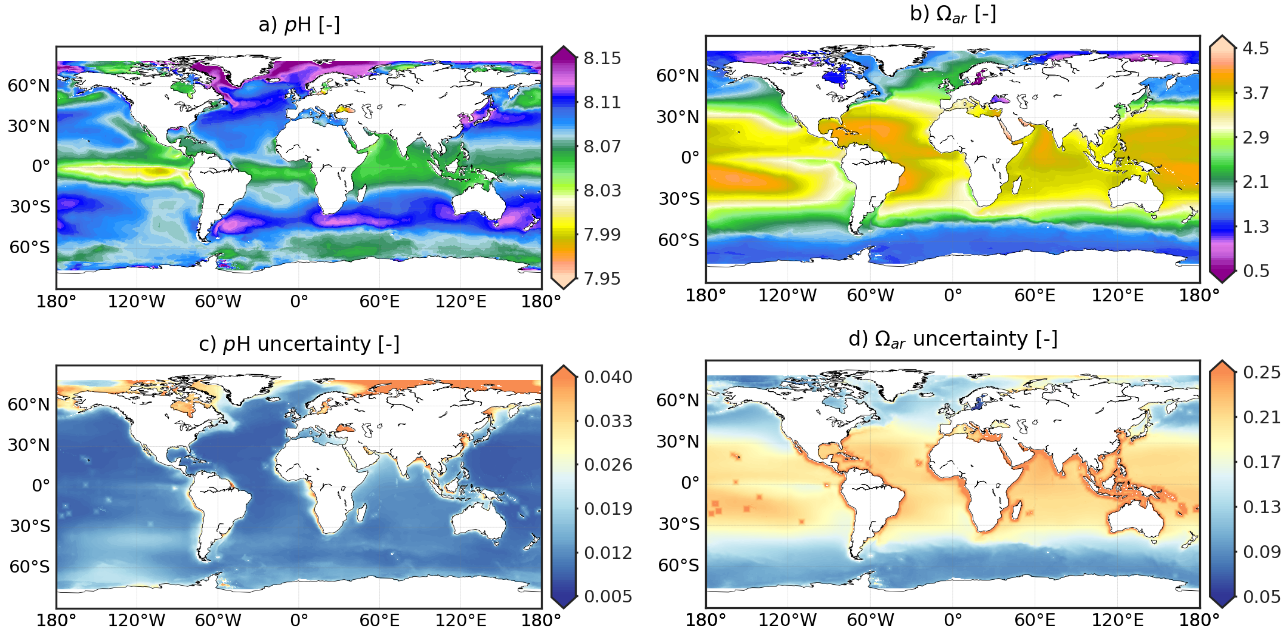

Figure 9. CMEMS-LSCE pH and Ω_{ar} over the global ocean at a spatial resolution of $0.25°$. Temporal means of the model best estimate and 1σ-uncertainty per grid cell over 1985-2021 are calculated by using Eq. (5).

of their climatological means share common spatial patterns over the global ocean (Figs. 9b and A5a). Surface seawater is generally supersaturated, i.e., Ω_{ar} and Ω_{ca} greater than 1. The magnitude of surface ocean calcium carbonate saturation state varies with latitude. Values as large as 3.7-4.5 [5-7] for aragonite [calcite] are reconstructed in subtropical and tropical regions. Ω_{ar} and Ω_{ca} decrease toward the poles. In the Southern Ocean, surface seawater enriched in CO_2 from vertical mixing has Ω_{ar} [Ω_{ca}] values in the range of 1.5-2.1 [2-3.4]. Low saturation states are also computed in the Arctic and for waters of upwelling regimes (Fig. 9b). Locally Ω_{ar} drops below 1.3, and even fall under the $CaCO_3$ dissolution threshold of 1 (Gattuso and Hansson, 2011) in the Arctic water runoff and Baltic sea.

The uncertainty (1σ) of pH, Ω_{ar}, and Ω_{ca} propagated the speciation of the CO_2 system takes into account the ensemble spread of $p$$CO_2$ estimates and analysis errors of other variables (Sect. 3.3). Monthly pH uncertainty estimates fall in the 95% confidence interval of $[0.008, 0.036]$ with a global mean value of 0.011. These estimates are in close agreement with the global uncertainty between 0.01-0.022 pH units calculated by Jiang et al. (2019), Iida et al. (2021), and Gregor and Gruber (2021). pH uncertainty is typically larger than 0.03 in the Arctic and in coastal regions (Figs. 9c). In contrast, the reconstructions of Ω_{ar} and Ω_{ca} are subject to high uncertainty ($\sigma > 0.175$) between 30°S-30°N (Fig. 9d and A5b). Regarding the σ-to-μ ratio, mean uncertainty estimates per cell for the saturation states in the (sub-) tropical band are relatively small compared to the mean of the best monthly estimates (Figs. A9-ef). The Arctic and the coastal oceans remain the regions with largest reconstruction uncertainties for Ω_{ar} and Ω_{ca}, as well as for $p$$CO_2$ and pH (Figs. A9-ab). Excluding these regions, $R(\sigma, \mu)$ (Eq. 8) is less than 0.3% for pH and 8% for Ω_{ar} and Ω_{ca}.

The monthly CMEMS-LSCE reconstruction at $0.25°$ resolution is assessed against pH measurements from GLODAPv2.2022 bottle data (Table 2). For the period 1985-2021, the global RMSD amounts to 0.022 [0.060] pH units and r^2 scores at 0.70 [0.45] over the open [coastal] ocean (Table 4). Model bias lies within $[-0.01, 0.01]$ pH units and RMSD is below 0.02 pH units over the open ocean, except for high latitudes over $60°$ (Figs. 8-ef). At local scale, the ~~eight coastal~~ time series from Sutton et al. (2019) are used for further evaluation (Tables A2 and A3). There exists much ~~less~~ fewer evaluation data for pH than for pCO$_2$, e.g., only 2 months of monitoring pH at COASTALLA and FIRSTLANDING ~~(Table A3). Monthly time series of CMEMS-LSCE~~ or devoid of pH ~~are coherent with these~~ measurements at equatorial observing systems. CMEMS-LSCE reconstructs pH ~~measurements (Tables A2 and A3). Measurement uncertainty of pH at these coastal sites is reported to be around 0.02~~ over the open ocean with rather high scores, e.g., at BOBOA (RMSD $= 0.011$ and $r^2 = 0.71$) and KEO (RMSD $= 0.014$ and $r^2 = 0.86$). Referring to the eight coastal sites evaluated for p~~H units.~~ CO$_2$ in Section 5.1, RMSD can be as small as 0.035 and 0.04 pH units at CCE2 and GRAYSREEF while it is over 0.05 pH units at the other stations (e.g., COASTALLA: 0.068, CAPEARAGO: 0.069). Similar to the pCO$_2$ time series (Fig. 5, Sect. 5.1), pH has been monitored with low sampling frequency (roughly ~~a~~ few days in the tracking month) and the temporal sampling deviation of instantaneous observations from monthly averages ($\sigma^t_{p\mathrm{H}}$) is significant. This temporal sampling uncertainty of pH contributes to the mismatch between model estimates and observations. For example, $\sigma^t_{p\mathrm{H}}$ amounts to 0.048 pH units at CCE2 and 0.020 pH units at GRAYSREEF, and reaches highest values of 0.078 pH units at COASTALLA and 0.086 pH units at CAPEARAGO. Although model-observation misfit and model uncertainty remain high over the coastal sector (see also Figs. 8-ef and 9c), their estimates do not surpass 1% of the global mean pH (8.082). The reconstructed pH time series reproduce measurement variability with relatively high correlation, r^2 in ~~$[0.21, 0.69]$~~ $[0.21, 0.94]$, that reinforces the reliability of CMEMS-LSCE pH data.

5.3.2 Ocean acidification: key features from global to local scales

The monthly, $0.25°$ CMEMS-LSCE datasets of pH, Ω_{ar}, and Ω_{ca} are at the basis of of two CMEMS ocean indicators monitoring surface ocean acidification from 1985 to 2021: (1) annual global means and (2) global trend maps.

In Fig. 10, we present annual global means of surface ocean pH and saturation states for aragonite (Ω_{ar}). An illustration of calcite (Ω_{ca}) is provided in the Appendix (Fig. A13a). For each variable, the calculation of annual global area-weighted means of best estimates (line) and 1σ-uncertainties (envelope) follows Eq. (7). The trends reported in the legend result from linear least-squares regression on annual global means of 100-ensembles of the carbonate system variables. These ensembles are generated with Gaussian distribution having the mean and variance as best model estimate μ and squared uncertainty (σ^2) at monthly time steps and $0.25°$-grid cells, respectively. pH decreases from 8.110 ± 0.017 in 1985 to 8.049 ± 0.014 in 2021 with a descend rate of -0.017 ± 0.004 decade^{-1}. Similar trends are found for the surface ocean saturation states with respect to calcium carbonate minerals. The global mean estimates of Ω_{ar} [Ω_{ca}] amount to 3.141 ± 0.198 [4.807 ± 0.302] and 2.862 ± 0.174 [4.372 ± 0.266] for the open and coastal oceans. The saturation state declines at a rate of -0.080 ± 0.029 decade^{-1} with respect to aragonite while the reduction is steeper for calcite (-0.114 ± 0.045 decade^{-1}).

Global trend maps of surface ocean pH, Ω_{ar}, and Ω_{ca} over the entire period are illustrated in Figs. 11 and A13b. Linear least-squares regression is used to estimate secular trends at every $0.25°$-grid cell. The linear fits of each variable against time rely on

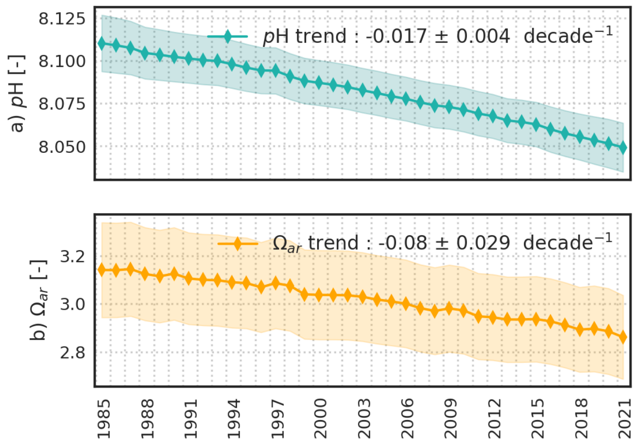

Figure 10. Yearly global area-weighted mean of surface seawater pH reported on total scale (a) and surface ocean saturation states with respect to aragonite (b). Global means of the best estimate (μ, plain line) and of uncertainty (σ, envelop) are computed with Eq. (7a). Trend and uncertainty in the legend are computed with linear regressions on the 100-member ensemble of yearly global means for each variable.

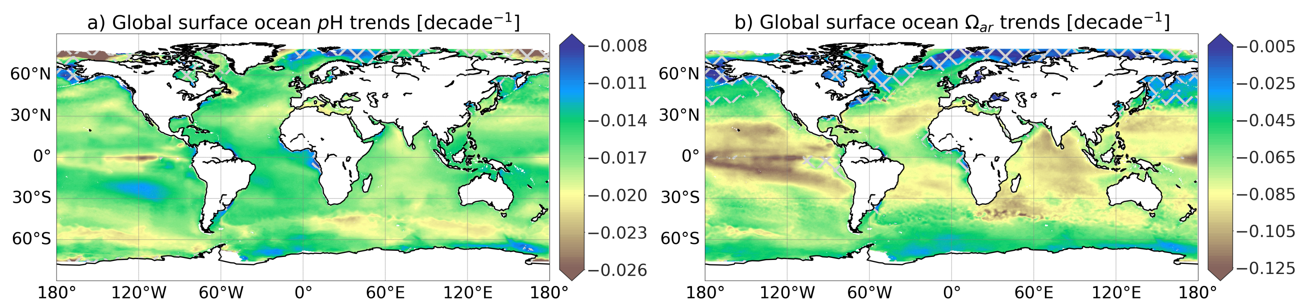

Figure 11. Global trend maps of surface seawater pH reported on total scale (a) and surface ocean saturation states with respect to aragonite (b). Linear trend of CMEMS-LSCE pH and Ω_{ar} is estimated per $0.25°$-grid cell over 1985-2021. Cross-hatching covers the regions ~~where~~ with uncertainty over 10% [20%] of pH [Ω_{ar}] trend estimates.

the 100-member ensemble generated with the best estimates and propagated uncertainties of pH, Ω_{ar}, and Ω_{ca} (see Figs. A14 for examples). Regression slope and residual standard deviation estimates are defined as linear trend and uncertainty of pH, Ω_{ar}, and Ω_{ca}. Hatched area represents pH [Ω_{ar} and Ω_{ca}] trend estimates (μ) with highest uncertainties (σ), i.e., σ-to-μ ratio (Eq. 8) above 10% [20%]. These regions include a portion of the Arctic, Antarctic, equatorial Pacific, and coastal ocean (Figs. 11, A11, and A12). 95% of pH trend estimates over the global ocean is in the range of $[-0.022, -0.012]$ decade^{-1} (Fig. 11a). In the broad open ocean of the tropics and subtropics, pH has been declining around -0.018 decade^{-1} to -0.012 decade^{-1}. Faster decrease rates are found in the Indian Ocean and Southern Ocean with values between -0.022 and -0.018 decade^{-1}. Fastest reductions are computed for the eastern equatorial Pacific and the Arctic with rates exceeding -0.025 decade^{-1}. A similar magnitude of pH trends over these regions is also found in (Lauvset et al., 2015; Leseurre et al., 2022; Ma et al., 2023). The spatial distribution of saturation states with respect to calcium carbonate minerals generally shows the opposite latitudinal pattern (Figs. 11b and A13b). The magnitude of Ω_{ar} [Ω_{ca}] trends over the 30°S-30°N band can be as large as $-0.086\ \mathrm{decade}^{-1}$ [$-0.134\ \mathrm{decade}^{-1}$] to the greatest extent of $-0.186\ \mathrm{decade}^{-1}$ [$-0.275\ \mathrm{decade}^{-1}$] (e.g., eastern equatorial Pacific). Trends of Ω_{ar} and Ω_{ca} computed in polar and subpolar northern hemisphere regions are not significant.

Table 5. Secular trend estimates of pH and Ω_{ar} at seven time-series stations (Bates et al., 2014). Trend and uncertainty estimates are reported as $\mu \pm \sigma$. Monthly time series in the CMEMS-LSCE datasets are extracted at the grid box nearest to each station location (Fig. A1b). For the first three stations, this study calculates linear trends starting in the year 1985. Brackets show values computed over the full period 1985-2021.

Stations	Coordinates	Time span	pH trend [decade^{-1}]		Ω_{ar} trend [decade^{-1}]	
			Bates et al. (2014)	This sudy	Bates et al. (2014)	This sudy
1. Iceland Sea	68.00°N 12.66°W	1983-2012	-0.014 ± 0.005	-0.010 ± 0.001 (-0.014 ± 0.001)	-0.018 ± 0.027	-0.013 ± 0.011 (-0.025 ± 0.008)
2. Irminger Sea	64.30°N 28.00°W	1983-2012	-0.026 ± 0.006	-0.014 ± 0.001 (-0.016 ± 0.001)	-0.080 ± 0.040	-0.006 ± 0.011 (-0.039 ± 0.009)
3. BATS	32.00°N 64.00°W	1983-2012	-0.017 ± 0.001	-0.014 ± 0.001 (-0.016 ± 0.001)	-0.095 ± 0.007	-0.079 ± 0.016 (-0.074 ± 0.010)
4. ESTOC	29.04°N 15.50°W	1995-2012	-0.018 ± 0.002	-0.018 ± 0.002 (-0.019 ± 0.001)	-0.115 ± 0.023	-0.103 ± 0.031 (-0.089 ± 0.011)
5. HOT*	22.75°N 158.00°W	1988-2012	-0.016 ± 0.001	-0.016 ± 0.001 (-0.019 ± 0.001)	-0.084 ± 0.011	-0.100 ± 0.020 (-0.102 ± 0.011)
6. CARIACO*	10.50°N 64.66°W	1995-2012	-0.025 ± 0.004	-0.017 ± 0.003 (-0.018 ± 0.001)	-0.066 ± 0.028	-0.059 ± 0.053 (-0.099 ± 0.018)
7. Munida	45.70°S 171.50°E	1998-2012	-0.013 ± 0.003	-0.017 ± 0.002 (-0.017 ± 0.001)	-0.085 ± 0.026	-0.088 ± 0.032 (-0.070 ± 0.009)

*Stations with direct observations of pH.

Trend estimates derived from reconstructions of pH and Ω_{ar} are evaluated at seven time series stations (Bates et al., 2014) in Table 5. Time series locations are shown in Fig. A1b. With the exception of CARIACO and HOT ~~excepted~~ for which pH measurements are available, long-term trend estimates by Bates et al. (2014) rely on time series of pH and Ω_{ar} calculated via speciation from measurements of A_T and DIC. ~~A~~ 100-member ~~ensemble~~ ensembles of monthly time series of pH and Ω_{ar} are extracted from the 0.25°-grid box nearest to each monitoring station. Linear least-squares regression is then used to infer estimates of their secular trends and associated uncertainties (see Fig. A14 for illustration). Trend estimates derived from CMEMS-LSCE reconstructions at HOT, BATS, ESTOC, and Munida are in line with previous studies for both pH and Ω_{ar} (Dore et al., 2009; González-Dávila and Santana-Casiano, 2009; Bates et al., 2014). The magnitude of the trend estimate at Irminger Sea for 1985-2012 (pH: $-0.014 \pm 0.001\ \mathrm{decade}^{-1}$, Ω_{ar}: $-0.006 \pm 0.011\ \mathrm{decade}^{-1}$) is smaller than that determined by Bates et al. (2014). However, the CMEMS-LSCE pH trend is consistent with the estimate by Pérez et al. (2021)

(-0.017 ± 0.002 decade^{-1}). Moreover, 1σ-uncertainty reported for both pH and Ω_{ar} trend estimates by Bates et al. (2014) is large at this station (pH: -0.025 ± 0.006 decade^{-1}, Ω_{ar}: -0.080 ± 0.040 decade^{-1}) highlighting the associated uncertainty. Long-term trends of pH and Ω_{ar} are also under-estimated at the Iceland Sea monitoring site, but the bias is not as large as at Irminger Sea (Table 5). Low data sampling frequency at these two stations (Table 1, Bates et al., 2014) could be on account of trend estimate deviation. At CARIACO, the CMEMS-LSCE time series yields a decrease in Ω_{ar} of -0.059 ± 0.053 decade^{-1}, relatively close to Bates et al. (2014) (-0.066 ± 0.028 decade^{-1}). The decrease in pH derived from CMEMS-LSCE is, however, larger than in Bates et al. (2014).

6 Summary ~~Conclusions and Discussion~~

This study presents the CMEMS-LSCE product, a dataset of six carbonate system variables (Table ~~??~~6) covering the global surface ocean at a spatial resolution of 0.25° for every month in the period 1985-2021 (444 months). Datasets of individual carbonate system variables are built on the combination of the three methods. First, we adapt an ensemble of 100 feed-forward neural network models (CMEMS-LSCE-FFNN, Chau et al., 2022b) to estimate surface ocean partial pressure of CO_2 (pCO_2) at the pre-defined data resolution. Second, the high-resolution total alkalinity (A_T) reconstruction is obtained by using locally interpolated alkalinity regression (LIAR, Carter et al., 2016, 2018). Finally, surface ocean pH, total dissolved inorganic carbon (DIC), and saturation states with respect to aragonite (Ω_{ar}) and calcite (Ω_{ca}) are calculated with the carbonate system speciation software (CO2SYS, Lewis and Wallace, 1998; Van Heuven et al., 2011; Orr et al., 2018), given the global monthly reconstructions of pCO_2 and A_T and other environmental input data (Sect. 3). Results are 2D-fields of the best estimate and associated uncertainty (1σ) of carbonate system variables available at each grid box of $1\text{month} \times 0.25° \times 0.25°$. 1σ-uncertainty is referred to as the ensemble standard deviation of 100 FFNN outputs for pCO_2 while it is propagated through the processing chain of LIAR and CO2SYS taking into account different uncertainty sources of input parameters for other variables.

Multiple observation-based datasets, which are not used for the CMEMS-LSCE reconstructions at monthly and 0.25° resolutions, serve as benchmarks in the assessments of product quality from global to local scales (e.g., Tables 3, 4, and A3; Figs. 2-5 and 7-8). A summary of the primary statistics for all the six carbonate variables is presented Table 6. Over the full period 1985-2021, CMEMS-LSCE yields global RMSDs of ~~14.29~~14.3 µatm and ~~27.55~~27.6 µatm in comparison with SOCATv2022 pCO_2 for the open and coastal oceans, respectively. Temporal variability of observation-based data is well reproduced with r^2 of 0.83 for the open ocean and 0.74 for the coastal domain. In comparison to CMEMS-LSCE at monthly and 1° resolutions (Chau et al., 2022b), the reconstructions over coastal areas are improved at higher resolution~~(Figs. 2-4). Furthermore, the~~. The monthly, 0.25° reconstruction outperforms its 1° counterpart in reproducing horizontal and temporal gradients of pCO_2 over a variety of oceanic regions as well as at nearshore time series stations (Figs. 2-5). Evaluations with GLODAPv2022 bottle data and time series stations results in good reconstruction skills for A_T, DIC, and pH at monthly and 0.25° resolutions (Tables 4 and A3, Figs. 7 and 8). At the global scale, the open-ocean reconstruction scores a RMSD smaller than 23 µmol kg^{-1} and a r^2 of 0.9 in A_T and DIC. The model-observation deviation is higher in the coastal zone. However, it does not exceed 5% of the global mean values and r^2 is above 0.6 for both coastal A_T and DIC. Regarding pH, the CMEMS-LSCE reconstruction provides estimates with RMSD$= 0.022$ [0.060] and $r^2 = 0.7$ [0.45] over the open [coastal] ocean. From the statistics in Tables 3 and 4, the Indian Ocean and the Southern Ocean have poor data density (Fig. A2) but generally show the best global reconstruction among the ocean basins. Thus, model evaluation with different numbers of observation data might not reflect a fair comparison of skill scores (e.g., RMSD and r^2) between regions. Data density is much higher in the Arctic, Atlantic, and Pacific than in the Indian and Southern Oceans. The increased data density reveals stronger spatio-temporal variability, for instance, related to coastal dynamics or upwelling than resolved in the two latter basins. RMSD and r^2 computed on the lower data variability result in better model scores.

The spatial distribution of long-term mean 1σ-uncertainty estimates (Figs. 1b, 6cd, and 9cd) indicates higher confidence levels for open-ocean estimates than over the coastal sector. The evaluation of temporal mean 1σ-uncertainty estimates relative to climatological mean values μ (Figs. 1a, 6ab, and 9ab) results in σ-to-μ ratio (Eq. 8) below 5% and 8% for $p\mathrm{CO_2}$ and Ω_{ar}, 2% for $\mathrm{A_T}$ and DIC, and 0.4% for pH over the open ocean (Fig. A9). The σ-to-μ ratio reaches values as high as 10% to 20% for $p\mathrm{CO_2}$ and Ω_{ar} in the coastal domain. The global mean of open-ocean 1σ-uncertainty estimates (Eq. 7a) for CMEMS-LSCE $p\mathrm{CO_2}$ (~~8.48~~8.5 µatm), $\mathrm{A_T}$ (~~16.66~~16.7 µmol kg^{-1}), DIC (~~15.75~~15.8 µmol kg^{-1}), pH (0.011), and Ω_{ar} (0.180) are in line with those reported by previous studies despite being derived from different statistics. For instance, Iida et al. (2021) calculated 1σ-uncertainty based on the median absolute deviation of regression model fits from open-ocean observations. Their approach yielded global σ-averages of 17.8 µatm, 11.5 µmol kg^{-1}, 0.018, and 0.110 for $p\mathrm{CO_2}$, normalized DIC, pH, and Ω_{ar}, respectively. In Gregor and Gruber (2021), the authors propagated the sum squared errors (global RMSD and measurement uncertainties) of $p\mathrm{CO_2}$ (15 µatm) and $\mathrm{A_T}$ (22 µmol kg^{-1}) obtaining global uncertainty estimates of 19 µmol kg^{-1} in DIC and 0.022 in pH. Mean uncertainty estimates over the coastal region are on the order of twofold that computed for the open ocean for these four variables (Table 6), corroborating results by Gregor and Gruber (2021) (Fig. 7).

Table 6. Summary in global evaluation statistics for CMEMS-LSCE surface ocean carbonate system datasets at monthly, 0.25° resolutions over the period 1985-2021. μ and σ stand for the global area-weighted means of monthly best estimates and 1σ-uncertainties for each variable (Eq. 7). RMSD (Eq. 10) and r^2 (Eq. 11) are computed with SOCATv2022 for $p\mathrm{CO_2}$ and GLODAPv2.2022 for pH, $\mathrm{A_T}$, and DIC. The division between the coastal (C) and open (O) oceans is at 400 km on a distance from the shore line (Fig. A1a).

Variables	Standard names	Units	Sector	μ	σ	RMSD	r^2
1. $p\mathrm{CO_2}$	Partial pressure of $\mathrm{CO_2}$ in surface seawater	µatm	(O)	~~364.48~~364.5	~~8.48~~8.5	~~14.29~~14.3	0.83
			(C)	~~359.35~~359.4	~~17.10~~17.1	~~27.55~~27.6	0.74
2. $\mathrm{A_T}$	Total alkalinity in surface seawater	µmol kg^{-1}	(O)	~~2305.78~~2305.8	~~16.66~~16.7	~~22.09~~22.1	0.90
			(C)	~~2263.02~~2263.0	~~38.36~~38.4	~~82.01~~82.0	0.72
3. DIC	Surface ocean dissolved inorganic carbon	µmol kg^{-1}	(O)	~~2031.12~~2031.1	~~15.75~~15.8	~~22.67~~22.7	0.90
			(C)	~~2008.65~~2008.7	~~33.40~~33.4	~~72.39~~72.4	0.62
4. pH	Surface seawater pH reported on total scale	-	(O)	8.082	0.011	0.022	0.70
			(C)	8.082	0.021	0.060	0.45
5. Ω_{ar}	Saturation state for surface seawater with respect to aragonite	-	(O)	3.059	0.180	-	-
			(C)	2.864	0.206		
6. Ω_{ca}	Saturation state for surface seawater with respect to calcite	-	(O)	4.674	0.275	-	-
			(C)	4.384	0.314		

Our high-resolution carbon data product opens the door to various analyses of the marine carbonate system from global to local scale. This study exemplifies an application of the data for monitoring ocean acidification over recent years. The monitoring indicators derived from the monthly, $0.25°$ surface ocean CMEMS-LSCE product consist of (1) yearly global means of surface ocean pH and saturation states with respect aragonite Ω_{ar} and calcite Ω_{ca} and (2) global maps of multi-annual trends of surface ocean pH, Ω_{ar}, and Ω_{ca} (Figs. 10, 11, and A13). In 1985, the global mean surface ocean pH was 8.110 ± 0.017. It was 8.049 ± 0.014 in 2021 (Fig. 10a). Over the same 37-year time period, Ω_{ar} decreased from 3.141 ± 0.198 to 2.862 ± 0.174 (Fig. 10b). The rate of decline of surface ocean pH and Ω_{ar} was respectively $-0.017 \pm 0.004\ \mathrm{decade}^{-1}$ and $-0.080 \pm 0.029\ \mathrm{decade}^{-1}$ since 1985 (see also results for Ω_{ca} in Sect. 5.3.2). Estimates of pH trend lie between $[-0.022, -0.012]\ \mathrm{decade}^{-1}$ across most of the open ocean (Fig. 11a). In general, surface ocean pH decreased more rapidly in the Indian Ocean and Southern Ocean than the tropics and subtropics. These findings are in close agreement with the suggestions by Lauvset et al. (2015) and Ma et al. (2023) but future studies would need to include analyses of underlying drivers to provide insight into regional differences in pH changes. By contrast, the greatest reduction in surface ocean saturation states (Fig. 11b) was computed for the two latter regions. The global trend maps of pH and Ω_{ar} highlight the Eastern Equatorial Pacific as one of the vulnerable regions with respect to ocean acidification. In this area, the decline rate of pH exceeds $-0.025\ \mathrm{decade}^{-1}$ and $-0.186\ \mathrm{decade}^{-1}$ for Ω_{ar}. The comparison of multi-annual trends of pH and Ω_{ar} at time series stations (Table 5 and Fig. A14) highlighted the consistency between CMEMS-LSCE estimates and previous studies (Dore et al., 2009; González-Dávila and Santana-Casiano, 2009; Bates et al., 2014; Pérez et al., 2021). For most of these sites, the trends evaluated for 1985-2021 are greater than those relative to the sub-period before the year 2012. The faster rate of ocean acidification over the full period compared to the pre-2012 probably reflects a steeper acceleration in ocean uptake of anthropogenic CO_2 in the last decade. The global maps of CMEMS-LSCE pH, Ω, and their trend estimates would be potential indicators for ocean acidification along with the SDG 14.3.1 - "Average marine acidity (pH) measured at agreed suite of representative sampling stations" (https://sdgs.un.org/goals/goal14: last access 31/07/2023).

The production chain of CMEMS-LSCE carbonate system variables will be maintained and further improvements with the aim to reduce model-observation misfit and improve the quantification of model uncertainty are on the way forward. Being at the core of the chain, model upgrades of CMEMS-LSCE-FFNN will be tackled first. At the time, SOCAT does not provide open-ocean data of CO_2 fugacity gridded at monthly, $0.25°$ resolutions. Our ensemble-based approach draws thus on two SOCATv2022 data sources: a "downscaled" version of the $1°$-open-ocean data and the $0.25°$-coastal-ocean data (see Sect. 2.1). Open-ocean SOCAT datasets gridded at finer regular resolutions (if accessible) will be updated to gain more accuracy in our model fitting. Selections of data products for predictors needed for model input are equally important. For instance, the CMEMS SSS product used here results in a globally good reconstruction of total alkalinity (Table 4). However, the temporal variability in CMEMS SSS data does not match that in observations (Fig. A10) and this feature is retained in time series of total alkalinity (Fig. 7). Despite best efforts in determining overall product uncertainty in estimates of carbonate system variables, part of input uncertainty is still not taken into account or only partially quantified due to lack of time-space varying uncertainty fields associated with predictor variables (e.g. SSH, Chl-a, MLD, nutrient concentrations). Moreover, temporal sampling bias in pCO_2 and pH is likely to contribute to deviations between observations and model output (Fig. 5 and Table A3). The total ~~measurement~~ analytical error uncertainty should be considered with great care during reconstruction and model output evaluation.

The CMEMS-LSCE approach leads as the first series of long-term reconstructions of $p\mathrm{CO_2}$, $p\mathrm{H}$, $\mathrm{A_T}$, DIC, Ω_{ca} and Ω_{ar} extending seamlessly from the global open ocean to coastal regions at monthly, $0.25°$ resolutions. Future use cases recommended for this high-resolution product include (1) estimation of monthly to interannual variations, long-term trends of carbonate system variables, as well as of air-sea $\mathrm{CO_2}$ exchanges at the surface layer from local scale to large ocean basins, (2) analyses in interactions between these variables and effects of other physical and biogeochemical factors on ocean acidification and changes in the marine carbonate system, (3) assessments of horizontal and temporal gradients of carbonate system variables in the coastal-open ocean continuum, (4) evaluation or combination with other model- or observation-based products (e.g., Biogeochemistry Argo, Southern Ocean Carbon and Climate Observations and Modeling), and (5) improvements in coastal reconstructions based on observation system simulation experiments (e.g., with finer spatio-temporal model resolutions). The CMEMS-FFNN surface ocean carbon product at monthly, $0.25°$ resolutions will be accessible through the CMEMS data portal (see Sect. 7).

7 Data availability

The CMEMS-LSCE datasets (netCDF format) of six carbonate system variables have been delivered to the European Copernicus Marine Environment Monitoring Service (CMEMS, Product ID: MULTIOBS_GLO_BIO_CARBON_SURFACE_REP_015_008, DOI: 10.48670/moi-00047). Since November 2022, the product with monthly and $1°$ resolutions is available at the CMEMS portal (Chau et al., 2022a, b). The CMEMS-LSCE data product at monthly and $0.25°$ resolutions proposed in this study will replace its coarser resolution version in due course. For the time being, the high-resolution data product described in this manuscript can be accessed via repository under data DOI: 10.14768/a2f0891b-763a-49e9-af1b-78ed78b16982 (Chau et al., 2023).

Appendix A: ~~Definitions of ocean carbonate system variables~~

~~Chemical reactions of dissolved $\mathrm{CO_2}$ in seawater follow a series of the following equilibria,~~

$$\begin{aligned}
\mathrm{CO_2(g)} &\rightleftharpoons \mathrm{CO_2(aq)},\\
\mathrm{CO_2(aq)+H_2O} &\rightleftharpoons \mathrm{H^+(aq)+HCO_3^-(aq)},\\
\mathrm{HCO_3^-(aq)} &\rightleftharpoons \mathrm{H^+(aq)+CO_3^{2-}(aq)},
\end{aligned}$$

~~where (g) and (aq) stand for a gas or the species in an aqueous solution. $\mathrm{CO_2(aq)}$ refers to the combination of aqueous $\mathrm{CO_2}$ and its weak acid $\mathrm{H_2CO_3}$. $\mathrm{HCO_3^-}$ and $\mathrm{CO_3^{2-}}$ are bicarbonate and carbonate ions.~~

~~Definitions of the essential variables involved in the carbonate system equilibria are on the list below (see in Dickson et al., 2007; Dickso~~

~~.~~

i) ~~Surface ocean pCO_2 is partial pressure of CO_2 in air which is in equilibrium with that in water sample. It is not the same as surface ocean fugacity of CO_2 (fCO_2). pCO_2 can be converted from fCO_2 via~~

$$\underline{pCO_2 = fCO_2 \exp\left(-P\frac{B+2\delta}{RT^*}\right).}$$

~~where P is total atmospheric pressure at surface water, T^* is absolute temperature, R is the gas constant, and B and δ are cross-virial coefficients (Körtzinger, 1999).~~

ii) ~~Seawater pH is a negative logarithmic scale of total concentration of hydrogen ions (H^+) in aqueous solution. Total H^+ is the sum of concentrations of free H^+ and HSO_4 ions. The pH scale typically ranges from 0 to 14. $p\mathrm{H} = 7$ is the threshold specifying whether a water sample is in acidic (i.e., $p\mathrm{H} < 7$) or basic (i.e., $p\mathrm{H} > 7$) conditions.~~

iii) ~~Total alkalinity (A_T) measures the capacity of seawater against acidification. By definition, A_T is total concentration of dissolved alkaline substances corresponding to the ability in H^+ attracting over H^+ releasing. The major contributions to alkalinity includes bicarbonate (HCO_3^-), carbonate (CO_3^{2-}), and hydroxide (OH^-) ions. Total alkalinity can be approximated with~~

$$\underline{A_T =}[\underline{HCO_3^-}]\underline{+2}[\underline{CO_3^{2-}}]\underline{+}[\underline{OH^-}]\underline{-}[\underline{H^+}]\underline{.}$$

iv) ~~Total dissolved inorganic carbon (DIC) is the sum in concentrations of the three primary aqueous species in seawater,~~

$$\underline{\mathrm{DIC} =}[\underline{HCO_3^-}]\underline{+}[\underline{CO_3^{2-}}]\underline{+}[\underline{CO_2(aq)}]\underline{.}$$

v) ~~Calcium carbonate saturation state (Ω) is defined as follows,~~

$$\underline{\Omega = \frac{[Ca^{2+}][CO_3^{2-}]}{K_{sp}},}$$

~~where $[Ca^{2+}]$ is the concentration of dissolved calcium ions and K_{sp} is the solubility of calcium carbonate in seawater. $CaCO_3$ has two principal minerals: aragonite and calcite. Aragonite, which is more soluble than calcite ($\Omega_{ar} < \Omega_{ca}$), is produced by many marine shells and skeletons including corals, pteropods, clams, and mussels. A Ω_{ar} value greater than 1, i.e., preferable conditions in shell formation, indicates supersaturated seawater with respect to aragonite, and vice versa.~~

vi) ~~Revelle factor (RF) measures the buffer capacity for the carbonate system in seawater that decreases as pH increases. Revelle factor is expressed by the ratio between instantaneous changes of dissolved CO_2 $\left(\frac{[\Delta CO_2(aq)]}{[CO_2(aq)]}\right)$ and of DIC $\left(\frac{[\Delta DIC]}{[DIC]}\right)$ in seawater,~~

$$\underline{\mathrm{RF} = \frac{[\Delta CO_2(aq)]}{[CO_2(aq)]}\left(\frac{[\Delta \mathrm{DIC}]}{[\mathrm{DIC}]}\right)^{-1}.}$$

Author contributions. TTTC, FC, and MG developed the CMEMS-LSCE-FFNN model at a quarter-degree resolution. TTTC has prepared script codes and executed the experiments with support from FC in setting and running the model at the HPC resources of TGCC. TTTC, MG, NM, and FC shaped the first manuscript version. All the authors contribute to the manuscript revision.

Competing interests. The author and co-authors have declared that they have no competing interests.

Acknowledgements. This research has been supported by the MOB TAC project of the European Copernicus Marine Environment Monitoring Service (CMEMS) (https://marine.copernicus.eu/about/producers/mob-tac, last access: 14 March 2023). It was granted access to the HPC resources of TGCC under the allocation A0110102201 made by GENCI. The Surface Ocean CO_2 Atlas (SOCAT, www.socat.info, last access: 20 March 2023) is an international effort ~~,~~ endorsed by the International Ocean Carbon Coordination Project (IOCCP), the Surface Ocean Lower Atmosphere Study (SOLAS) and the Integrated Marine Biogeochemistry and Ecosystem Research program (IMBER), to deliver a uniformly quality-controlled surface ocean CO_2 database. The Global Ocean Data Analysis Project (GLODAP, www.glodap.info, last access: 21 August 2023) provides access to ocean surface-to-bottom quality controlled data of carbonate system variables collected through international cruises. We thank Anna Conchon for her help in testing and wrapping LIAR and CO2SYS Matlab toolboxes. We are grateful for constructive comments from two anonymous reviews to refine the manuscript.

Appendix

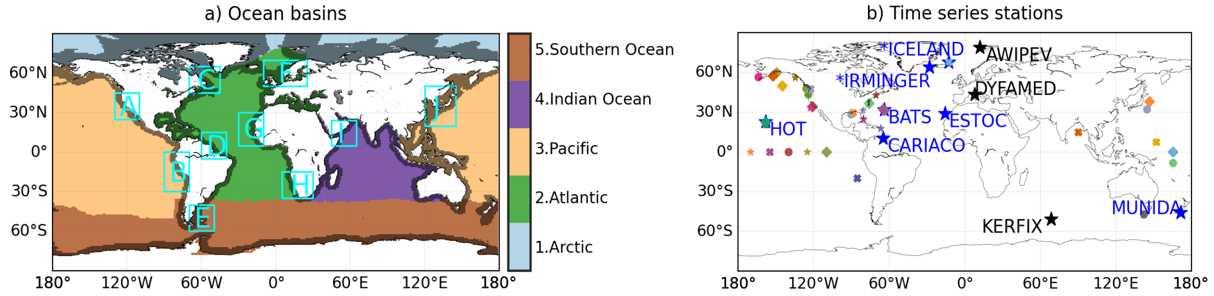

Figure A1. a) Ocean basins (https://github.com/RECCAP2-ocean/RECCAP2-shared-resources/tree/master/data/regions, last access: 11/7/2022): coastal mask (grey, approximately 400 km from the ~~shore line~~shoreline), feature regions ~~analyzed~~ analysed in this study (cyan box, Table A1); b) Location of time series stations recording in situ observations used in data evaluation (Table 2): blue stars ~~(Bates et al., 2014)~~for ocean acidification (Bates et al., 2014), black ~~star (Coppola et al., 2021)~~stars for A_T and DIC (Metzl and Lo Monaco, 1998; Coppola et al., 2021; Gattuso et al., 2023), and other coloured scattered objects ~~(Sutton et al., 2019)~~for pCO$_2$ and pH (Sutton et al., 2019). Asterisk (*) marks the two stations with also A_T and DIC observations (Olafsson et al., 2010) available for assessments.

Table A1. Information of feature regions ~~analyzed~~ analysed in this study (Fig. A1a - cyan boxes).

Notations	Regions	Coordinates	
		Latitude	Longitude
A	California Current System	25°N-45°N	130°W-110°W
B	Humboldt Current System	30°S-0°	90°W-70°W
C	Labrador Sea	45°N-65°N	70°W-45°W
D	Amazon river mouth	5°S-15°N	60°W-40°W
E	Western South Atlantic	60°S-40°S	70°W-50°W
F	Northern Europe	50°N-70°N	10°W-25°E
G	Canary Current System	5°N-30°N	30°W-10°W
H	Benguela Current System	35°S-15°S	5°E-20°E
I	Western Arabian Sea	5°N-24°N	45°E-65°E
J	Sea of Japan	30°N-50°N	120°E-150°E

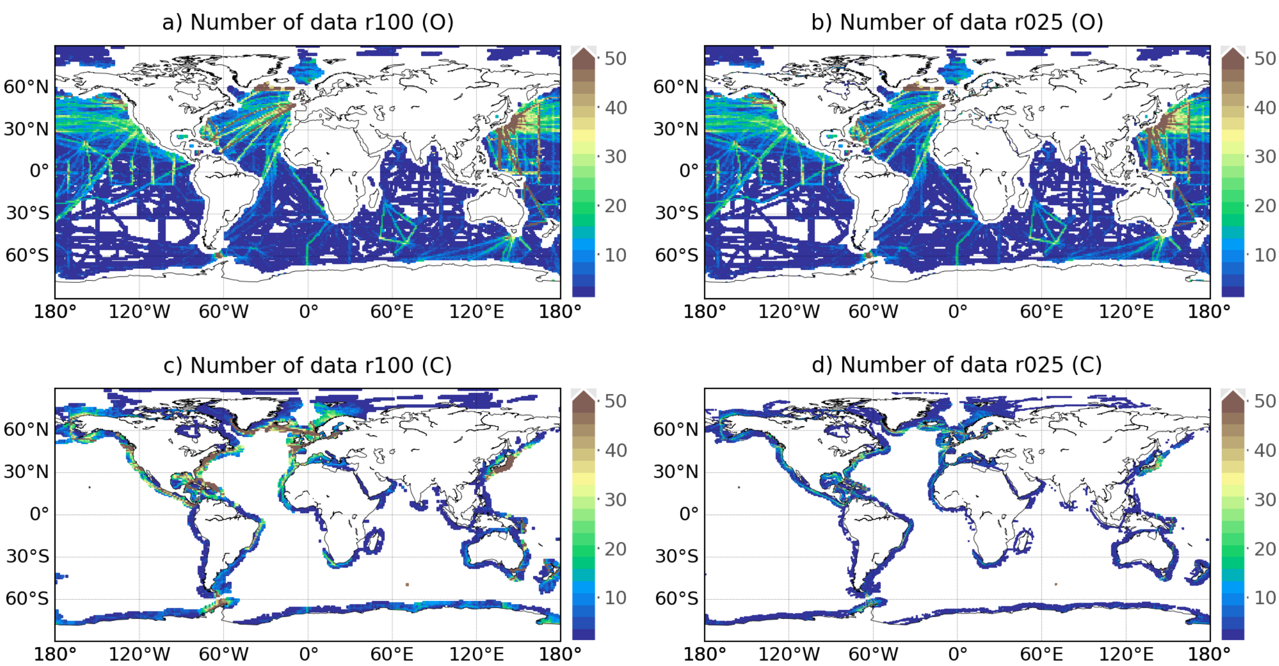

Figure A2. Spatial distribution of total months in 1985-2021 containing SOCATv2022 gridded data. Left: 1°-data product (r100), right: 0.25°-data product (r025). Open-ocean data (O) in each 0.25°-grid box is created by setting conservatively the open-ocean SOCATv2022 data at the 1°-grid box containing it. The coastal-ocean SOCATv2022 data (C) are assigned within 400 km from the shoreline (Fig. A1a).

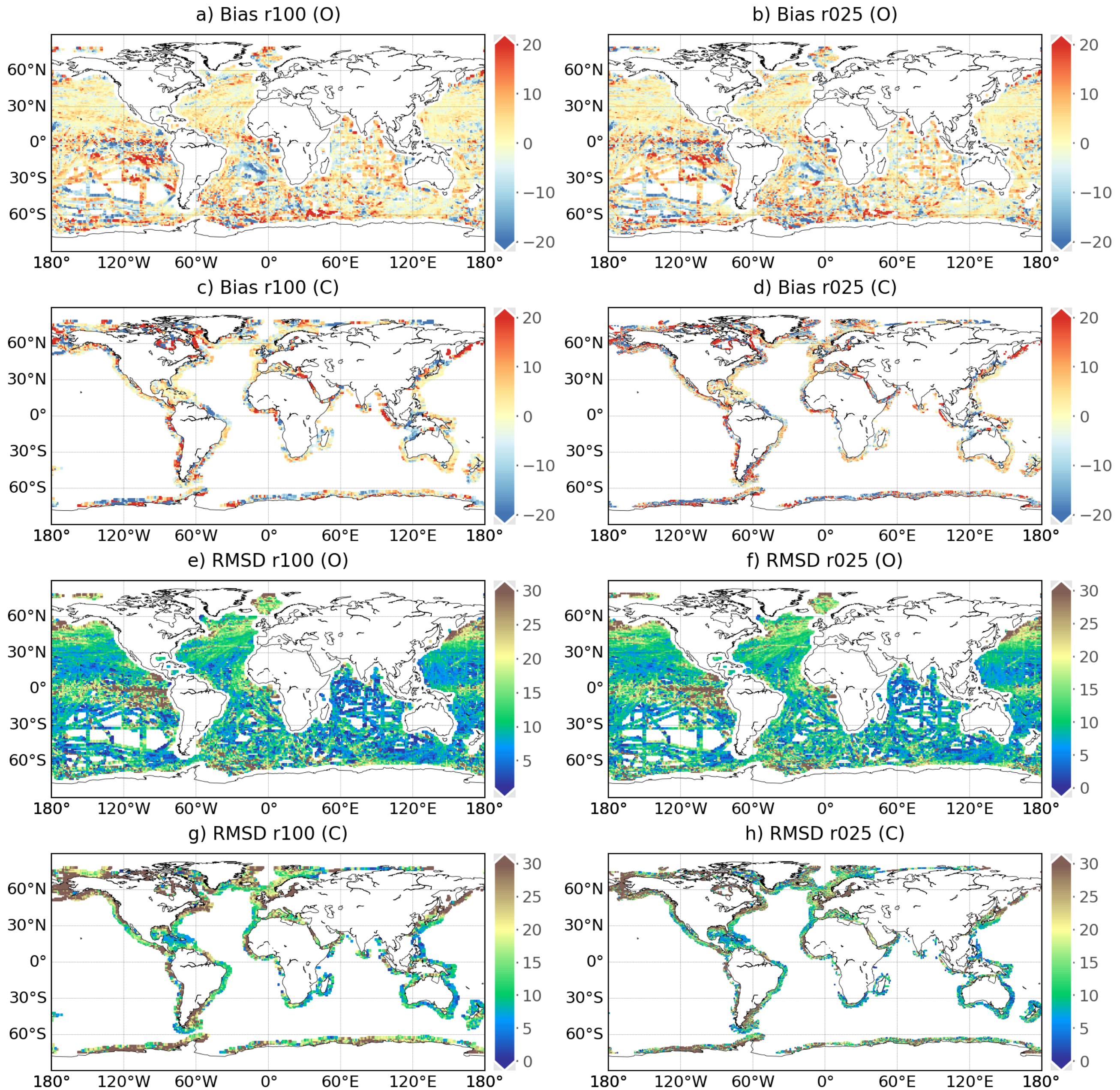

Figure A3. Global maps of mean model-data difference (Bias, abcd) and root-of-mean-square-deviation (RMSD, efgh) between the reconstruction and SOCATv2022 $p\mathrm{CO_2}$ [$\mu\,\mathrm{atm}$] over 1985-2021. Left: CMEM-LSCE-FFNN with a resolution of 1° (r100), right: CMEM-LSCE-FFNN with a resolution of 0.25° (r025). Open-ocean data (O) in each 0.25°-grid box used for evaluation is created by setting conservatively the open-ocean SOCATv2022 data value at the 1°-grid box containing it. Coastal-ocean data (C) are extracted from each of the two SOCATv2022 gridded data products.

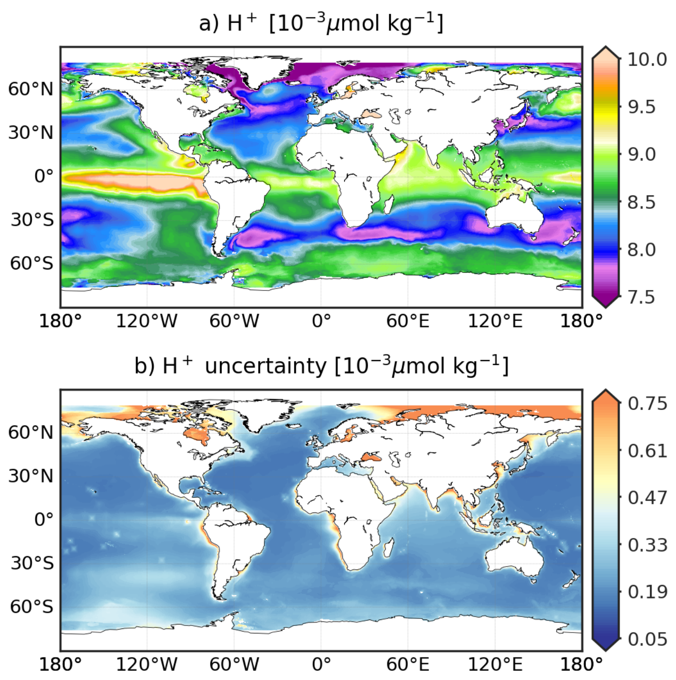

Figure A4. CMEMS-LSCE H^+ over the global ocean at a spatial resolution of $0.25°$. Temporal means of the model best estimate and 1σ-uncertainty per grid cell over 1985-2021 are calculated by using Eq. (5).

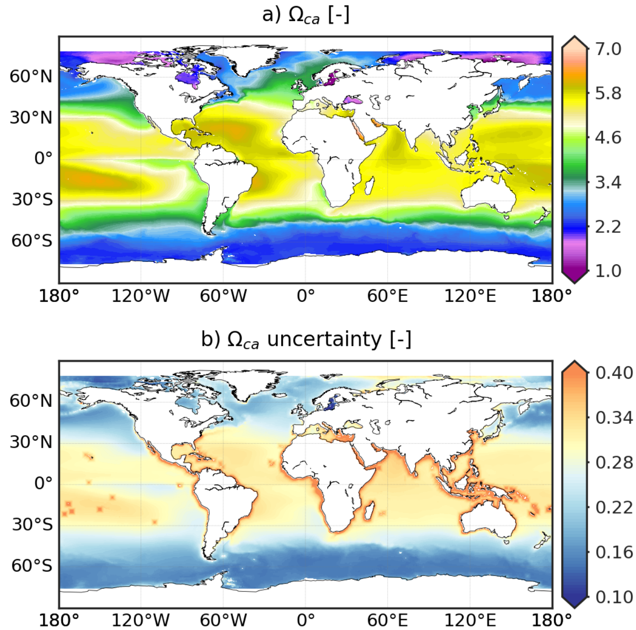

Figure A5. CMEMS-LSCE Ω_{ca} over the global ocean at a spatial resolution of $0.25°$. Temporal means of the model best estimate and 1σ-uncertainty per grid cell over 1985-2021 are calculated by using Eq. (5).

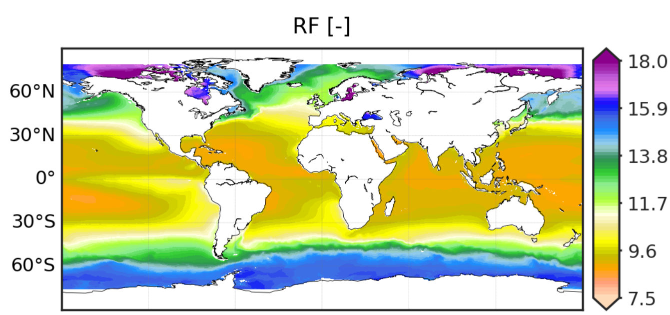

Figure A6. CMEMS-LSCE Revelle Factor (RF) over the global ocean at a spatial resolution of $0.25°$. Temporal means of the model best estimate per grid cell over 1985-2021 are calculated by using Eq. (5).

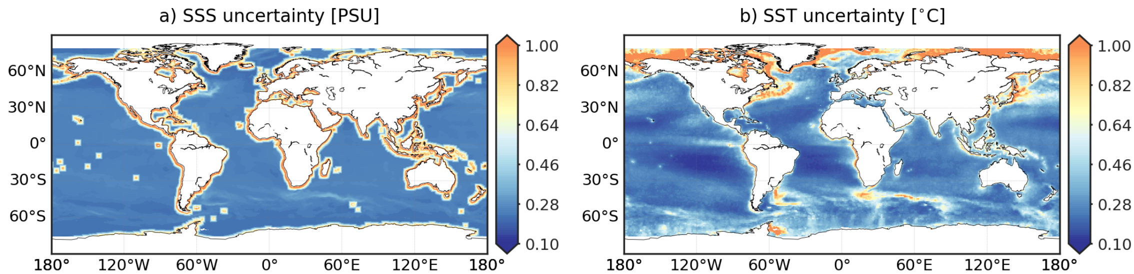

Figure A7. Spatial distribution of CMEMS SSS and SST product uncertainty over the global ocean at a spatial resolution of $0.25°$. 1σ-uncertainty is computed per grid cell by using Eq. (5) over 1985-2021.

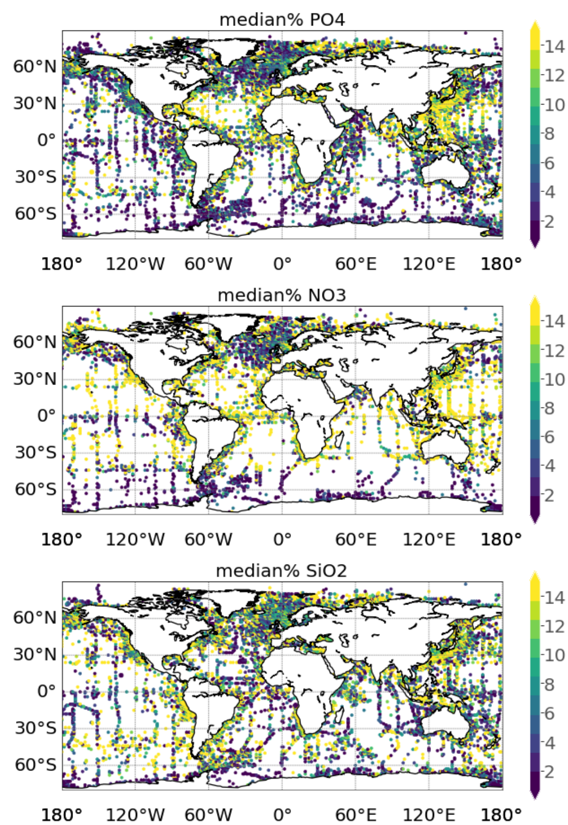

Figure A8. Median percentage of analysis error uncertainty against of climatological mean of surface WOA18 nutrient data: phosphate (PO_4), nitrate (NO_3), and silicate (SiO_2).

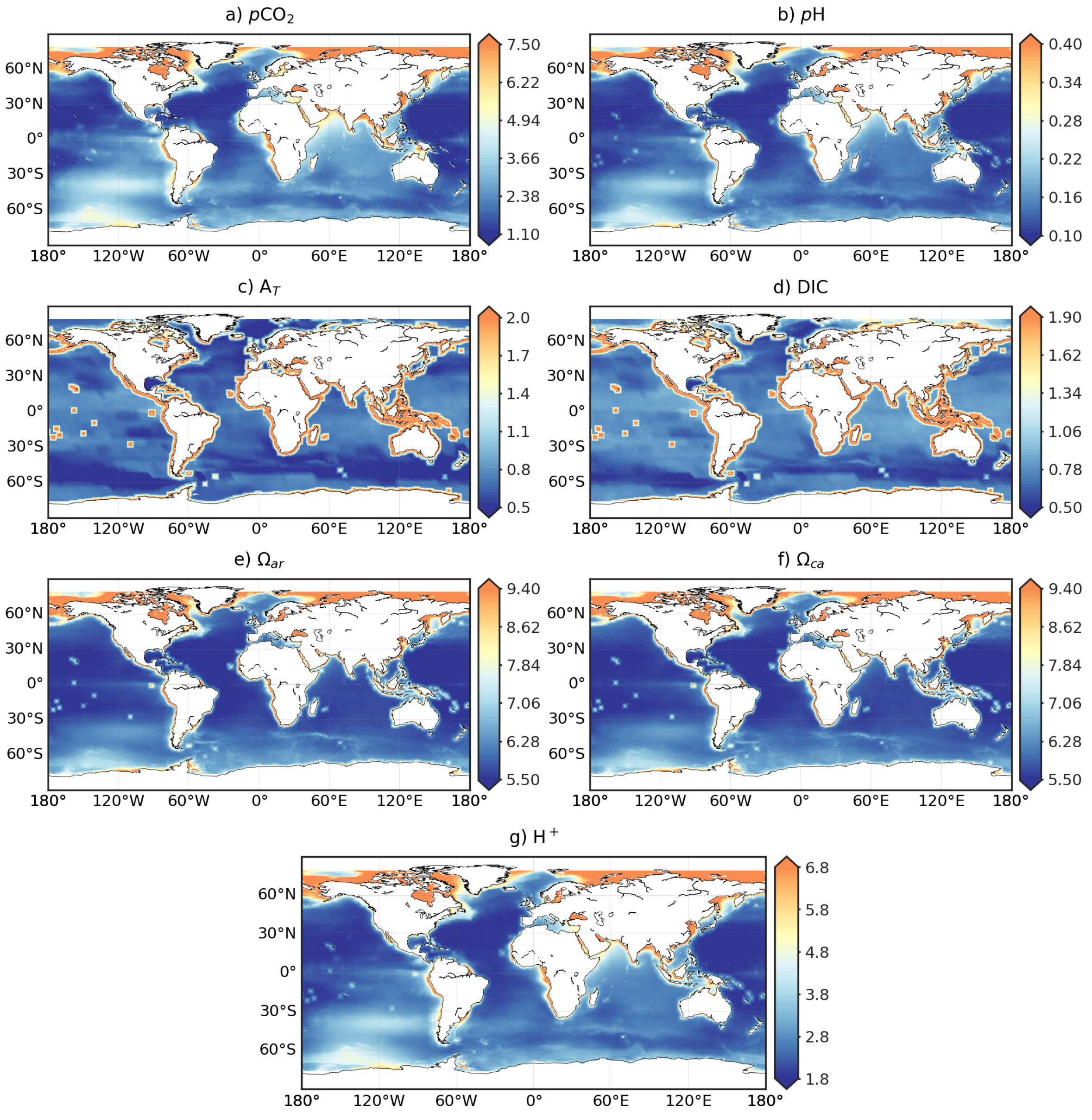

Figure A9. Spatial distribution of $R(\sigma, \mu)$ [%] (Eq 8), i.e., the ratio of model uncertainty (σ) against model best estimate (μ).

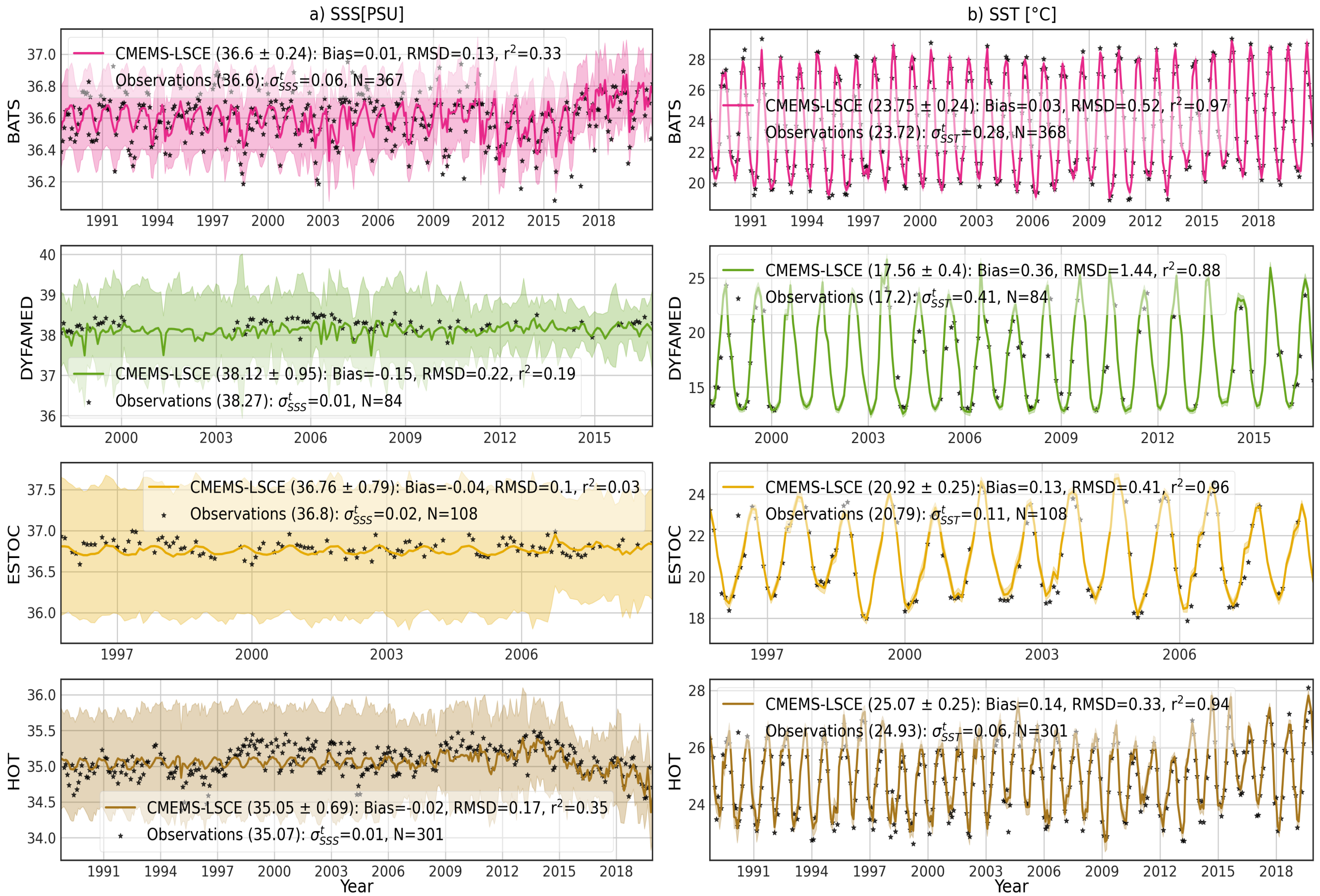

Figure A10. Monthly time series of SSS and SST at BATS, DYFAMED, ESTOC, and HOT stations (Table 2 and Fig. A1b): ~~model best estimate~~ CMEMS data (curve), 1σ-uncertainty (envelope), and monthly average of observations (point). Means of ~~the best estimate~~ CMEMS data and 1σ-uncertainty ($\mu \pm \sigma$) calculated over the observing time span are shown in brackets if accessible. Statistics include the number of months with observations (N), Bias, RMSD, and r^2. σ^t_{SSS} [σ^t_{SST}] stands for temporal standard deviation from monthly averages of SSS and SST observations. Temporal variations in SSS observations are poorly described in the CMEMS SSS time series (Table 1) used in CMEMS-LSCE reconstructions.

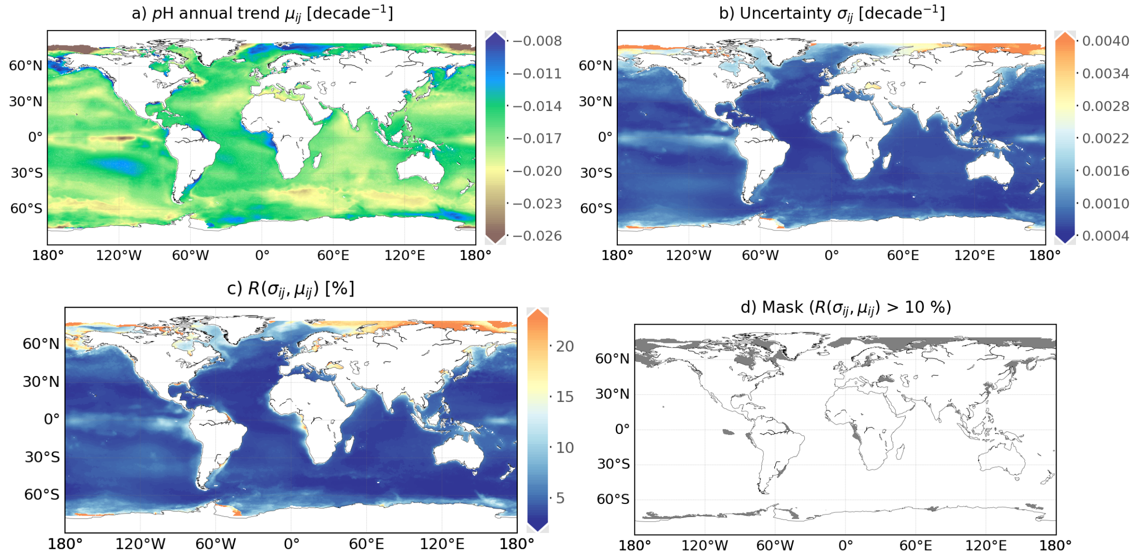

Figure A11. a) Global surface seawater pH trend over the period 1985-2021, b) 1σ-uncertainties associated to trend estimates, c) σ-to-μ ratio $R(\sigma,\mu)[\%]$ (Eq. 8) between uncertainty estimates (b) and the best trend estimates (a), d) mask applied over the regions where $R(\mu,\sigma) > 10\%$.

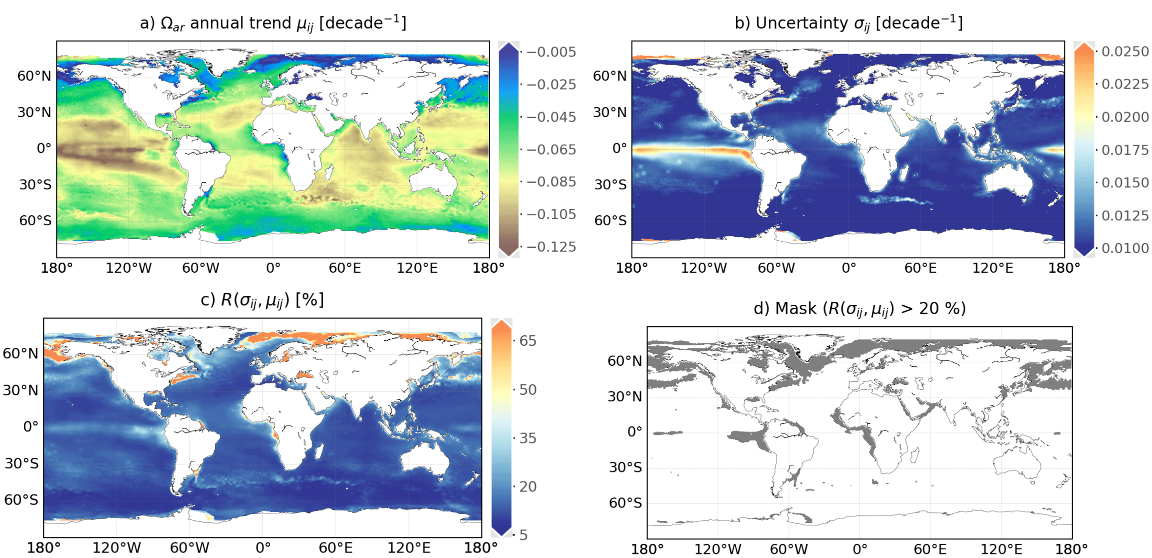

Figure A12. a) Global surface seawater Ω_{ar} trend over the period 1985-2021, b) 1σ-uncertainties associated to trend estimates, c) σ-to-μ ratio $R(\sigma,\mu)[\%]$ (Eq. 8) between uncertainty estimates (b) and the best trend estimates (a), d) mask applied over the regions where $R(\mu,\sigma) > 20\%$.

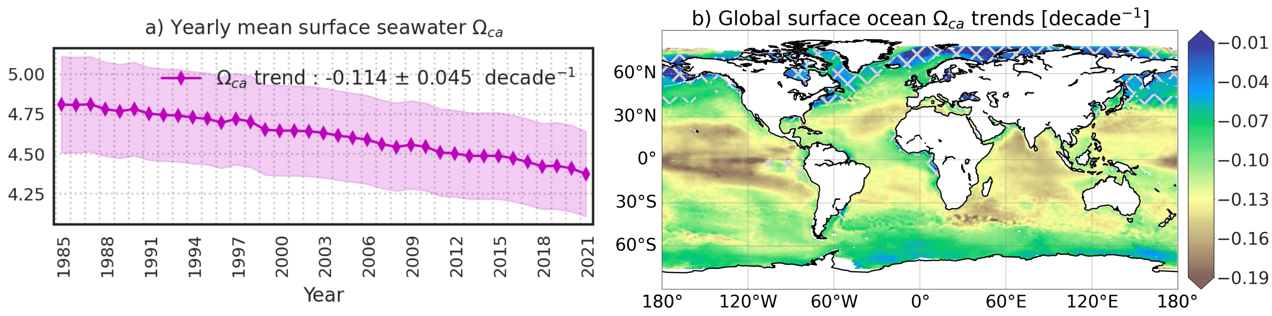

Figure A13. a) Yearly global area-weighted mean of surface ocean saturation states with respect to calcite (Ω_{ca}): Global means of the best estimate (μ, plain line) and uncertainty (σ, envelop) are computed with Eq. (7a). b) Global trend maps of Ω_{ca} over 1985-2021: Cross-hatching covers the regions ~~where~~ with uncertainty of a trend estimate over 20% of the trend value.

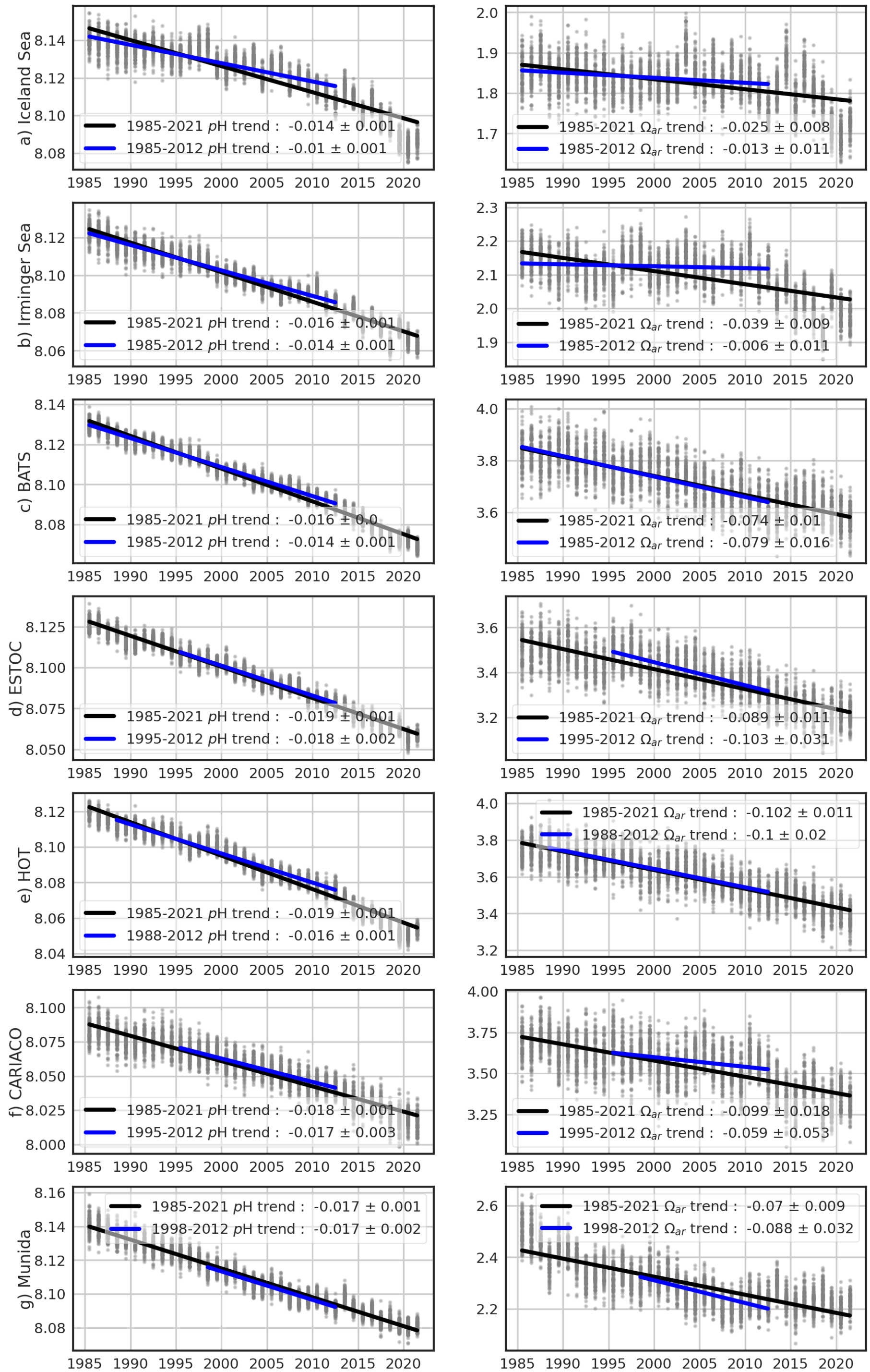

Figure A14. Linear trend estimates learned on 100-member ensemble (grey points) of yearly mean time series of pH and Ω_{ar} at different stations (Bates et al., 2014). $\mu \pm \sigma$ present linear slope and residual standard deviation. Black or blue lines stand for linear fits over the full or sub-period in 1985-2021 (see Table 5 for comparison).

Table A2. Information of moored time series of ~~coastal-surface-ocean~~ surface-ocean pCO_2 and pH observations (Sutton et al., 2019).

Stations	Abbreviations	Coordinates	Date range
Ala Wai Water Quality Buoy Pacific island	ALAWAI	21.3°N, 157.9°W	06/2008-12/2020
Bay of Bengal Ocean Indian Ocean	BOBOA	15.0°N, 90.0°W	11/2013-12/2017
Bermuda Testbed Mooring	BTM	31.5°N, 64.2°W	10/2005f-12/2006
Cape Arago	CAPEARAGO	43.3°N, 124.5°W	06/2017-12/2020
Cape Elizabeth	CAPEELIZABETH	47.4°N, 124.7°W	06/2006-05/2020
California Current Ecosystem 2	CCE2	34.3°N, 120.8°W	01/2010-06/2021
Chá b˘a Buoy in the Northwest Enhanced Moored Observatory and Olympic Coast NMS	CHABA	47.9°N, 126°W	07/2010-09/2020
Chuuk Lagoon Ocean Acidification Mooring	CHUUK	7.5°N, 151.9°E	11/2011-12/2017
Cheeca Rocks Ocean Acidification Mooring in Florida Keys National Marine Sanctuary	CHEECAROCKS	24.9°N, 80.6°W	12/2011-12/2021
Coastal Louisiana buoy	COASTALLA	28.5°N, 90.3°W	07/2017-08/2020
Central Gulf of Mexico Ocean Observing System Station 01	COASTALMS	30.0°N, 88.6°W	05/2009-05/2017
Crescent Reef Bermuda Buoy	CRESCENTREEF	32.4°N, 64.8°W	11/2010-12/2014
Coral Reef Instrumented Monitoring Platform 1	CRIMP1	21.4°N, 157.8°W	12/2005-12/2007
Coral Reef Instrumented Monitoring Platform 2	CRIMP2	21.5°N, 157.8°W	06/2008-12/2019
Chesapeake Bay Interpretive Buoy System Ocean Acidification Buoy at First Landing	FIRSTLANDING	37.0°N, 76.1°W	04/2018-09/2020
NANOOS ORCA buoy in Dabob Bay	DABOB	47.8°N, 122.8°W	06/2011-01/2016
Gulf of Alaska Ocean Acidification Mooring	GAKOA	59.9°N, 149.4°W	05/2011-12/2017
NDBC Buoy 41008 in Gray's Reef National Marine Sanctuary	GRAYSREEF	31.4°N, 80.9°W	07/2006-08/2018
Coastal Western Gulf of Maine Mooring	GULFOFMAINE	43.0°N, 70.5°W	07/2006-06/2021
Hog Reef Bermuda Buoy	HOGREEF	32.5°N, 64.8°W	12/2010-12/2017
North Atlantic Ocean Acidification Mooring	ICELAND	68.0°N, 12.7°W	08/2013-06/2017
Kaneohe Bay Ocean Acidification Offshore Observatory	KANEOHE	21.5°N, 157.8°W	09/2011-12/2019
Kuroshio Extension Observatory	KEO	32.3°N, 144.6°E	09/2007-12/2019
Kilo Nalu Water Quality Buoy at South Shore Oahu	KILONALU	21.3°N,157.9°W	08/2008-12/2018
Kodiak Alaska Ocean Acidification Mooring	KODIAK	57.7°N,152.3°W	03/2013-12/2015
La Parguera Ocean Acidification Mooring	LAPARGUERA	18.0°N, 67.1°W	01/2009-12/2018
Southeastern Bering Sea Mooring Site 2	M2	56.5°N,164.0°W	05/2013-09/2017
Newport Hydrographic Line Station 10 Ocean Acidification Mooring	NH10	44.9°N, 124.8°W	04/2014-12/2016
Ocean Station Papa	PAPA	50.1°N, 144.8°W	06/2007-12/2019
Southeast Alaska Ocean Acidification Mooring	SEAK	56.3°N, 134.7°W	03/2013-12/2015
Southern Ocean Flux Station	SOFS	46.8°S, 142.0°E	11/2011-12/2020
Stratus	STRATUS	19.7°S, 85.6°W	10/2006-12/2017
National Data Buoy Center (NDBC) Tropical Atmosphere Ocean	TAO110W	0.0°N, 110.0°W	09/2009-12/2018
NDBC Tropical Atmosphere Ocean	TAO125W	0.0°N, 125.0°W	05/2004-12/2020
NDBC Tropical Atmosphere Ocean	TAO140W	0.0°N, 140.0°W	05/2004-4/2019
NDBC Tropical Atmosphere Ocean	TAO155W	0.0°N, 155.0°W	01/2010-07/2020
NDBC Tropical Atmosphere Ocean	TAO165E	0.0°N, 165.0°E	02/2010-12/2019
NDBC Tropical Atmosphere Ocean	TAO170W	0.0°N, 170.0°W	07/2005-12/2017
NDBC Tropical Atmosphere Ocean	TAO8S165E	8.0°S, 165.0°E	06/2009-11/2011
ORCA buoy at Twanoh in Hood Canal	TWANOH	47.4°N,123.0°W	08/2009-12/2020
Woods Hole Oceanographic Institution Hawaii Ocean Time-series Station	WHOTS	22.7°N, 158.0°W	12/2004-12/2018

Table A3. Statistics computed between CMEMS-LSCE datasets (0.25°) and time series of $p\mathrm{CO_2}$ and pH measurements (Sutton et al., 2019) at open-ocean (O) and coastal stations (C): total numbers of monthly mean observations (N), temporal standard deviation of observations from their monthly averages (σ^t), RMSD (Eq. 10), and r^2 (Eq. 11). See Table A2 and Fig. A1b for stations' information and locations.

Stations	$p\mathrm{CO_2}$ [μatm]				pH [-]			
	N	σ^t	RMSD	r^2	N	σ^t	RMSD	r^2
~~1.~~ O1. BOBOA	42	9.9	9.6	0.69	19	0.010	0.011	0.71
O2. BTM	15	7.2	11.4	0.98	0	–	–	–
O3. CHUUK	66	10.9	23.5	0.60	33	0.014	0.033	0.78
O5. CRESCENTREEF	41	13.6	45.0	0.93	0	–	–	–
O5. HOGREEF	60	23.3	47.8	0.85	0	–	–	–
O6. ICELAND	24	8.1	16.9	0.68	4	0.007	0.092	0.94
O7. KEO	130	9.0	10.1	0.92	48	0.010	0.014	0.86
O8. PAPA	135	5.7	8.7	0.60	103	0.007	0.017	0.40
O9. SOFS	61	7.1	7.8	0.81	0	–	–	–
O10. STRATUS	116	6.3	9.2	0.80	10	0.004	0.042	0.43
O11. TAO110W	67	22.8	17.7	0.79	0	–	–	–
O12. TAO125W	124	16.5	16.0	0.43	0	–	–	–
O13. TAO140W	92	11.4	12.0	0.44	0	–	–	–
O14. TAO155W	45	11.3	12.2	0.75	0	–	–	–
O15. TAO165E	39	9.1	19.8	0.76	0	–	–	–
O16. TAO170W	87	9.0	17.9	0.45	0	–	–	–
O17. TAO8S165E	29	7.1	10.5	0.49	0	–	–	–
O18. WHOTS	143	4.7	8.0	0.80	23	0.004	0.01	0.57
C1. ALAWAI	112	20.3	22.8	0.32	0	–	–	–
C2. CAPEARAGO	33	~~65.60~~ 65.6	~~79.86~~79.9	0.19	31	0.086	0.069	0.22
~~2.~~ C3. CAPEELIZABETH	92	~~42.54~~ 42.5	~~41.44~~ 41.4	0.52	11	0.061	0.057	0.69
~~3.~~ C4. CCE2	127	~~45.31~~ 45.3	~~32.44~~ 32.4	0.16	58	0.048	0.035	0.24
~~4.~~ C5. CHABA	75	51.2	65.3	0.44	42	0.056	0.064	0.58
C6. CHEECAROCKS	73	~~44.05~~ 44.1	~~62.42~~ 62.4	0.25	40	0.038	0.066	0.21
~~5.~~ C7. COASTALLA	22	~~59.15~~ 59.2	~~57.41~~ 57.4	0.52	2	0.078	0.068	~~–~~–
~~6.~~ C8. COASTALMS	41	~~43.04~~ 43.0	~~42.50~~42.5	0.51	15	0.062	0.065	0.25
~~7.~~ C9. CRIMP1	23	26.4	95.6	0.62	0	–	–	–
C10. CRIMP2	119	85.4	90.7	0.58	0	–	–	–
C11. DABOB	24	55.0	89.3	0.74	0	–	–	–
C12. FIRSTLANDING	17	~~69.98~~ 70.0	~~77.32~~ 77.3	0.49	2	0.061	0.042	~~–~~–
~~8.~~ C13. GAKOA	64	20.3	66.0	0.73	0	–	–	–
C14. GRAYSREEF	96	~~20.12~~ 20.1	~~38.34~~ 38.3	0.65	49	0.020	0.040	0.66
C15. GULFOFMAINE	144	26.7	31.2	0.54	77	0.029	0.042	0.27
C16. KANEOHE	49	20.9	23.5	0.36	35	0.025	0.034	0.25
C17. KILONALU	69	14.3	11.6	0.56	0	–	–	–
C18. KODIAK	34	31.7	62.1	0.78	0	–	–	–
C19. LAPARGUERA	103	12.9	41.6	0.41	48	0.012	0.038	0.33
C20. M2	23	25.4	55.8	0.24	0	–	–	–
C21. NH10	25	64.6	31.4	0.46	15	0.058	0.048	0.42
C22. SEAK	31	53.4	141.3	0.82	0	–	–	–
C23. TWANOH	57	126.2	199.9	0.33	0	–	–	–

Table A4. Statistics computed between CMEMS-LSCE datasets ($0.25°$) and time series of A_T and DIC measurements ($0-10$ m depth): total numbers of monthly mean observations (N), temporal standard deviation of observations from their monthly averages (σ^t), RMSD (Eq. 10), and r^2 (Eq. 11). See Table 2 and Fig. A1b for stations' information and locations.

Stations	A_T [μmol kg^{-1}]				DIC [μmol kg^{-1}]			
	N	σ^t	RMSD	r^2	N	σ^t	RMSD	r^2
1. AWIPEV	52	15.8	32.0	0.33	52	17.7	29.6	0.71
2. BATS	303	2.4	9.6	0.34	351	1.9	8.2	0.82
3. DYFAMED	84	1.3	145.7	0.12	84	2.0	124.7	0.61
4. ESTOC	298	1.3	8.3	0.03	108	1.4	11.2	0.47
5. HOT	298	0.8	12.5	0.32	298	0.6	10.6	0.70
6. ICELAND	27	2.5	13.4	0.24	27	0.8	13.7	0.79
7. IRMINGER	29	1.8	8.4	0.30	23	1.7	14.6	0.84
8. KERFIX	23	1.0	7.4	0.22	23	3.4	14.0	0.52

References

Bakker, D., Alin, S., Becker, M., Bittig, H., Castaño-Primo, R., Feely, R. A., Gritzalis, T., Kadono, K., Kozyr, A., Lauvset, S. K., Metzl, N., Munro, D., Nakaoka, S.-i., Nojiri, Y., O'Brien, K., Olsen, A., Pfeil, B., Pierrot, D., Steinhoff, T., Sullivan, K., Sutton, A., Sweeney, C., Tilbrook, B., Wada13, C., Wanninkhof, R., Wranne, A. W., et al.: SOCAT version 2022 for quantification of ocean CO_2 uptake, https://www.socat.info/wp-content/uploads/2022/06/2022_Poster_SOCATv2022_release.pdf, 2022.

Bakker, D. C. E., Pfeil, B., Landa, C. S., Metzl, N., O'Brien, K. M., Olsen, A., Smith, K., Cosca, C., Harasawa, S., Jones, S. D., Nakaoka, S., Nojiri, Y., Schuster, U., Steinhoff, T., Sweeney, C., Takahashi, T., Tilbrook, B., Wada, C., Wanninkhof, R., Alin, S. R., Balestrini, C. F., Barbero, L., Bates, N. R., Bianchi, A. A., Bonou, F., Boutin, J., Bozec, Y., Burger, E. F., Cai, W.-J., Castle, R. D., Chen, L., Chierici, M., Currie, K., Evans, W., Featherstone, C., Feely, R. A., Fransson, A., Goyet, C., Greenwood, N., Gregor, L., Hankin, S., Hardman-Mountford, N. J., Harlay, J., Hauck, J., Hoppema, M., Humphreys, M. P., Hunt, C. W., Huss, B., Ibánhez, J. S. P., Johannessen, T., Keeling, R., Kitidis, V., Körtzinger, A., Kozyr, A., Krasakopoulou, E., Kuwata, A., Landschützer, P., Lauvset, S. K., Lefèvre, N., Lo Monaco, C., Manke, A., Mathis, J. T., Merlivat, L., Millero, F. J., Monteiro, P. M. S., Munro, D. R., Murata, A., Newberger, T., Omar, A. M., Ono, T., Paterson, K., Pearce, D., Pierrot, D., Robbins, L. L., Saito, S., Salisbury, J., Schlitzer, R., Schneider, B., Schweitzer, R., Sieger, R., Skjelvan, I., Sullivan, K. F., Sutherland, S. C., Sutton, A. J., Tadokoro, K., Telszewski, M., Tuma, M., van Heuven, S. M. A. C., Vandemark, D., Ward, B., Watson, A. J., and Xu, S.: A multi-decade record of high-quality fCO_2 data in version 3 of the Surface Ocean CO_2 Atlas (SOCAT), Earth System Science Data, 8, 383–413, https://doi.org/10.5194/essd-8-383-2016, 2016.

Bates, N. R., Astor, Y. M., Church, M. J., Currie, K., Dore, J. E., González-Dávila, M., Lorenzoni, L., Muller-Karger, F., Olafsson, J., and Santana-Casiano, J. M.: A time-series view of changing surface ocean chemistry due to ocean uptake of anthropogenic CO_2 and ocean acidification, Oceanography, 27, 126–141, 2014.

~~Bopp, L., Resplandy, L., Orr, J. C., Doney, S. C., Dunne, J. P., Gehlen, M., Halloran, P., Heinze, C., Ilyina, T., Séférian, R., Tjiputra, J., and Vichi, M.: Multiple stressors of ocean ecosystems in the 21st century: projections with CMIP5 models, Biogeosciences, 10, 6225–6245, , 2013.~~

Bresnahan, P. J., Takeshita, Y., Wirth, T., Martz, T. R., Cyronak, T., Albright, R., Wolfe, K., Warren, J. K., and Mertz, K.: Autonomous in situ calibration of ion-sensitive field effect transistor pH sensors, Limnology and Oceanography: Methods, 19, 132–144, 2021.

Broullón, D., Pérez, F. F., Velo, A., Hoppema, M., Olsen, A., Takahashi, T., Key, R. M., Tanhua, T., González-Dávila, M., Jeansson, E., et al.: A global monthly climatology of total alkalinity: a neural network approach, Earth System Science Data, 11, 1109–1127, 2019.

Canadell, J. G., Monteiro, P. M., Costa, M. H., Da Cunha, L. C., Cox, P. M., Alexey, V., Henson, S., Ishii, M., Jaccard, S., Koven, C., et al.: Global carbon and other biogeochemical cycles and feedbacks In Climate Change 2021: The Physical Science Basis. Contribution of Working Group I to the Sixth Assessment Report of the Intergovernmental Panel on Climate Change, Cambridge University Press, https://doi.org/10.1017/9781009157896.007, 2021.

Carter, B. R., Williams, N. L., Gray, A. R., and Feely, R. A.: Locally interpolated alkalinity regression for global alkalinity estimation, Limnology and Oceanography: Methods, 14, 268–277, https://doi.org/https://doi.org/10.1002/lom3.10087, 2016.

Carter, B. R., Feely, R. A., Williams, N. L., Dickson, A. G., Fong, M. B., and Takeshita, Y.: Updated methods for global locally interpolated estimation of alkalinity, pH, and nitrate, Limnology and Oceanography: Methods, 16, 119–131, https://doi.org/https://doi.org/10.1002/lom3.10232, 2018.

Chau, T. T. T., Gehlen, M., and Chevallier, F.: Global ocean surface carbon product, Research Report CMEMS-MOB-QUID-015-008, Le Laboratoire des Sciences du Climat et de l'Environnement, https://doi.org/10.48670/moi-00047, quality Information Document, 2022a.

Chau, T. T. T., Gehlen, M., and Chevallier, F.: A seamless ensemble-based reconstruction of surface ocean pCO_2 and air–sea CO_2 fluxes over the global coastal and open oceans, Biogeosciences, 19, 1087–1109, https://doi.org/10.5194/bg-19-1087-2022, 2022b.

Chau, T. T. T., Gehlen, M., Metzl, N., and Chevallier, F.: CMEMS-LSCE: A global 0.25-degree, monthly reconstruction of the surface ocean carbonate system, ESPRI/IPSL [dataset], https://doi.org/10.14768/a2f0891b-763a-49e9-af1b-78ed78b16982, 2023.

Chevallier, F.: On the parallelization of atmospheric inversions of CO_2 surface fluxes within a variational framework, Geoscientific Model Development, 6, 783–790, https://doi.org/10.5194/gmd-6-783-2013, 2013.

Chevallier, F., Fisher, M., Peylin, P., Serrar, S., Bousquet, P., Bréon, F.-M., Chédin, A., and Ciais, P.: Inferring CO2 sources and sinks from satellite observations: Method and application to TOVS data, Journal of Geophysical Research: Atmospheres, 110, https://doi.org/https://doi.org/10.1029/2005JD006390, 2005.

Chevallier, F., Ciais, P., Conway, T. J., Aalto, T., Anderson, B. E., Bousquet, P., Brunke, E. G., Ciattaglia, L., Esaki, Y., Fröhlich, M., Gomez, A., Gomez-Pelaez, A. J., Haszpra, L., Krummel, P. B., Langenfelds, R. L., Leuenberger, M., Machida, T., Maignan, F., Matsueda, H., Morguí, J. A., Mukai, H., Nakazawa, T., Peylin, P., Ramonet, M., Rivier, L., Sawa, Y., Schmidt, M., Steele, L. P., Vay, S. A., Vermeulen, A. T., Wofsy, S., and Worthy, D.: CO2 surface fluxes at grid point scale estimated from a global 21 year reanalysis of atmospheric measurements, Journal of Geophysical Research: Atmospheres, 115, https://doi.org/https://doi.org/10.1029/2010JD013887, 2010.

~~Cooley, S., Schoeman, D., Bopp, L., Boyd, P., Donner, S., Ito, S.-i., Kiessling, W., Martinetto, P., Ojea, E., Racault, M.-F., et al.: Oceans and coastal ecosystems and their services, in: IPCC AR6 WGII, Cambridge University Press, 2022.~~

Coppola, L., Boutin, J., Gattuso, J.-P., Lefevre, D., and Metzl, N.: The Carbonate System in the Ligurian Sea, chap. 4, pp. 79–103, John Wiley & Sons, Ltd, https://doi.org/https://doi.org/10.1002/9781119706960.ch4, 2020.

Coppola, L., Diamond, R. E., and Carval, T.: Dyfamed observatory data. SEANOE [dataset], https://doi.org/0.17882/43749, 2021.

Denvil-Sommer, A., Gehlen, M., Vrac, M., and Mejia, C.: LSCE-FFNN-v1: a two-step neural network model for the reconstruction of surface ocean pCO_2 over the global ocean, Geoscientific Model Development, 12, 2091–2105, https://doi.org/10.5194/gmd-12-2091-2019, 2019.

Dickson, A. G.: Standard potential of the reaction -AgCl(s)+1/2H-2(g)=Ag(s)+HCl(aq) and the standard acidity constant of the ion HSO4- in synthetic sea-water from 273.15-K to 318.15-K, Journal of Chemical Thermodynamics, 22, 113–127, https://doi.org/doi:10.1016/0021-9614(90)90074-z, 1990.

Dickson, A. G.: The carbon dioxide system in seawater: equilibrium chemistry and measurements in Guide to best practices for ocean acidification research and data reporting, https://www.pmel.noaa.gov/co2/files/dickson_thecarbondioxidesysteminseawater_equilibriumchemistryandmeasurementspp17-40.pdf, 2010.

Dickson, A. G., Sabine, C. L., and Christian, J. R.: Guide to best practices for ocean CO2 measurements., North Pacific Marine Science Organization, 2007.

~~Doney, S. C.: The growing human footprint on coastal and open-ocean biogeochemistry, science, 328, 1512–1516, 2010.~~

Doney, S. C., Fabry, V. J., Feely, R. A., and Kleypas, J. A.: Ocean acidification: the other CO2 problem, Annual review of marine science, 1, 169–192, 2009.

Doney, S. C., Busch, D. S., Cooley, S. R., and Kroeker, K. J.: The impacts of ocean acidification on marine ecosystems and reliant human communities, Annual Review of Environment and Resources, 45, 2020.

Dore, J. E., Lukas, R., Sadler, D. W., Church, M. J., and Karl, D. M.: Physical and biogeochemical modulation of ocean acidification in the central North Pacific, Proceedings of the National Academy of Sciences, 106, 12 235–12 240, 2009.

Droghei, R., Buongiorno Nardelli, B., and Santoleri, R.: A new global sea surface salinity and density dataset from multivariate observations (1993–2016), Frontiers in Marine Science, 5, 84, 2018.

Fabry, V. J., Seibel, B. A., Feely, R. A., and Orr, J. C.: Impacts of ocean acidification on marine fauna and ecosystem processes, ICES Journal of Marine Science, 65, 414–432, 2008.

Feely, R. A., Wanninkhof, R., Takahashi, T., and Tans, P.: Influence of El Niño on the equatorial Pacific contribution to atmospheric CO_2 accumulation, Nature, 398, 597–601, 1999.

Feely, R. A., Sabine, C. L., Takahashi, T., and Wanninkhof, R.: Uptake And Storage Of Carbon Dioxide In The Ocean: The Global CO_2 Survey, OCEANOGRAPHY-WASHINGTON DC-OCEANOGRAPHY SOCIETY-, 14, 18–32, 2001.

Fischer, P., Schwanitz, M., Loth, R., Posner, U., Brand, M., and Schröder, F.: First year of practical experiences of the new Arctic AWIPEV-COSYNA cabled Underwater Observatory in Kongsfjorden, Spitsbergen, Ocean Science, 13, 259–272, https://doi.org/10.5194/os-13-259-2017, 2017.

Friedlingstein, P., O'Sullivan, M., Jones, M. W., Andrew, R. M., Gregor, L., Hauck, J., Le Quéré, C., Luijkx, I. T., Olsen, A., Peters, G. P., Peters, W., Pongratz, J., Schwingshackl, C., Sitch, S., Canadell, J. G., Ciais, P., Jackson, R. B., Alin, S. R., Alkama, R., Arneth, A., Arora, V. K., Bates, N. R., Becker, M., Bellouin, N., Bittig, H. C., Bopp, L., Chevallier, F., Chini, L. P., Cronin, M., Evans, W., Falk, S., Feely, R. A., Gasser, T., Gehlen, M., Gkritzalis, T., Gloege, L., Grassi, G., Gruber, N., Gürses, O., Harris, I., Hefner, M., Houghton, R. A., Hurtt, G. C., Iida, Y., Ilyina, T., Jain, A. K., Jersild, A., Kadono, K., Kato, E., Kennedy, D., Klein Goldewijk, K., Knauer, J., Korsbakken, J. I., Landschützer, P., Lefèvre, N., Lindsay, K., Liu, J., Liu, Z., Marland, G., Mayot, N., McGrath, M. J., Metzl, N., Monacci, N. M., Munro, D. R., Nakaoka, S.-I., Niwa, Y., O'Brien, K., Ono, T., Palmer, P. I., Pan, N., Pierrot, D., Pocock, K., Poulter, B., Resplandy, L., Robertson, E., Rödenbeck, C., Rodriguez, C., Rosan, T. M., Schwinger, J., Séférian, R., Shutler, J. D., Skjelvan, I., Steinhoff, T., Sun, Q., Sutton, A. J., Sweeney, C., Takao, S., Tanhua, T., Tans, P. P., Tian, X., Tian, H., Tilbrook, B., Tsujino, H., Tubiello, F., van der Werf, G. R., Walker, A. P., Wanninkhof, R., Whitehead, C., Willstrand Wranne, A., Wright, R., Yuan, W., Yue, C., Yue, X., Zaehle, S., Zeng, J., and Zheng, B.: Global Carbon Budget 2022, Earth System Science Data, 14, 4811–4900, https://doi.org/10.5194/essd-14-4811-2022, 2022.

Garcia, H., Weathers, K., Paver, C., Smolyar, I., Boyer, T., Locarnini, M., Zweng, M., Mishonov, A., Baranova, O., Seidov, D., et al.: World ocean atlas 2018. Vol. 4: Dissolved inorganic nutrients (phosphate, nitrate and nitrate+ nitrite, silicate), https://archimer.ifremer.fr/doc/00651/76336/, 2019.

Gattuso, J.-P. and Hansson, L.: Ocean acidification, Oxford university press, 2011.

Gattuso, J.-P., ~~Magnan, A., Billé, R., Cheung, W. W. L., Howes, E. L., Joos, F., Allemand, D., Bopp, L., Cooley, S. R., Eakin, C. M., Hoegh-Guldberg, O., Kelly, R. P., Pörtner, H.-O., Rogers, A. D., Baxter, J. M., Laffoley, D., Osborn, D., Rankovic, A., Rochette, J., Sumaila, U. R., Treyer~~Alliouane, S., and ~~Turley, C.: Contrasting futures for ocean and society from different anthropogenic CO₂ emissions scenarios, Science~~Fischer, P.: High-frequency, ~~349, aac4722, , 2015.~~ year-round time series of the carbonate chemistry in a high-Arctic fjord (Svalbard), Earth System Science Data, 15, 2809–2825, https://doi.org/10.5194/essd-15-2809-2023, 2023.

Gehlen, M., Gruber, N., Gangstø, R., Bopp, L., and Oschlies, A.: Biogeochemical consequences of ocean acidification and feedbacks to the earth system, Ocean acidification, 1, 230–248, 2011.

González-Dávila, M. and Santana-Casiano, J.: Sea surface and atmospheric fco2 data measured during the estoc time series cruises from 1995-2009, CDIAC, Oak Ridge National Laboratory, US Department of Energy, Oak Ridge, Tennessee. doi, 10, 2009.

Good, S., Fiedler, E., Mao, C., Martin, M. J., Maycock, A., Reid, R., Roberts-Jones, J., Searle, T., Waters, J., While, J., and Worsfold, M.: The Current Configuration of the OSTIA System for Operational Production of Foundation Sea Surface Temperature and Ice Concentration Analyses, Remote Sensing, 12, https://www.mdpi.com/2072-4292/12/4/720, 2020.

Gregor, L. and Gruber, N.: OceanSODA-ETHZ: a global gridded data set of the surface ocean carbonate system for seasonal to decadal studies of ocean acidification, Earth System Science Data, 13, 777–808, https://doi.org/10.5194/essd-13-777-2021, 2021.

Gregor, L., Lebehot, A. D., Kok, S., and Scheel Monteiro, P. M.: A comparative assessment of the uncertainties of global surface ocean CO_2 estimates using a machine-learning ensemble (CSIR-ML6 version 2019a) – have we hit the wall?, Geoscientific Model Development, 12, 5113–5136, https://doi.org/10.5194/gmd-12-5113-2019, 2019.

Gruber, N., Clement, D., Carter, B. R., Feely, R. A., Van Heuven, S., Hoppema, M., Ishii, M., Key, R. M., Kozyr, A., Lauvset, S. K., et al.: The oceanic sink for anthropogenic CO2 from 1994 to 2007, Science, 363, 1193–1199, 2019.

Hauck, J., Zeising, M., Le Quéré, C., Gruber, N., Bakker, D. C., Bopp, L., Chau, T. T. T., Gürses, Ö., Ilyina, T., Landschützer, P., Lenton, A., Resplandy, L., Rödenbeck, C., Schwinger, J., and Séférian, R.: Consistency and Challenges in the Ocean Carbon Sink Estimate for the Global Carbon Budget, Frontiers in Marine Science, 7, 852, https://doi.org/10.3389/fmars.2020.571720, 2020.

Hoffmann, L. J., Breitbarth, E., Boyd, P. W., and Hunter, K. A.: Influence of ocean warming and acidification on trace metal biogeochemistry, Marine Ecology Progress Series, 470, 191–205, 2012.

Hopkins, F. E., Suntharalingam, P., Gehlen, M., Andrews, O., Archer, S. D., Bopp, L., Buitenhuis, E., Dadou, I., Duce, R., Goris, N., et al.: The impacts of ocean acidification on marine trace gases and the implications for atmospheric chemistry and climate, Proceedings of the Royal Society A, 476, 20190 769, 2020.

Ibánhez, J. S. P., Diverrès, D., Araujo, M., and Lefèvre, N.: Seasonal and interannual variability of sea-air CO_2 fluxes in the tropical Atlantic affected by the Amazon River plume, Global Biogeochemical Cycles, 29, 1640–1655, 2015.

Iida, Y., Takatani, Y., Kojima, A., and Ishii, M.: Global trends of ocean CO2 sink and ocean acidification: an observation-based reconstruction of surface ocean inorganic carbon variables, Journal of Oceanography, 77, 323–358, 2021.

Jiang, L.-Q., Carter, B. R., Feely, R. A., Lauvset, S. K., and Olsen, A.: Surface ocean pH and buffer capacity: past, present and future, Scientific reports, 9, 1–11, 2019.

~~Jiang, L.-Q., Dunne, J., Carter, B. R., Tjiputra, J. F., Terhaar, J., Sharp, J. D., Olsen, A., Alin, S., Bakker, D. C. E., Feely, R. A., Gattuso, J.-P., Hogan, P., Ilyina, T., Lange, N., Lauvset, S. K., Lewis, E. R., Lovato, T., Palmieri, J., Santana-Falcón, Y., Schwinger, J., Séférian, R., Strand, G., Swart, N., Tanhua, T., Tsujino, H., Wanninkhof, R., Watanabe, M., Yamamoto, A., and Ziehn, T.: Global Surface Ocean Acidification Indicators From 1750 to 2100, Journal of Advances in Modeling Earth Systems, 15, e2022MS003 563, , 2023.~~

Jones, S., Le Quéré, C., and Rödenbeck, C.: Autocorrelation characteristics of surface ocean pCO2and air-sea CO2 fluxes, Global biogeochemical cycles, 26, 2012.

Key, R. M., Kozyr, A., Sabine, C. L., Lee, K., Wanninkhof, R., Bullister, J. L., Feely, R. A., Millero, F. J., Mordy, C., and Peng, T.-H.: A global ocean carbon climatology: Results from Global Data Analysis Project (GLODAP), Global Biogeochemical Cycles, 18, https://doi.org/https://doi.org/10.1029/2004GB002247, 2004.

~~Kwiatkowski, L., Torres, O., Bopp, L., Aumont, O., Chamberlain, M., Christian, J. R., Dunne, J. P., Gehlen, M., Ilyina, T., John, J. G., Lenton, A., Li, H., Lovenduski, N. S., Orr, J. C., Palmieri, J., Santana-Falcón, Y., Schwinger, J., Séférian, R., Stock, C. A., Tagliabue, A., Takano, Y., Tjiputra, J., Toyama, K., Tsujino, H., Watanabe, M., Yamamoto, A., Yool, A., and Ziehn, T.: Twenty-first century ocean warming, acidification, deoxygenation, and upper-ocean nutrient and primary production decline from CMIP6 model projections, Biogeosciences, 17, 3439–3470, , 2020.~~

Körtzinger, A.: Determination of carbon dioxide partial pressure (pCO_2), chap. 9, pp. 149–158, John Wiley & Sons, Ltd, https://doi.org/https://doi.org/10.1002/9783527613984.ch9, 1999.

Landschützer, P., Gruber, N., and Bakker, D. C.: Decadal variations and trends of the global ocean carbon sink, Global Biogeochemical Cycles, 30, 1396–1417, 2016.

Landschützer, P., Ilyina, T., and Lovenduski, N. S.: Detecting Regional Modes of Variability in Observation-Based Surface Ocean pCO_2, Geophysical Research Letters, 46, 2670–2679, 2019.

Landschützer, P., Laruelle, G. G., Roobaert, A., and Regnier, P.: A uniform $p\mathrm{CO}_2$ climatology combining open and coastal oceans, Earth System Science Data, 12, 2537–2553, https://doi.org/10.5194/essd-12-2537-2020, 2020.

Laruelle, G. G., Landschützer, P., Gruber, N., Tison, J.-L., Delille, B., and Regnier, P.: Global high-resolution monthly pCO_2 climatology for the coastal ocean derived from neural network interpolation, Biogeosciences, 14, 4545–4561, 2017.

Lauvset, S. K. and Gruber, N.: Long-term trends in surface ocean pH in the North Atlantic, Marine Chemistry, 162, 71–76, 2014.

Lauvset, S. K., Gruber, N., Landschützer, P., Olsen, A., and Tjiputra, J.: Trends and drivers in global surface ocean pH over the past 3 decades, Biogeosciences, 12, 1285–1298, https://doi.org/10.5194/bg-12-1285-2015, 2015.

Lauvset, S. K., Lange, N., Tanhua, T., Bittig, H. C., Olsen, A., Kozyr, A., Alin, S., Álvarez, M., Azetsu-Scott, K., Barbero, L., Becker, S., Brown, P. J., Carter, B. R., da Cunha, L. C., Feely, R. A., Hoppema, M., Humphreys, M. P., Ishii, M., Jeansson, E., Jiang, L.-Q., Jones, S. D., Lo Monaco, C., Murata, A., Müller, J. D., Pérez, F. F., Pfeil, B., Schirnick, C., Steinfeldt, R., Suzuki, T., Tilbrook, B., Ulfsbo, A., Velo, A., Woosley, R. J., and Key, R. M.: GLODAPv2.2022: the latest version of the global interior ocean biogeochemical data product, Earth System Science Data, 14, 5543–5572, https://doi.org/10.5194/essd-14-5543-2022, ~~2022.~~ 2022a.

Lauvset, S. K., Lange, N., Tanhua, T., Bittig, H. C., Olsen, A., Kozyr, A., Alin, S., Álvarez, M., Azetsu-Scott, K., Barbero, L., Becker, S., Brown, P. J., Carter, B. R., da Cunha, L. C., Feely, R. A., Hoppema, M., Humphreys, M. P., Ishii, M., Jeansson, E., Jiang, L.-Q., Jones, S. D., Lo Monaco, C., Murata, A., Müller, J. D., Pérez, F. F., Pfeil, B., Schirnick, C., Steinfeldt, R., Suzuki, T., Tilbrook, B., Ulfsbo, A., Velo, A., Woosley, R. J., and Key, R. M.: Global Ocean Data Analysis Project version 2.2022 (GLODAPv2.2022) (NCEI Accession 0257247), NOAA National Centers for Environmental Information [dataset], https://doi.org/10.25921/1f4w-0t92, 2022b.

Lee, K., Tong, L. T., Millero, F. J., Sabine, C. L., Dickson, A. G., Goyet, C., Park, G.-H., Wanninkhof, R., Feely, R. A., and Key, R. M.: Global relationships of total alkalinity with salinity and temperature in surface waters of the world's oceans, Geophysical research letters, 33, 2006.

Leseurre, C., Lo Monaco, C., Reverdin, G., Metzl, N., Fin, J., Mignon, C., and Benito, L.: Summer trends and drivers of sea surface fCO_2 and pH changes observed in the southern Indian Ocean over the last two decades (1998–2019), Biogeosciences, 19, 2599–2625, https://doi.org/10.5194/bg-19-2599-2022, 2022.

Lewis, E. and Wallace, D.: CO2SYS-Program developed for the CO2 system calculations, Carbon Dioxide Inf Anal Center Report ORNL/CDIAC-105, https://doi.org/https://doi.org/10.15485/1464255, 1998.

Lueker, T. J., Dickson, A. G., and Keeling, C. D.: Ocean pCO2 calculated from dissolved inorganic carbon, alkalinity, and equations for K1 and K2: validation based on laboratory measurements of CO2 in gas and seawater at equilibrium, Marine chemistry, 70, 105–119, 2000.

Ma, D., Gregor, L., and Gruber, N.: Four Decades of Trends and Drivers of Global Surface Ocean Acidification, Global Biogeochemical Cycles, 37, e2023GB007 765, https://doi.org/https://doi.org/10.1029/2023GB007765, e2023GB007765 2023GB007765, 2023.

Maritorena, S., d'Andon, O. H. F., Mangin, A., and Siegel, D. A.: Merged satellite ocean color data products using a bio-optical model: Characteristics, benefits and issues, Remote Sensing of Environment, 114, 1791–1804, https://doi.org/https://doi.org/10.1016/j.rse.2010.04.002, 2010.

Menemenlis, D., Campin, J., Heimbach, P., Hill, C., Lee, T., Nguyen, A., Schodlok, M., and Zhang, H.: ECCO2: High Resolution Global Ocean and Sea Ice Data Synthesis, 2008, OS31C-1292, 2008.

Menviel, L., Spence, P., Yu, J., Chamberlain, M., Matear, R., Meissner, K., and England, M. H.: Southern Hemisphere westerlies as a driver of the early deglacial atmospheric CO2 rise, Nature Communications, 9, 1–12, 2018.

Metzl, N. and Lo Monaco, C.: OISO - Ocean Indien Service d'Observation [dataset], https://doi.org/10.18142/228, 1998.

Michaels, A. F. and Knap, A. H.: Overview of the US JGOFS Bermuda Atlantic Time-series Study and the Hydrostation S program, Deep Sea Research Part II: Topical Studies in Oceanography, 43, 157–198, 1996.

Millero, F. J., Woosley, R., Ditrolio, B., and Waters, J.: Effect of ocean acidification on the speciation of metals in seawater, Oceanography, 22, 72–85, 2009.

Mucci, A.: The solubility of calcite and aragonite in seawater at various salinities, temperatures, and one atmosphere total pressure, American Journal of Science, 283, 780–799, 1983.

Nardelli, B. B., Droghei, R., and Santoleri, R.: Multi-dimensional interpolation of SMOS sea surface salinity with surface temperature and in situ salinity data, Remote Sensing of Environment, 180, 392–402, 2016.

Olafsson, J., Olafsdottir, S., Benoit-Cattin, A., and Takahashi, T.: The Irminger Sea and the Iceland Sea time series measurements of sea water carbon and nutrient chemistry 1983–2008, Earth System Science Data, 2, 99–104, 2010.

Olivier, L., Boutin, J., Reverdin, G., Lefèvre, N., Landschützer, P., Speich, S., Karstensen, J., Labaste, M., Noisel, C., Ritschel, M., Steinhoff, T., and Wanninkhof, R.: Wintertime process study of the North Brazil Current rings reveals the region as a larger sink for CO_2 than expected, Biogeosciences, 19, 2969–2988, https://doi.org/10.5194/bg-19-2969-2022, 2022.

Olsen, A., Key, R. M., Van Heuven, S., Lauvset, S. K., Velo, A., Lin, X., Schirnick, C., Kozyr, A., Tanhua, T., Hoppema, M., et al.: The Global Ocean Data Analysis Project version 2 (GLODAPv2)–an internally consistent data product for the world ocean, Earth System Science Data, 8, 297–323, 2016.

Orr, J. C., Fabry, V. J., Aumont, O., Bopp, L., Doney, S. C., Feely, R. A., Gnanadesikan, A., Gruber, N., Ishida, A., Joos, F., et al.: Anthropogenic ocean acidification over the twenty-first century and its impact on calcifying organisms, Nature, 437, 681–686, 2005.

Orr, J. C., Epitalon, J.-M., Dickson, A. G., and Gattuso, J.-P.: Routine uncertainty propagation for the marine carbon dioxide system, Marine Chemistry, 207, 84–107, https://doi.org/https://doi.org/10.1016/j.marchem.2018.10.006, 2018.

Palmiéri, J., Orr, J., Dutay, J.-C., Béranger, K., Schneider, A., Beuvier, J., and Somot, S.: Simulated anthropogenic CO_2 storage and acidification of the Mediterranean Sea, Biogeosciences, 12, 781–802, 2015.

Park, P. K.: OCEANIC CO2 SYSTEM: AN EVALUATION OF TEN METHODS OF INVESTIGATION1, Limnology and Oceanography, 14, 179–186, https://doi.org/https://doi.org/10.4319/lo.1969.14.2.0179, 1969.

Pérez, F. F., Olafsson, J., Ólafsdóttir, S. R., Fontela, M., and Takahashi, T.: Contrasting drivers and trends of ocean acidification in the subarctic Atlantic, Scientific Reports, 11, 1–16, 2021.

Pfeil, B., Olsen, A., Bakker, D. C., Hankin, S., Koyuk, H., Kozyr, A., Malczyk, J., Manke, A., Metzl, N., Sabine, C. L., et al.: A uniform, quality–controlled Surface Ocean CO_2 Atlas (SOCAT), Earth System Science Data, 5, 125–143, 2013.

Rödenbeck, C., Keeling, R. F., Bakker, D. C., Metzl, N., Olsen, A., Sabine, C., and Heimann, M.: Global surface-ocean pCO_2 and sea–air CO_2 flux variability from an observation-driven ocean mixed-layer scheme, Ocean Science, 9, 193–216, 2013.

~~Rödenbeck, C., Bakker, D. C. E., Gruber, N., Iida, Y., Jacobson, A. R., Jones, S., Landschützer, P., Metzl, N., Nakaoka, S., Olsen, A., Park, G.-H., Peylin, P., Rodgers, K. B., Sasse, T. P., Schuster, U., Shutler, J. D., Valsala, V., Wanninkhof, R., and Zeng, J.: Data-based estimates~~

~~of the ocean carbon sink variability – first results of the Surface Ocean pCO_2 Mapping intercomparison (SOCOM), Biogeosciences, 12, 7251–7278, , 2015.~~

Rose, A.: Vision: human and electronic, Springer Science & Business Media, 2013.

Sabine, C. L., Key, R. M., Feely, R. A., and Greeley, D.: Inorganic carbon in the Indian Ocean: Distribution and dissolution processes, Global Biogeochemical Cycles, 16, 15–1, 2002.

Sabine, C. L., Hankin, S., Koyuk, H., Bakker, D. C. E., Pfeil, B., Olsen, A., Metzl, N., Kozyr, A., Fassbender, A., Manke, A., Malczyk, J., Akl, J., Alin, S. R., Bellerby, R. G. J., Borges, A., Boutin, J., Brown, P. J., Cai, W.-J., Chavez, F. P., Chen, A., Cosca, C., Feely, R. A., González-Dávila, M., Goyet, C., Hardman-Mountford, N., Heinze, C., Hoppema, M., Hunt, C. W., Hydes, D., Ishii, M., Johannessen, T., Key, R. M., Körtzinger, A., Landschützer, P., Lauvset, S. K., Lefèvre, N., Lenton, A., Lourantou, A., Merlivat, L., Midorikawa, T., Mintrop, L., Miyazaki, C., Murata, A., Nakadate, A., Nakano, Y., Nakaoka, S., Nojiri, Y., Omar, A. M., Padin, X. A., Park, G.-H., Paterson, K., Perez, F. F., Pierrot, D., Poisson, A., Ríos, A. F., Salisbury, J., Santana-Casiano, J. M., Sarma, V. V. S. S., Schlitzer, R., Schneider, B., Schuster, U., Sieger, R., Skjelvan, I., Steinhoff, T., Suzuki, T., Takahashi, T., Tedesco, K., Telszewski, M., Thomas, H., Tilbrook, B., Vandemark, D., Veness, T., Watson, A. J., Weiss, R., Wong, C. S., and Yoshikawa-Inoue, H.: Surface Ocean CO_2 Atlas (SOCAT) gridded data products, Earth System Science Data, 5, 145–153, https://doi.org/10.5194/essd-5-145-2013, 2013.

Sarma, V. V. S. S., Lenton, A., Law, R. M., Metzl, N., Patra, P. K., Doney, S., Lima, I. D., Dlugokencky, E., Ramonet, M., and Valsala, V.: Sea–air CO_2 fluxes in the Indian Ocean between 1990 and 2009, Biogeosciences, 10, 7035–7052, https://doi.org/10.5194/bg-10-7035-2013, 2013.

Sarma, V. V. S. S., Sridevi, B., Metzl, N., Patra, P. K., Lachkar, Z., Chakraborty, K., Goyet, C., Levy, M., Mehari, M., and Chandra, N.: Air-Sea Fluxes of CO_2 in the Indian Ocean Between 1985 and 2018: A Synthesis Based on Observation-Based Surface CO_2, Hindcast and Atmospheric Inversion Models, Global Biogeochemical Cycles, 37, e2023GB007 694, https://doi.org/https://doi.org/10.1029/2023GB007694, 2023.

Skjelvan, I., Lauvset, S. K., Johannessen, T., Gundersen, K., and Skagseth, Ø.: Decadal trends in ocean acidification from the Ocean Weather Station M in the Norwegian Sea, Journal of Marine Systems, 234, 103 775, https://doi.org/10.1016/j.jmarsys.2022.103775, 2022.

Steinberg, D. K., Carlson, C. A., Bates, N. R., Johnson, R. J., Michaels, A. F., and Knap, A. H.: Overview of the US JGOFS Bermuda Atlantic Time-series Study (BATS): a decade-scale look at ocean biology and biogeochemistry, Deep Sea Research Part II: Topical Studies in Oceanography, 48, 1405–1447, 2001.

Sutton, A. J., Feely, R. A., Maenner-Jones, S., Musielwicz, S., Osborne, J., Dietrich, C., Monacci, N., Cross, J., Bott, R., Kozyr, A., et al.: Autonomous seawater pCO_2 and pH time series from 40 surface buoys and the emergence of anthropogenic trends, Earth System Science Data, 11, 421–439, 2019.

Takahashi, T., Sutherland, S. C., Wanninkhof, R., Sweeney, C., Feely, R. A., Chipman, D. W., Hales, B., Friederich, G., Chavez, F., Sabine, C., Watson, A., Bakker, D. C., Schuster, U., Metzl, N., Yoshikawa-Inoue, H., Ishii, M., Midorikawa, T., Nojiri, Y., Körtzinger, A., Steinhoff, T., Hoppema, M., Olafsson, J., Arnarson, T. S., Tilbrook, B., Johannessen, T., Olsen, A., Bellerby, R., Wong, C., Delille, B., Bates, N., and de Baar, H. J.: Climatological mean and decadal change in surface ocean pCO_2, and net sea–air CO_2 flux over the global oceans, Deep Sea Research Part II: Topical Studies in Oceanography, 56, 554–577, https://doi.org/https://doi.org/10.1016/j.dsr2.2008.12.009, 2009.

Takahashi, T., Sutherland, S. C., Chipman, D. W., Goddard, J. G., Ho, C., Newberger, T., Sweeney, C., and Munro, D.: Climatological distributions of pH, pCO2, total CO2, alkalinity, and CaCO3 saturation in the global surface ocean, and temporal changes at selected locations, Marine Chemistry, 164, 95–125, 2014.

Thomsen, J., Haynert, K., Wegner, K. M., and Melzner, F.: Impact of seawater carbonate chemistry on the calcification<? xmltex\newline?> of marine bivalves, Biogeosciences, 12, 4209–4220, 2015.

~~Torres, O., Kwiatkowski, L., Sutton, A. J., Dorey, N., and Orr, J. C.: Characterizing mean and extreme diurnal variability of ocean CO2 system variables across marine environments, Geophysical Research Letters, 48, e2020GL090 228, 2021.~~

Uppstrom, L.: The boron/chlorinity ratio of deep-sea water from the Pacific Ocean, Deep Sea Res., 21, 161–162, 1974.

Van Heuven, S., Pierrot, D., Rae, J., Lewis, E., and Wallace, D.: CO2SYS v 1.1, MATLAB program developed for CO2 system calculations, ORNL/CDIAC-105b. Oak Ridge, TN: Oak Ridge National Laboratory, https://cdiac.ess-dive.lbl.gov/ftp/co2sys/CO2SYS_calc_MATLAB_v1.1/, 2011.

Woosley, R. J.: Evaluation of the temperature dependence of dissociation constants for the marine carbon system using pH and certified reference materials, Marine Chemistry, 229, 103 914, 2021.

Zeebe, R. E. and Wolf-Gladrow, D.: CO2 in seawater: equilibrium, kinetics, isotopes, 65, Gulf Professional Publishing, 2001.